University of Alberta

Arterial Spin Labeling MRI of Cerebral Perfusion

by

Alison M. Campbell

A thesis submitted to the Faculty of Graduate Studies and Research in partial fulfillment of the requirements for the degree of Master of Science

Department of Biomedical Engineering

Edmonton, Alberta
Spring 2006

Library and Archives Canada

Published Heritage Branch

395 Wellington Street
Ottawa ON K1A 0N4
Canada

Bibliothèque et Archives Canada

Direction du Patrimoine de l'édition

395, rue Wellington
Ottawa ON K1A 0N4
Canada

Your file Votre référence
ISBN: 0-494-13798-3
Our file Notre référence
ISBN: 0-494-13798-3

NOTICE:
The author has granted a non-exclusive license allowing Library and Archives Canada to reproduce, publish, archive, preserve, conserve, communicate to the public by telecommunication or on the Internet, loan, distribute and sell theses worldwide, for commercial or non-commercial purposes, in microform, paper, electronic and/or any other formats.

The author retains copyright ownership and moral rights in this thesis. Neither the thesis nor substantial extracts from it may be printed or otherwise reproduced without the author's permission.

AVIS:
L'auteur a accordé une licence non exclusive permettant à la Bibliothèque et Archives Canada de reproduire, publier, archiver, sauvegarder, conserver, transmettre au public par télécommunication ou par l'Internet, prêter, distribuer et vendre des thèses partout dans le monde, à des fins commerciales ou autres, sur support microforme, papier, électronique et/ou autres formats.

L'auteur conserve la propriété du droit d'auteur et des droits moraux qui protège cette thèse. Ni la thèse ni des extraits substantiels de celle-ci ne doivent être imprimés ou autrement reproduits sans son autorisation.

In compliance with the Canadian Privacy Act some supporting forms may have been removed from this thesis.

While these forms may be included in the document page count, their removal does not represent any loss of content from the thesis.

Conformément à la loi canadienne sur la protection de la vie privée, quelques formulaires secondaires ont été enlevés de cette thèse.

Bien que ces formulaires aient inclus dans la pagination, il n'y aura aucun contenu manquant.

Canada

ABSTRACT

Arterial spin labeling (ASL) is a completely noninvasive magnetic resonance imaging (MRI) technique that uses blood water as an endogenous tracer to assess cerebral blood flow (CBF). We applied a pulsed arterial spin labeling (PASL) sequence at 1.5 Tesla to determine potential methodological problems in multi-slice ASL imaging. Results indicate that slice interactions in 2D-EPI acquisition schemes reduce perfusion-weighted signal in ASL images, causing an underestimation of blood flow in distal slices. As preliminary work for the application of ASL to stroke, the same PASL sequence was used to assess CBF and arterial transit times in the elderly. Due to an increase in transit times, a longer inversion time (TI) is required for PASL imaging in the elderly to reduce intravascular signal and increase tissue signal, and accurately quantify CBF. Overall, ASL is a promising technique that can provide reliable and reproducible CBF measurements in normal brain tissue as well as a variety of pathologies.

ACKNOWLEDGEMENTS

There are many people without whom this thesis would not have been possible. I would like to thank my supervisor, Dr. Christian Beaulieu, who has guided me through my degree and provided unending encouragement and support. Your knowledge of MRI and your enthusiasm for research has been invaluable to my work. I am extremely grateful for your patience and for the time you have invested in helping me accomplish my goals.

I would like to thank the Beaulieu Lab, Jacob, Rob, Yusuf, Luis, and Lindsay for their support, friendship, and countless hours in the scanner. Lindsay, thank you for your work with the teenagers, I recognize that imaging 51 volunteers takes many hours. As well, thanks to Atiyah who is a constant source of encouragement, and Jason who never failed to amuse me even on the worst of days, and was always there to remind me of what is truly important in life.

I would like to thank my committee members, Dr. Rick Snyder and Dr. Derek Emery, for being extremely accommodating throughout the years. Dr. Snyder, I sincerely appreciate you going beyond your duty as Graduate Chair to lend a helping hand during the tough times. As well, thank you Maisie for dealing with my endless paperwork, and Beau for rebuilding my computer during my moments of crisis.

I would like to thank NSERC for providing two full-time studentships, and the University of Alberta for granting me numerous tuition scholarships. Thanks to Dr. Stefan Thesen at Siemens for providing the PASL Q2TIPS sequence we used on our 1.5T scanner.

I'd like to thank my parents who have always emphasized the importance of education and afforded the encouragement I needed to complete my research. I'd like to thank Marcia, Scott, and Steph for always being there, and my friends in Edmonton who never got tired of hearing me talk about my thesis. Finally, I'd like to give a very special thank you to Dr. Piktel, Loretta, Nancy, Trish, Joanna, and the rest of the crew who were there to pull, push, or drag me through to the finish line. You have given me the strength to move forward and pursue my dreams.

TABLE OF CONTENTS

CHAPTER 1: Introduction 1

1.1 Introduction 2
1.1.1 Cerebral Perfusion 4
1.1.2 Perfusion Regulation 7
1.1.3 Perfusion Thresholds 9
1.2 Measurement of Cerebral Blood Flow 11
1.2.1 The Original Techniques 11
1.2.2 Dynamic Susceptibility Contrast MRI 12
1.2.3 Arterial Spin Labeling 17
1.3 Pulsed Arterial Spin Labeling 20
1.3.1 Labeling Schemes 20
1.3.2 The General Kinetic Model for CBF Quantification 22
1.3.3 Transit Time Insensitive Sequences 24
1.4 Implementation of PASL Imaging 28
1.4.1 TR Optimization 29
1.4.2 TI_1 Optimization 30
1.4.3 Reproducibility of ASL Perfusion Values 31
1.4.4 CBF Quantification 36
1.5 Scope of Thesis 38

CHAPTER 2: Comparison of Multi-slice and Single Slice Acquisitions for Pulsed Arterial Spin Labeling Measurements of Cerebral Perfusion 40

2.1 Introduction 41
2.2 Materials and Methods 43
2.2.1 MR Imaging 43
2.2.2 Data Processing 46
2.3 Results 48
2.4 Discussion 53

CHAPTER 3: Pulsed Arterial Spin Labeling Parameter Optimization for an Elderly Population 57

3.1 Introduction 58
3.2 Materials and Methods 59
3.2.1 MR Scanning 59
3.2.2 Data Processing 61
3.3 Results 63
3.3.1 ASL Difference Signal 63
3.3.2 Transit Time 65
3.3.3 Cerebral Blood Flow 66
3.4 Discussion 67

CHAPTER 4: Discussion **69**

4.1 Multi-slice and Single Slice PASL for CBF Measurement 70
4.2 PASL Parameter Optimization for the Elderly 71
4.2.1 Future Directions 72
4.3 High Field ASL Imaging 73
4.3.1 SNR Increase with Main Magnetic Field Strength 73
4.3.2 ASL Pulse Sequence Development at 3T 75
4.4 Imaging Evaluation of Stroke 77
4.4.1 Evaluation and Treatment of Acute Stroke 77
4.4.2 Diffusion- and Perfusion-Weighted MRI 78
4.4.3 ASL Assessment of Perfusion in Stroke 79
4.4.4 MRI Stroke Research Program 82
4.5 Future Directions 84
4.5.1 Q2TIPS Sequence Development 84
4.5.2 Tagging Schemes 84
4.5.3 3D Image Acquisition Techniques 85
4.6 Conclusions 86

REFERENCES **89**

LIST OF TABLES

Table 2-1: Average CBF in single slice and multi-slice studies 53
Table 3-1: Gray matter CBF in the young and elderly 66
Table 4-1: Assessment of cerebrovascular disease using ASL 81

LIST OF FIGURES

Figure 1-1: Major blood vessels supplying the brain 6
Figure 1-2: Exchange of oxygen and nutrients through the capillary wall 7
Figure 1-3: Biochemical consequences of reduced cerebral perfusion 10
Figure 1-4: DSC-MRI raw images and corresponding signal intensity plot 14
Figure 1-5: Creating the tag and control images 18
Figure 1-6: Tag and control (raw) images and ASL difference signal images 19
Figure 1-7: EPISTAR, FAIR, and PICORE tagging profiles 21
Figure 1-8: QUIPSS II modification of a traditional PASL sequence 25
Figure 1-9: Movement of tagged water during the inversion time in QUIPSS II 26
Figure 1-10: Q2TIPS pulse sequence 27
Figure 1-11: Q2TIPS difference signal images 29
Figure 1-12: TI_1 optimization 31
Figure 1-13: Stability of gray matter ΔM SNR with TI_2 33
Figure 1-14: Stability of gray matter CBF with PICORE-Q2TIPS 35
Figure 1-15: Quantitative CBF map 37
Figure 2-1: Location of the tagging plane and imaging slices in studies 1, 2, and 3 45
Figure 2-2: ASL single slice and multi-slice perfusion images in study 1 49
Figure 2-3: ASL single slice and multi-slice perfusion images in study 2 49
Figure 2-4: ASL single slice and multi-slice perfusion images in study 3 49
Figure 2-5: Mean gray matter SNR ± SD in both single slice and multi-slice acquisitions 51
Figure 3-1: Average GM difference signal normalized to M_{ob} ($\Delta M / M_{ob}$) 63
Figure 3-2: Perfusion-weighted difference images at different values of TI_2 64
Figure 3-3: Multi-slice perfusion-weighted difference images 65
Figure 4-1: ASL images of a 91-year-old stroke patient (time from onset = 20 hours) 72
Figure 4-2: FAIR difference images at 3T 75
Figure 4-3: Summation of 10 ASL difference images at 3T 76
Figure 4-4: DWI and PWI images (DSC-MRI) of an acute stroke patient 79
Figure 4-5: DWI, DSC-MRI, and ASL images of an acute stroke patient 83

LIST OF ABBREVIATIONS, SYMBOLS AND NOMENCLATURE

α	tagging efficiency, the fraction of the desired difference in magnetization generated by the tag and control pulses
ΔM	ASL difference signal
ΔR_2, ΔR_2^*	change in transverse relaxation rate
Δt	arterial transit time
λ	blood-brain partition coefficient of water
τ	time width of the tagged bolus
ω	delay time between saturation and inversion, $TI_2 - TI_1$
ACA	anterior cerebral artery
ADC	apparent diffusion coefficient
AIF	arterial input function
ASL	arterial spin labeling
ATP	adenosine triphosphate
B_0	main magnetic field strength
BA	basilar artery
BBB	blood-brain barrier
BW	bandwidth
$C_a(t)$	arterial contrast agent concentration
CASL	continuous arterial spin labeling
CBF	cerebral blood flow
CBV	cerebral blood volume
$CMRO_2$	cerebral metabolic rate of oxygen
CNR	contrast-to-noise ratio
CO_2	carbon dioxide
CSF	cerebrospinal fluid
CT	computed tomography
$C_t(t)$	tissue contrast agent concentration
DSC-MRI	dynamic susceptibility contrast enhanced MRI
DTI	diffusion-tensor imaging
DWI	diffusion-weighted imaging
EPI	echo-planar imaging
EPISTAR	echo-planar imaging and signal targeting with alternating radio-frequency
f	cerebral blood flow (s^{-1})
FAIR	flow-sensitive alternating inversion recovery
fMRI	functional magnetic resonance imaging
FOCI	frequency offset corrected inversion radio-frequency pulse
FOV	field of view
FSE	fast spin-echo sequence
Gd-DTPA	gadolinium-diethylenetriaminepentaacetic acid
GE-EPI	gradient-echo echo-planar imaging

GM	gray matter
GRASE	gradient- and spin-echo sequence
ICA	internal carotid artery
IR-EPI	inversion recovery echo-planar imaging
JMRI	Journal of Magnetic Resonance Imaging
k	proportionality constant relating tissue contrast agent concentration to change in relaxation rate
MCA	middle cerebral artery
M_{ob}	T_2*-weighted equilibrium signal of blood
M_{ot}	T_2*-weighted equilibrium signal of tissue
M_{owm}	T_2*-weighted equilibrium signal of white matter
MRA	magnetic resonance angiography
MRI	magnetic resonance imaging
MRS	magnetic resonance spectroscopy
MT	magnetization transfer
MTT	mean transit time
NO	nitrous oxide
P_aCO_2	arterial pressure of carbon dioxide
PASL	pulsed arterial spin labeling
PET	positron emission tomography
PICORE	proximal inversion with a control for off-resonance effects
PWI	perfusion-weighted imaging
q(t)	correction factor for the effects of capillary/tissue exchange, incomplete water extraction, and venous outflow
Q2TIPS	quantitative imaging of perfusion using a single subtraction second version with thin-slice TI_1 periodic saturation
QUIPSS	quantitative imaging of perfusion using a single subtraction
R	ratio of blood signal to white matter signal
R(t)	residue function, fraction of contrast agent remaining in tissue
R_2, R_2*	transverse relaxation rate
rCBF	regional cerebral blood flow
rCBV	regional cerebral blood volume
RF	radio-frequency
rOEF	relative oxygen extraction fraction
rt-PA	recombinant tissue plasminogen activator
S(t)	signal intensity
sech	hyperbolic secant radio-frequency pulse
SE-EPI	spin-echo echo-planar imaging
SENSE	sensitivity encoding
SNR	signal-to-noise ratio
SPECT	single photon emission computed tomography
T	tesla
T_1	longitudinal (spin-lattice) relaxation time
T_{1b}	longitudinal relaxation time of blood
T_{1t}	longitudinal relaxation time of tissue

T_2	transverse (spin-spin) relaxation time
T_{2b}*	transverse relaxation time of blood
T_{2wm}*	transverse relaxation time of white matter
TE	echo time
T_{ex}	time of water exchange between blood and tissue
TI	inversion time
TI_1	time of saturation
TI_{1s}	periodic saturation stop time
TI_2	time of inversion
TR	repetition time
TR_{slice}	slice repetition time
TTP	time-to-peak
V_c	cutoff velocity
VS-ASL	velocity selective arterial spin labeling
WM	white matter
XeCT	xenon-enhanced computed tomography

CHAPTER 1: Introduction

1.1 Introduction

Magnetic resonance imaging (MRI) is a powerful technique for the evaluation of brain structure and function. During the last 20 years tremendous progress has been made in MR imaging which has increased our knowledge of the human brain and numerous cerebral diseases. MRI has developed into an imaging modality that is applied routinely in the clinical setting to assess both acute and chronic pathologies. The noninvasive nature of MRI makes it suitable for use in long term studies and in the assessment of children.

One of the greatest advantages of MRI is its flexibility to generate variable contrast between different tissues and pathologies. Conventional MRI provides excellent structural information by exploiting the distinct longitudinal and transverse relaxation times (T_1 and T_2 respectively) of different tissue compartments. Conventional techniques can be combined with: magnetic resonance angiography (MRA), to evaluate arteries in the head and neck for the presence of stenosis or aneurysm; magnetic resonance spectroscopy (MRS), to measure relative concentrations of cerebral metabolites; functional magnetic resonance imaging (fMRI), to evaluate normal brain functioning and neurocognitive disorders (e.g. schizophrenia, bipolar disorder, and depression); and diffusion-tensor imaging (DTI) to measure the directionality and magnitude of water diffusion, map white matter tracts, and assess white matter disease and brain development. Structural MR imaging is often supplemented with methods that investigate physiologic aspects of the brain, such as diffusion-weighted imaging (DWI), and perfusion-weighted imaging (PWI). The widespread availability of MR scanners capable of ultrafast imaging (e.g. echo-planar imaging, EPI) has led to an increase in the clinical application of DWI and PWI.

Techniques for the assessment of tissue perfusion are of considerable clinical importance, especially in the areas of acute stroke, chronic cerebrovascular disease, brain tumors,

Alzheimer's disease, and epilepsy. Therapy for acute stroke depends on ensuring an accurate diagnosis and excluding diseases that clinically mimic cerebral ischemia, such as brain tumours or hemorrhagic stroke Because stroke is characterized by reduced blood flow, imaging of brain perfusion has become an important part in the evaluation of potential stroke patients. Where available, perfusion-weighted MR imaging (PWI) combined with diffusion-weighted MR imaging (DWI) is the method of choice for determining the physiological status of tissue and helping to guide the direction of treatment (Chalela *et al.*, 2000, Schellinger *et al.*, 2003, Kidwell *et al.*, 2004).

In chronic cerebrovascular disease, patients often present with intra- and/or extracranial high grade stenotic lesions of the cerebral vessels (e.g. internal carotid artery (ICA) stenosis) which cause resting cerebral hypoperfusion and reduced cerebrovasculature reserve capacity (Nighoghossian *et al.*, 1994, Widder *et al.*, 1994). While it is well known that chronic cerebrovascular abnormalities can lead to cortical and white matter borderzone ischemia (Leblanc *et al.*, 1987, Carpenter *et al.*, 1990), reduced cerebral perfusion or perfusion reserve has also been found to be predictive of stroke (Bogousslavsky *et al.*, 1990, Widder *et al.*, 1994, Webster *et al.*, 1995, Gur *et al.*, 1996). Perfusion MR imaging is capable of quantifying both hypoperfusion and reduced reserve capacity, therefore it provides important diagnostic information for patients with chronic cerebrovascular disorders (Detre & Alsop, 1999, Detre *et al.*, 1999).

There are two main categories of MRI perfusion techniques: dynamic susceptibility contrast enhanced MRI (DSC-MRI), and arterial spin labeling (ASL). DSC-MRI is a bolus tracking technique that uses exogenous contrast to assess multiple hemodynamic parameters (i.e. cerebral blood flow, cerebral blood volume (CBV), mean transit time (MTT), and time-to-peak (TTP)). Alternatively, arterial spin labeling is a completely noninvasive technique that uses blood water as an endogenous tracer to measure cerebral blood flow. Both ASL and DSC have been validated with $H_2{}^{15}O$ PET for assessing cerebral blood flow in humans (Ostergaard *et al.*, 1998b, Ye *et al.*, 2000).

This thesis focuses on the measurement of cerebral perfusion using arterial spin labeling. In the first chapter we present the basic theory of ASL, including the mechanism for generating the perfusion signal as well as techniques for CBF quantification. The implementation of ASL at our site along with preliminary results is also discussed. Chapters 2 and 3 are essentially journal articles which comprise our main body of work in ASL. In Chapter 2 we compare multi-slice and single slice pulsed ASL acquisitions for the assessment of cerebral perfusion, and in Chapter 3 we optimize pulsed ASL parameters for an elderly population. In the final chapter we introduce our preliminary ASL work at high field and in stroke patients, and discuss potential future directions.

1.1.1 Cerebral Perfusion

The brain is the most complex organ in the human body and has captured the interest of the world's most prominent scientists for thousands of years. Pythagoras was the first to emphasize the importance of the brain when he claimed the brain was the locus of the soul. In the 3rd century B.C., Herophylos of Chalcedon continued in the ideas of Pythagoras and studied the anatomy and function of the brain. He established the brain as the centre of intelligence and consciousness and identified many brain structures such at the meninges, sinuses, veins and arteries. As well, he discovered the function of nerves, and was able to separate them into sensory and motor branches (Bell, 1984). The understanding of the human brain was slow to advance until human dissections began in the 13th century. At this time, the structure and location of the cerebral vasculature was determined with considerable success. Finally, in the 17th century the focus on vascular anatomy was shifted to physiology when William Harvey discovered the circulation of the blood (Harvey, 1628). This prompted research into the purpose of the distribution of cerebral blood vessels, such as the Circle of Willis (Willis, 1684). From this point, many techniques were used to measure cerebrospinal fluid (CSF) pressure, volume of the brain, intracranial pressure, and pressure and flow in cerebral vessels.

The term perfusion refers to the delivery of blood at the capillary level, where the exchange of oxygen and nutrients between blood and tissue occurs. Cerebral blood flow (CBF) is usually defined as the volume of arterial blood (mL) delivered to a volume of tissue (mL) per unit time (min), although it can also be defined as a rate constant (s^{-1}). It is useful to describe perfusion as the rate of delivery of metabolic substrates, including oxygen and nutrients, and removal of metabolic products, thereby linking blood flow to local metabolism. Regional CBF was proven to be coupled to regional brain function and energy metabolism in the 1970's (Carter *et al.*, 1972, Raichle *et al.*, 1976), finally providing evidence to support the observation made by Roy and Sherrington in 1890: "....the brain possesses an intrinsic mechanism by which its vascular supply can be varied locally in correspondence with local variations of functional activity" (Roy & Sherrington, 1890). In fact, one of the primary functions of the brain is flow regulation, determining the rate of oxygen delivery and removal of waste according to regional energy metabolism.

The cerebral circulation is a vast and complex system which is designed to distribute oxygen and nutrients to brain tissue. Blood is supplied to the cerebral vasculature through two pairs of large vessels in the neck, the internal carotid arteries, arising from the common carotid arteries, and the vertebral arteries (Fig. 1-1). Inside the brain, the major arteries, including the anterior cerebral artery (ACA), middle cerebral artery (MCA), and posterior cerebral artery (PCA), branch into multiple smaller arteries and arterioles, which in turn divide until they form capillaries, vessels made from a single layer of endothelial cells.

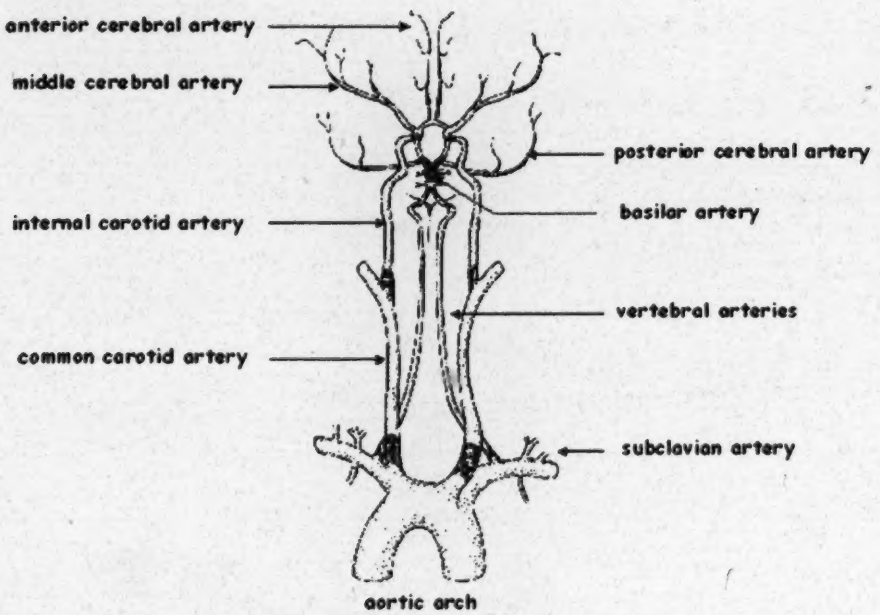

Figure 1-1: Major blood vessels supplying the brain

The common carotid arteries travel most of the length of the neck before branching into the external carotid arteries, supplying the face, and the internal carotid arteries, supplying approximately two thirds of the cerebrum. The vertebral arteries join in the brain to form the basilar artery which supplies the remaining third of the brain.

Typically only two capillaries arise from an arteriole in the nervous system, and run parallel to each other for about a centimeter before rejoining to form a small venule (Fig. 1-2). Unlike most systems in the body, substances are selectively passed from the blood to brain tissue through endothelial cells making up the capillary wall. The endothelial cells are major components of the blood-brain barrier (BBB), which prevents harmful substrates from passing into the brain.

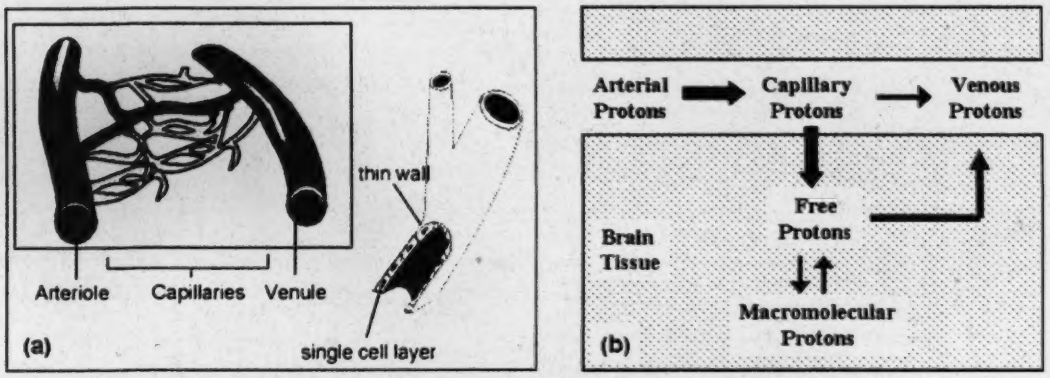

Figure 1-2: Exchange of oxygen and nutrients through the capillary wall

Capillaries permit the diffusion of oxygen and nutrients from the blood into tissues, and the waste products of metabolism from the tissues into blood. Although it is important that these molecules easily pass through the capillary wall, the brain must be protected from harmful substances (e.g. toxins), therefore cerebral vessels form a blood-brain barrier. The large surface area of the capillary network ensures that substrates can reach all brain regions by means of diffusion.

1.1.2 Perfusion Regulation

The human brain is only 2% of total body weight yet it consumes 20% of the cardiac output and oxygen consumption at rest, making it the most metabolically active organ in the human body (Kety, 1991). Cerebral metabolism is almost completely dependent on aerobic metabolism, therefore normal brain function requires regulation of cerebral blood flow to ensure a constant delivery of oxygen. Almost all of the oxygen supplied to brain tissue is used for the conversion of glucose to CO_2. Since neural tissue has no mechanism for storage of oxygen, there is an oxygen metabolic reserve of about 8-10 seconds (Paulson, 2002).

The cerebral circulation is regulated by four primary factors: metabolic stimuli, perfusion pressure, chemical stimuli, and neural stimuli (Lou *et al.*, 1987). As mentioned above, local metabolic activity is coupled to local blood flow in normal brain tissue; in fact, local

CBF varies in parallel to the local cerebral metabolic rate of oxygen ($CMRO_2$) (Lou *et al.*, 1987). Increased neuronal metabolic activity leads to the accumulation of vasodilating products (e.g. hydrogen ions, potassium, and glycolitic intermediates), which decrease vascular resistance thereby increasing blood flow until homeostasis is reestablished (Roy & Sherrington, 1890). Local increases in metabolic demand are rapidly met with increases in local blood flow and delivery of metabolic substrates.

Under non-pathological conditions, local perfusion is maintained through a wide range of arterial blood pressures, approximately 60 to 150 mmHg (Paulson *et al.*, 1990). This process is termed cerebral autoregulation and is controlled by local arterioles which possess an intrinsic autoregulatory capacity. Arterioles consist of endothelium surrounded by one or more layers of smooth muscle cells that can be stimulated to contract or dilate in order to maintain perfusion with changes in pressure. However, the vascular system cannot compensate for pressures below approximately 60 mmHg; cerebral vasodilation is maximal, and blood flow falls with pressure resulting in hypoxia. Similarly, pressure elevated above 150 mmHg can overwhelm resistance, leading to breakdown of the blood-brain barrier, and brain swelling.

Blood gases are the major chemical stimuli which can cause vasoconstriction or vasodilation of minor arteries approaching the capillary bed (Kety & Schmidt, 1948b, Reivich, 1964). An increase in blood levels of CO_2 causes vasodilation and higher blood rates, whereas a decrease below usual levels produces the reverse effect. A change in the arterial pressure of CO_2 (P_aCO_2) takes precedence over autoregulatory mechanisms. On the other hand, circulatory response to hypoxia is very poor, and elevated oxygen levels do not generate any response. Vasodilation occurs only when the oxygen partial pressure drops below approximately 50 mmHg.

Direct innervation of vessels appears to have relatively little role in cerebral blood flow, but when it does intervene it has priority over metabolic or autoregulatory processes (Tomita *et al.*, 2000). Sources of neural input to the brain's vessels include sympathetic,

parasympathetic, and peripheral sensory innervation. Brain stem and cerebellar nuclei have also been implicated in direct control of vessel diameter.

A loss of CBF regulatory capacity is most frequently attributed to damage of the control system (e.g. cerebral vessels). The most common vascular diseases to damage the control system are atherosclerosis, stroke, aneurysm, and hypertension, although the cerebral vasculature can also be impaired by brain tumors, epilepsy, Alzheimer's disease, and neuropsychiatric disorders such as, bipolar disorder, schizophrenia, and depression.

1.1.3 Perfusion Thresholds

Maintenance of normal cerebral blood flow is an important indicator of a healthy cerebral circulation and viable tissue. If perfusion regulation fails, global or focal blood flow may fall below the level required for normal brain function and tissue can become ischemic. Ischemic tissue is defined as having blood flow between two critical rates, the threshold for electrical failure and the threshold for membrane failure (Hossmann, 1994). Ischemia is also a time-dependent state; viable neurons that are not functioning properly undergo transient depolarizations which over time can compromise energy metabolism leading to infarction (Back, 1998).

In the presence of sufficient oxygen, the brain is highly efficient in deriving its energy from glucose and metabolic demands are easily met. Once cerebral perfusion drops below the critical 'threshold for ischemia', the resting neuronal membrane potential is lost, and a cascade of biochemical mechanisms is triggered within the tissue (Fig. 1-3) (Hossmann, 1994). Although the exact perfusion threshold for ischemia varies among individuals and pathologies, it is generally agreed to be approximately 20 mL/100mL/min. If perfusion continues to decline below approximately 12 mL/100mL/min neuronal energy metabolism fails, causing loss of cell ion homeostasis, acidosis, increased intracellular Ca^{2+}, excitotoxicity, free radical-mediated toxicity, and neuron death by necrosis or apoptosis (Macdonald & Stoodley, 1998). As a general rule,

neurons can endure many minutes to hours of ischemia when CBF is between 12 and 20 mL/100mL/min, however CBF less than 10 mL/100mL/min can only be tolerated for several minutes before infarction occurs (Latchaw *et al.*, 2003).

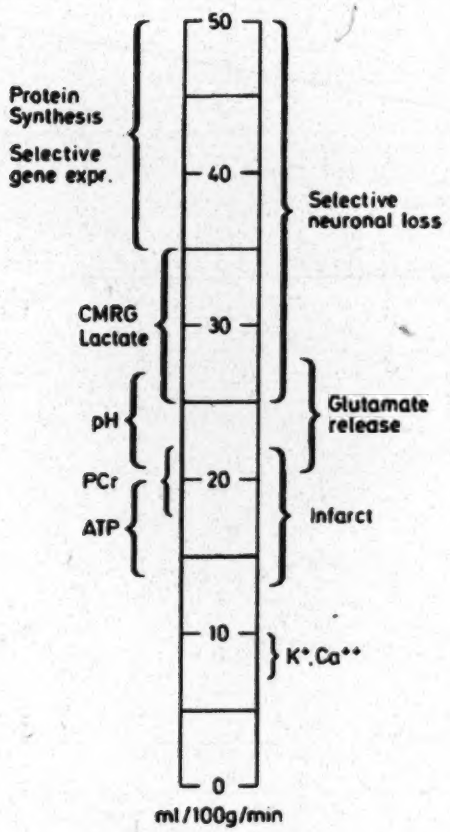

Figure 1-3: Biochemical consequences of reduced cerebral perfusion

The approximate gray matter perfusion thresholds in stroke have been determined as 55 mL/100mL/min for loss of protein synthesis, 35 mL/100mL/min for stimulation of anaerobic glycolysis (lactate release), 20 mL/100mL/min for synaptic release of transmitters (e.g. glutamate) and failure of energy metabolism, and 15 mL/100mL/min for anoxic depolarization (Hossmann, 1994). Normal human gray matter cerebral blood flow is approximately 60 mL/100mL/min. Adapted from (Hossmann, 1994).

1.2 Measurement of Cerebral Blood Flow

1.2.1 The Original Techniques

The quantitative measurement of cerebral blood flow (CBF) in humans was accomplished in 1945 by Seymour S. Kety and Carl F. Schmidt (Kety & Schmidt, 1945). CBF was determined following the inhalation of the diffusible inert gas nitrous oxide (NO), sampling of the jugular venous and peripheral arterial blood, and application of the Fick Principle (Fick, 1870). Kety and Schmidt calculated CBF in healthy normal men to be 54 ± 12 mL / 100 g brain / minute (Kety & Schmidt, 1948a). The Kety and Schmidt model was fundamental in advancing research of the cerebral circulation, and further work by Kety on the exchange of inert gas in the lungs and tissues helped develop techniques for regional blood flow measurements (Kety, 1951). The quantitative measurement of regional CBF was successfully carried out in humans in 1961 (Ingvar & Lassen, 1961). In the end, it was the original work by Kety in 1951 that produced the equations governing the action of inert gases as diffusible indicators, which eventually formed the basis of all clearance, autoradiographic, and computed tomographic techniques.

Currently, several imaging techniques are used clinically for the assessment of cerebral blood flow. Xenon-enhanced computed tomography (XeCT), involving inhalation of freely diffusible Xenon gas as a contrast material, has been used since the 1970's to quantitatively assess human CBF (Drayer *et al.*, 1978). Accurate and reliable quantitative measurements of CBF are possible with XeCT, although images are prone to motion artifacts and long acquisition times. Perfusion CT, which is a dynamic contrast bolus technique, can be used to accurately quantify CBV, MTT, and CBF, and has been widely accepted for the evaluation of acute stroke (Nabavi *et al.*, 1999, Nabavi *et al.*, 2001). A limitation of dynamic perfusion CT is its use of ionizing radiation and iodinated contrast material (Eastwood *et al.*, 2003). Single photon emission computed tomography (SPECT) uses gamma ray emitting radioisotopes (commonly ^{99m}Tc and ^{123}I) and gamma cameras to determine cerebral blood flow (Brooks & Di Chiro, 1976,

Jaszczak & Coleman, 1988). SPECT imaging is easy to perform, requiring only an intravenous injection of contrast, and is available in most large radiology departments, however images have low spatial resolution and only provide qualitative (relative) perfusion information (Latchaw *et al.*, 2003). Finally, positron emission tomography (PET) techniques measure emissions from radioactive metabolic chemicals, and apply kinetic wash-in and wash-out approaches to accurately produce quantitative images of hemodynamic parameters, such as CBF, CBV, relative oxygen extraction fraction (rOEF), and relative cerebral metabolic rate of oxygen ($rCMRO_2$) (Ter-Pogossian *et al.*, 1975, Brooks & Di Chiro, 1976). PET is often used as the 'gold-standard' for validation of other perfusion measurement techniques (Wintermark *et al.*, 2005). Readers are referred to the report by Wintermark *et al.* for a detailed overview of imaging techniques currently used to evaluate cerebral perfusion (Wintermark *et al.*, 2005).

Magnetic resonance imaging has become a powerful tool for the assessment of cerebral perfusion. Compared with PET, MRI is advantageous due to improved spatial and temporal resolution, no patient exposure to ionizing radiation, and the possibility to combine structural and functional information during a single imaging session. MRI techniques for the study of cerebral perfusion fall into two major categories: dynamic susceptibility contrast enhanced MR imaging (DSC-MRI), and arterial spin labeling (ASL).

1.2.2 Dynamic Susceptibility Contrast MRI

Cerebral perfusion MRI using exogenous contrast agents is a widely accepted technique for basic perfusion research and clinical applications (Villringer *et al.*, 1988, Rosen *et al.*, 1990). Dynamic susceptibility contrast MRI (DSC-MRI) is a bolus tracking technique used to derive hemodynamic parameters, such as cerebral blood flow (CBF), cerebral blood volume (CBV), and mean transit time (MTT), using tracer kinetic analysis. The technique involves injecting a bolus of paramagnetic contrast agent (gadolinium-based chelate, e.g. Gd-DTPA) into an antecubital vein, and tracking its first pass through the

cerebral vasculature by rapid MR imaging, most commonly echo-planar imaging (EPI). Overall, DSC-MRI uses changes in signal intensity caused by the paramagnetic contrast agent to infer contrast agent concentration within the tissue, and measure cerebral blood flow.

The contrast agents used in bolus tracking are compartmentalized in the vessels, creating microscopic susceptibility gradients between blood and tissue. Diffusion of extravascular protons through these gradients causes transverse relaxation and signal loss (Fig. 1-4) (Villringer *et al.*, 1988). The amount of signal loss depends on: vascular structure, contrast agent concentration, and the echo time (TE) of the acquisition sequence. The sensitivity of DSC-MRI to the microvasculature (i.e. capillaries) and macrovasculature depends on the acquisition method used (Speck *et al.*, 2000). Gradient-echo (GE) based techniques are relatively insensitive to vessel size, whereas spin-echo (SE) based techniques show a maximum sensitivity for vessels between 5 and 10 μm in diameter, the size of human cerebral capillaries (Weisskoff *et al.*, 1994, Boxerman *et al.*, 1995). GE-EPI techniques are advantageous because they allow for calculation of the arterial input function, and compared to SE-EPI, more slices can be acquired in the same time period, and images show higher contrast-to-noise ratio (CNR) and signal-to-noise ratio (SNR) (Simonsen *et al.*, 2000, Speck *et al.*, 2000). However, SE-EPI perfusion images demonstrate improved image quality, with fewer distortions and less signal loss in areas with high susceptibility gradients. Most importantly, spin-echo based images provide more information regarding signal alterations from small vessels, therefore they are more representative of true tissue perfusion at the capillary level (Baird & Warach, 1998).

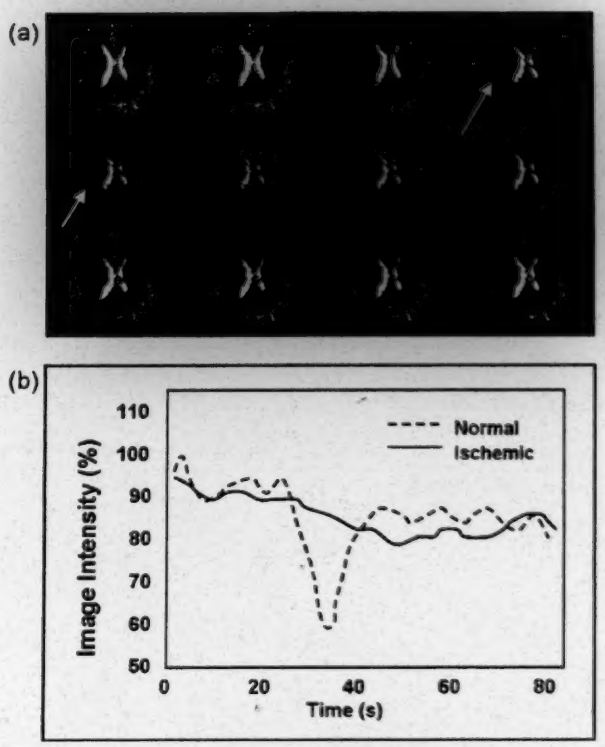

Figure 1-4: DSC-MRI raw images and corresponding signal intensity plot

An acute stroke patient was imaged using GE-EPI every 2 seconds after the injection of a bolus of contrast agent. The sequence of raw perfusion images in (a) show signal loss in perfused tissue as the contrast bolus passes through the slice, and high signal intensity in regions without flow (white arrows). The change in signal intensity with time for both normal and ischemic tissue is seen in (b). Ischemic tissue is identified as voxels showing little or no drop in signal intensity.

1.2.2.1 Absolute CBF Measurements by Bolus Tracking MRI

Quantification of CBF requires that the change in regional signal intensity, S(t), is converted to contrast agent concentration. The signal intensity in SE and GE sequences depends on both the transverse relaxation rate, R_2 and R_2*, and their rate changes, ΔR_2 and ΔR_2*. The transverse relaxation rate R_2* describes the rate of decay of transverse

magnetization that is caused by both molecular interactions and inhomogeneities in the main magnetic field (B_0), and accounts for the rate of signal loss in GE based sequences, whereas R_2 is the rate of decay of transverse magnetization that results from molecular interactions only, and describes signal loss in SE based sequences. By assuming a linear relationship between the change in transverse relaxation rate and tissue contrast agent concentration, the time course of the tissue tracer concentration, $C_t(t)$, and arterial tracer concentration, $C_a(t)$ (i.e. arterial input function, AIF), can be calculated from the signal intensities at baseline, S(0), and at time t, S(t),

$$C_t(t) = k \cdot \Delta R_2(t) = -k \cdot \log\left[\frac{S(t)}{S(0)}\right] / TE \qquad [1.1]$$

where k is the assumed proportionality constant. The calculation of tissue contrast agent concentration can also be described as the convolution between the arterial input function, $C_a(t)$, and the residue function, R(t), which describes the fraction of contrast agent remaining in the tissue at time t,

$$C_t(t) = CBF \cdot C_a(t) \otimes R(t) \qquad [1.2]$$

The relative cerebral blood flow is the height of the deconvolved response curve. It is important to note that the amount of signal loss is proportional to the concentration of contrast agent, and therefore proportional to CBF; the proportionality constant is k. A relative map of perfusion can be generated without determining k, however a quantitative value for k is required for absolute CBF measurement. Interestingly, the amount of signal loss is directly proportional to blood volume in healthy brain tissue, emphasizing that DSC-MRI is actually an *indirect* measure of cerebral blood flow and a *direct* measure of cerebral blood volume (Belliveau *et al.*, 1990, Belliveau *et al.*, 1991).

The quantification of CBF from raw DSC images involves three important processes: calibration of the proportionality constant k, selection of a robust mathematical approach

for deconvolution, and calculation of the arterial input function. The calculated CBF value can vary substantially with different combinations of deconvolution techniques, arterial input functions, and k values. Determination of an appropriate value for k requires co-registration of DSC images and CBF images acquired from an independent technique. Using PET and MRI data it has been shown that a common conversion factor can be used for perfusion quantification in healthy normal tissue (Ostergaard *et al.*, 1998a, Ostergaard *et al.*, 1998b). However, k must be calibrated separately for pathological tissues; in fact, researchers are unsure whether the proportionality between signal loss and contrast agent concentration holds in diseased tissue (Ostergaard *et al.*, 1998a).

The selection of an appropriate deconvolution technique is an important step in CBF calculation. Deconvolution approaches can be divided into two major categories: (a) model-dependent approaches, where R(t) is given a specific analytical expression based on an assumed vascular structure, or (b) model-independent approaches, where Eq. 1.2 is solved on a pixel-by-pixel basis to determine CBF · R(t) (Gobbel *et al.*, 1991, Rempp *et al.*, 1994). Experimental comparison of the various deconvolution methods has been carried out in numerous studies, however an optimal approach for all patients has yet to be determined (Ostergaard *et al.*, 1996b, Ostergaard *et al.*, 1996a, Smith *et al.*, 2000, Wirestam *et al.*, 2000).

The arterial input function (AIF) can be obtained from an artery within the slice of interest or from the middle cerebral artery supplying the slice, the difference being that more delay and dispersion of the bolus can occur if the MCA is chosen. As well, in cerebral ischemia the AIF can be chosen from the ipsilateral or contralateral side to the stroke. Several studies have tested different AIF sites and results indicate that perfusion-weighted lesion size and CBF values vary substantially with AIF location (Ostergaard *et al.*, 1996a, Wirestam *et al.*, 2000, Thijs *et al.*, 2004). Thijs *et al.* found that when the AIF was calculated from the MCA in the hemisphere contralateral to the stroke, the PWI lesion volumes were the largest, and they correlated best with final infarct volumes on

follow-up scans (Thijs *et al.*, 2004). Overall, optimal postprocessing methods for calculating absolute CBF values are yet to be determined.

Bolus tracking methods have been used to identify perfusion abnormalities in the brain in a wide variety of clinical applications, including characterization of tumours and acute stroke lesions. DSC techniques are appealing when qualitative or semi-quantitative results are required; DSC-MRI is straightforward to implement, acquisition times are short (40-60 seconds), and it is relatively sensitive to the microvasculature, resulting in good quality maps of CBF, CBV, and MTT. However, the use of exogenous paramagnetic contrast is potentially detrimental because it is expensive, it requires good intravenous access with a large bore catheter (18 gauge), and the concern of toxicity limits the number of injections in each subject. Alternatively, arterial spin labeling (ASL) is completely noninvasive, using blood water as an endogenous tracer for the direct measurement of cerebral blood flow. The noninvasive nature of ASL permits multiple measurements longitudinally or within a single imaging session, therefore ASL is an attractive method for basic science studies and clinical applications. Additionally, values for CBF obtained with ASL have been shown to be highly and linearly correlated with values from $H_2{}^{15}O$ PET (Ye *et al.*, 2000). The remainder of this chapter focuses on the measurement of perfusion using arterial spin labeling as well as the implementation of ASL at the University of Alberta.

1.2.3 Arterial Spin Labeling

1.2.3.1 Generating the Perfusion Signal

Arterial spin labeling is a magnetic resonance imaging technique for measuring perfusion that is completely noninvasive, since it uses an endogenous blood flow tracer. Basically, an MR image can be made sensitive to flow if incoming blood spins are in a different magnetic state than static brain tissue spins. Arterial spin labeling utilizes blood water as a freely diffusible tracer to determine the amount of blood that reaches capillaries and is

available for exchange with tissue. Arterial spins are labeled (inverted) in an artery upstream from the imaging region of interest. As labeled blood flows into the imaging area, there is an exchange of water between the microvasculature and tissue through the blood-brain barrier, yielding a change in tissue magnetization. The amount of signal change (i.e. magnetization change) is determined by blood flow and T_1 relaxation.

Two images are required to detect blood flow: one with upstream spin inversion (the tag image), and one without spin inversion (the control image) (Fig. 1-5). The tag image is subtracted from the control image to generate a perfusion-weighted image, known as an ASL difference signal image (ΔM) (Fig. 1-6). The difference signal in humans is inherently low (approximately 1% of the static tissue signal), resulting in low SNR, therefore lengthy signal averaging of tag-control pairs is required.

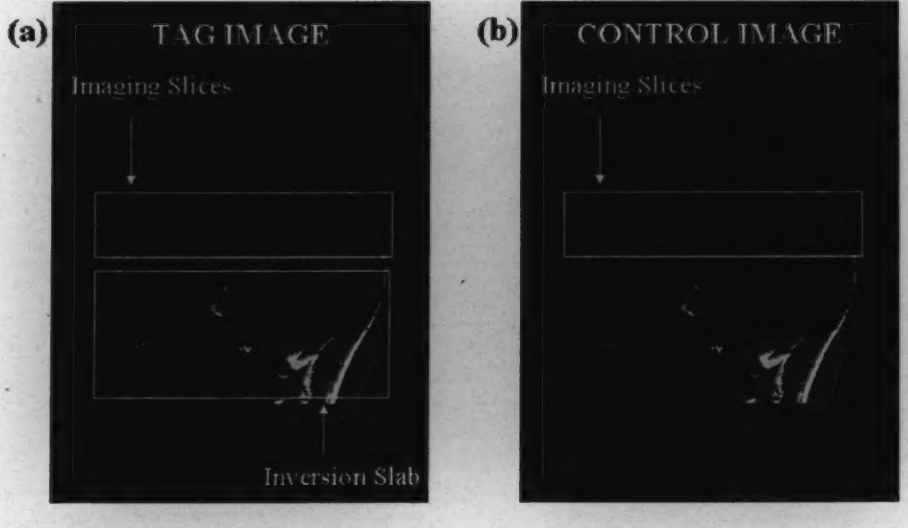

Figure 1-5: Creating the tag and control images

The tag image (a) is created by inverting water spins below the imaging slices. It is necessary that the control image (b) does not produce spin inversion in the same area as the tag image, so that the difference image can be sensitive to blood flow.

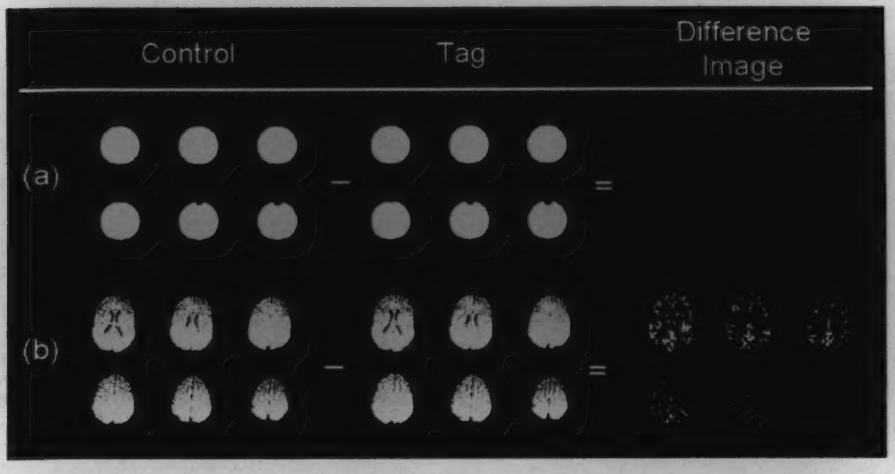

Figure 1-6: Tag and control (raw) images and ASL difference signal images

Control and tag images and subsequent difference images from (a) a water phantom without flow, and (b) a volunteer with normal cerebral blood flow. The sum of many tag-control pairs (50 in the example above) is required to produce perfusion-weighted images with adequate SNR and gray-white matter contrast.

1.2.3.2 CASL and PASL

In the original applications of ASL, arterial blood water was tagged continuously in the neck by flow-driven adiabatic inversion or pseudo-continuous saturation (Detre *et al.*, 1992, Williams *et al.*, 1992, Kwong *et al.*, 1995). This technique, known as continuous arterial spin labeling (CASL), inverts blood water along a plane that is defined by constant RF irradiation and a magnetic field gradient. Although the first CASL techniques were successful in producing qualitative perfusion maps in single slices, magnetization transfer (MT) effects induced from continuous labeling prevented the extension to multi-slice imaging. Either a hardware addition, a separate labeling coil (Zhang *et al.*, 1995), or a pulse sequence modification, amplitude modulation of the RF waveform (Alsop & Detre, 1998), is required to avoid MT effects.

Pulsed arterial spin labeling (PASL) was introduced as an alternative labeling technique that did not induce MT effects. The PASL inversion tag is applied over a large region rather than a plane, and is created from a rapid frequency sweep within the RF pulse. The RF pulse is typically a hyperbolic secant (sech) pulse or C-shaped frequency offset corrected inversion (FOCI) pulse (Ordidge *et al.*, 1996). The FOCI pulse is advantageous because of its high slice profile selectivity, which (a) reduces slice profile interactions and signal from static tissue, and (b) allows the tagging plane to be placed closer to the imaging slices, therefore reducing transit delays and increasing the perfusion signal (Yongbi *et al.*, 1999).

1.3 Pulsed Arterial Spin Labeling

1.3.1 Labeling Schemes

The first PASL sequence introduced was echo-planar imaging and signal targeting with alternating radio-frequency (EPISTAR) (Edelman *et al.*, 1994). The EPISTAR tag pulse inverts spins in a slab proximal to the imaging slice, and the control pulse inverts a slab distal to the imaging slice (Fig. 1-7). The purpose of inversion in the tag image is to generate an upstream bolus of tagged blood that flows into the imaging slices and alters tissue magnetization, whereas the inversion pulse is applied distal to the image slices in the control application in order to balance MT effects. In the next PASL sequence, flow-sensitive alternating inversion recovery (FAIR), the tag is created with an unselective inversion pulse that inverts all spins within the RF range of the coil, and the control is a slice selective inversion applied to the imaging slice (Kwong *et al.*, 1995, Kim, 1995, Schwarzbauer *et al.*, 1996). The third tagging scheme is a derivative of EPISTAR, called proximal inversion with a control for off-resonance effects (PICORE). PICORE uses the same tag as EPISTAR, but the control is an off-resonance inversion pulse applied at the same frequency as the tag in the absence of slab selective gradients (Wong *et al.*, 1997).

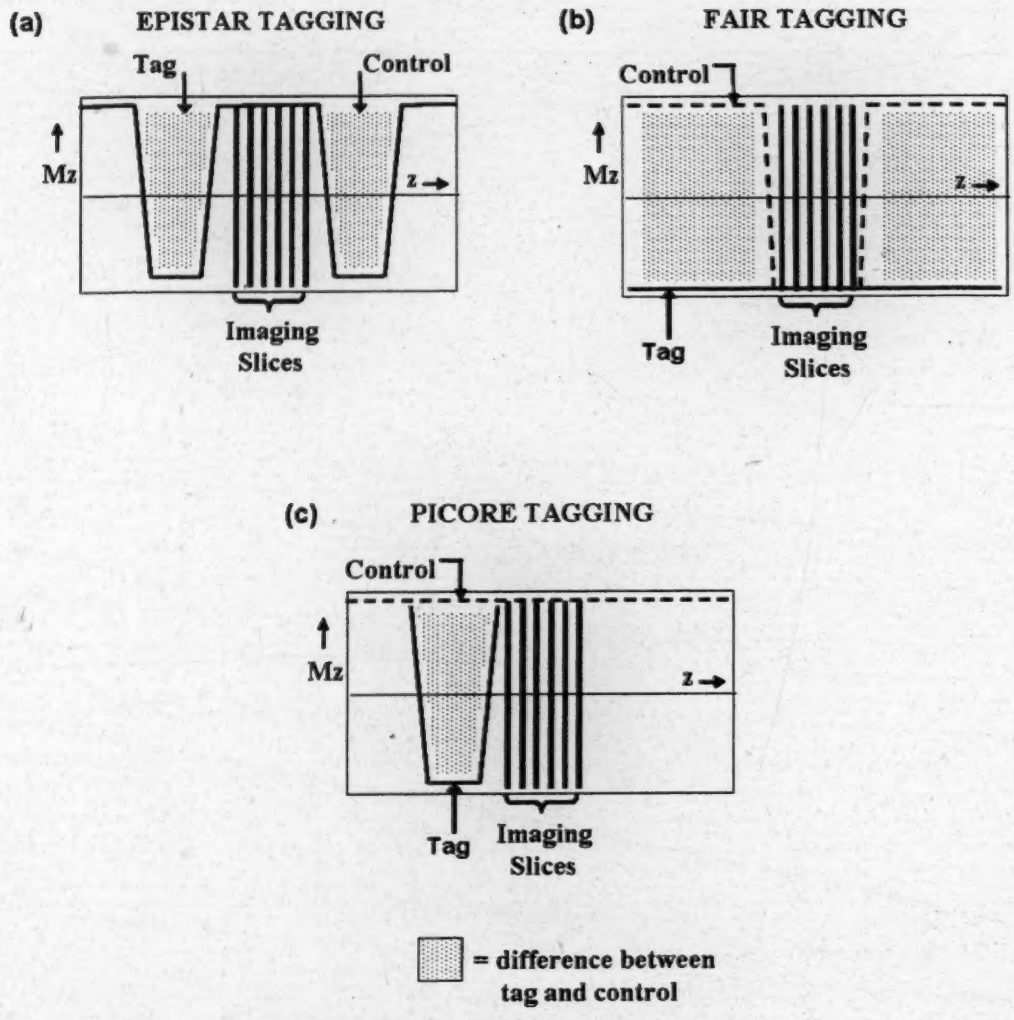

Figure 1-7: EPISTAR, FAIR, and PICORE tagging profiles

In the tag image of EPISTAR, FAIR, and PICORE the inversion pulse is applied, at least in part, to an area proximal to the imaging slices, generating a bolus of labeled blood (shaded regions). Inversion in the control image has no effect on incoming blood spins. The magnetic state of tissue spins in the image slices is always the same in tag and control images, whereas blood spins in the region proximal to the slices are always in a different magnetic state. Adapted from (Wong *et al.*, 1997).

EPISTAR, FAIR, and PICORE are the prototype PASL tagging schemes most frequently used in ASL research. In all three techniques the inversion pulse in the tag image generates a labeled bolus proximal to the imaging slices, yet the control image inversion pulse has a variety of effects on tissue depending on the scheme used. In general, it is essential in all PASL techniques that proximal blood spins in the control image are not affected by the inversion pulse, and that tissue in the imaging slices is left in the same magnetic state as the tag image. Therefore, subtraction of the tag image from the control image removes the signal from static tissue and generates a perfusion-weighted image.

1.3.2 The General Kinetic Model for CBF Quantification

Arterial spin labeling has always been considered a promising technique for blood flow quantification. The initial kinetic models for CBF quantification, which assumed single-compartment kinetics for water clearance and instantaneous exchange of water between blood and tissue, were specific to the applied tagging scheme (Detre *et al.*, 1992, Williams *et al.*, 1992). A more general model was proposed by Buxton *et al.* that describes the ASL difference signal (ΔM) at time t after application of the inversion pulse as (Buxton *et al.*, 1998),

$$\Delta M(t) = 0 \qquad 0 < t < \Delta t \qquad [1.3]$$

$$\Delta M(t) = 2M_{ob} f (t - \Delta t)\alpha \exp(-t/T_{1b}) q(T_{1b}, T_{1t}, T_{ex}, f, \lambda, TI) \qquad \Delta t < t < \Delta t + \tau \qquad [1.4]$$

$$\Delta M(t) = 2M_{ob} f \tau \alpha \exp(-t/T_{1b}) q(T_{1b}, T_{1t}, T_{ex}, f, \lambda, TI) \qquad \Delta t + \tau < t \qquad [1.5]$$

where M_{ob} is the T_2*-weighted equilibrium signal of blood, α is the fraction of the desired difference in magnetization generated by the tag and control pulses (between 0 and 1), and f is the cerebral blood flow in s^{-1}. Basically, the general kinetic model indicates that the ASL perfusion-weighted signal (control – tag) first appears in the imaging slice after a delay, Δt, the time it takes for blood to travel from the tagging plane to the slice, increases for a time τ, equal to the time width of the labeled bolus, and decays after this time according to the relaxation time of blood. The remaining term, q(t), describes the

effects of the capillary/tissue exchange, incomplete water extraction, and venous outflow. q(t) is a function of the longitudinal relaxation times of blood and tissue, T_{1b} and T_{1t}, the time of exchange of tagged water spins between blood and tissue, T_{ex}, the blood-brain partition coefficient of water, λ, the inversion time, TI, and blood flow.

The general kinetic model can be used to quantify cerebral blood flow (f). In Eq. 1.4, ΔM is the signal intensity that is measured directly from the ASL difference image that results from the subtraction of tag and control images. The inversion pulse in PASL imaging frequently produces complete inversion and α is normally given a value of 1. T_{1b} can either be measured in a separate experiment or assumed from literature results, and M_{ob} is calculated per individual using measurements taken from two separate MRI scans. In PASL imaging, q(t) has been determined to be between 0.85 and 1.0 depending on the timing parameters of the ASL sequence. Overall, cerebral blood flow can be calculated from Eqs. 1.3 through 1.5 after measuring ΔM and M_{ob}, and assuming values for T_{1b}, α, and q(t). A more detailed description of CBF quantification can be found in the Materials and Methods sections of Chapters 2 and 3.

The subtraction of two images (control – tag) at one delay time (TI) generates a qualitative map of perfusion that contains information about transit time and CBF. In order to generate a quantitative CBF image, data is required from a minimum of two delays so that any change in signal due to the variability in transit times can be measured. The transit time variation affects (1) the amount of blood delivered to the slice at the time of image acquisition, and (2) the amount of T_1 decay of the tag across the imaging slice (Alsop & Detre, 1996, Wong *et al.*, 1997). Because the delay time (TI) between inversion and image acquisition is on the order of T_{1b}, the 'transit time effect' can significantly alter the measured perfusion value. In general, it is possible to quantify CBF using the traditional PASL sequences and application of the general kinetic model. However, this is a time consuming process because the ASL signal must be measured at a minimum of two inversion times in order to eliminate/reduce transit time effects. Alternatively, a newer form of PASL imaging has been introduced by Wong *et al.* that is

relatively insensitive to the variability in transit times, and perfusion can be quantified using only one inversion time (Wong *et al.*, 1998b). The remainder of Chapter 1 outlines the pulse sequence design and CBF quantification model(s) of the 'transit time insensitive sequences', QUIPSS and Q2TIPS. These sequences were implemented at the University of Alberta for ASL research.

1.3.3 Transit Time Insensitive Sequences

1.3.3.1 QUIPSS II

There are several pulse sequence modifications that can be added to the prototype PASL tagging schemes. Quantitative imaging of perfusion using a single subtraction (QUIPSS II) is a modular feature that can be added to PICORE, FAIR, or EPISTAR, rendering them transit time insensitive (Wong *et al.*, 1998b). In QUIPSS II, a saturation pulse is applied to the tagging region at a time TI_1 after the tagging pulse (Fig. 1-8).

The saturation pulse clips the tail end of the tagged bolus, defining the time width of the tag. A delay time, Δt, is inserted following the saturation pulse, and images are acquired at TI_2. The delay allows time for tagged spins to move from the intravascular space into tissue, reducing intravascular signal (Fig. 1-9). QUIPSS II produces more accurate CBF values because it minimizes two major systematic errors: spatially varying transit delays, and contamination of tissue signal by intravascular tagged blood destined for more distal slices (Calamante *et al.*, 1999). As well, QUIPSS II is more time efficient than traditional sequences since it allows for CBF quantification in a single subtraction at one inversion time (TI_2). This is apparent in the simplification of the general kinetic model for QUIPSS quantification. The QUIPSS signal is no longer dependent on the timing parameters Δt and τ, but rather on the time width of the tag (TI_1), and Eqs. 1.3 through 1.5 can be written as (Wong *et al.*, 1998b),

$$\Delta M(TI_2) = 2M_{ob} f TI_1 \alpha \exp(-TI_2 / T_{1b}) q(T_{1b}, T_{1t}, T_{ex}, f, \lambda, TI_2) \qquad [1.6]$$

$$\text{if} \quad TI_1 < \tau \quad \text{and} \quad TI_2 > TI_1 + \Delta t$$

As long as the saturation pulse (at TI_1) is applied before all of the tagged blood has left the tagging region ($TI_1 < \tau$), and the image is acquired (at TI_2) after the entire bolus has been allowed to perfuse the imaging slice ($TI_2 > TI_1+\Delta t$), CBF can be quantified using Eq. 1.6. The ASL difference signal (ΔM) is measured at one inversion time (TI_2), TI_1 is the time of saturation, T_{1b} is assumed from literature values, M_{ob} is calculated using two alternate MR sequences, and q(t) is either measured or assumed to be 1. Therefore, cerebral blood flow (f) can be calculated on a pixel-by-pixel basis to generate an absolute CBF image.

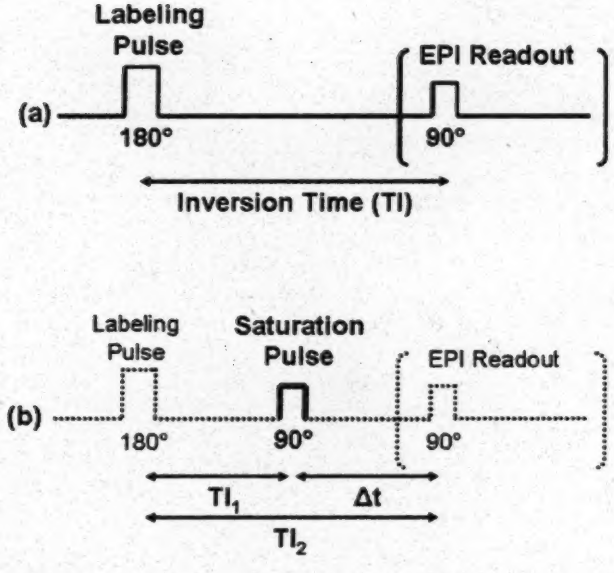

Figure 1-8: QUIPSS II modification of a traditional PASL sequence

The prototype PASL sequences (a) can be modified with the QUIPSS II saturation pulse (b). TI_1 is the time between inversion and saturation, and TI_2 is the time between inversion and imaging; $TI_2 - TI_1 = \Delta t$.

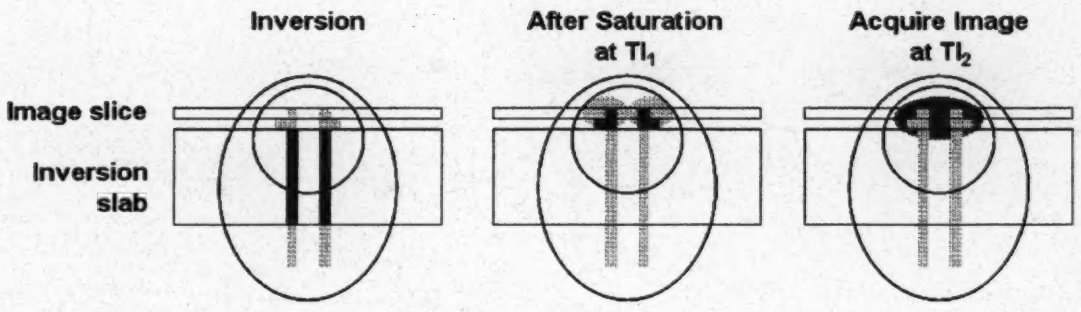

Figure 1-9: Movement of tagged water during the inversion time in QUIPSS II

Application of the inversion pulse (large rectangle) creates a wide slab of tagged blood that perfuses tissue (dark black area represents tagged blood in vessels). Saturation at TI_1 eliminates tagged blood remaining in the inversion slice. The additional delay before imaging, Δt, allows time for intravascular tag to perfuse the slice before image acquisition at TI_2. Adapted from (Wong *et al.*, 1998b).

1.3.3.2 Q2TIPS

The QUIPSS II pulse sequence has been modified to remove residual errors caused by incomplete saturation of the tagging region and spatial mismatch of the inversion and saturation slice profiles, both of which can lead to perfusion overestimation. In QUIPSS II with thin-slice TI_1 periodic saturation (Q2TIPS), the 15-lobe sinc saturation pulse in QUIPSS II is replaced by a periodic train of thin-slice sinc saturation pulses (Fig. 1-10) (Luh *et al.*, 1999). The slice profile of a sinc-shaped pulse is easily altered with B_1 inhomogeneity. The saturation pulses in Q2TIPS produce slice profiles on the distal end of the tagging region that closely match the sharply defined slice profile of the sech (or FOCI) inversion pulse.

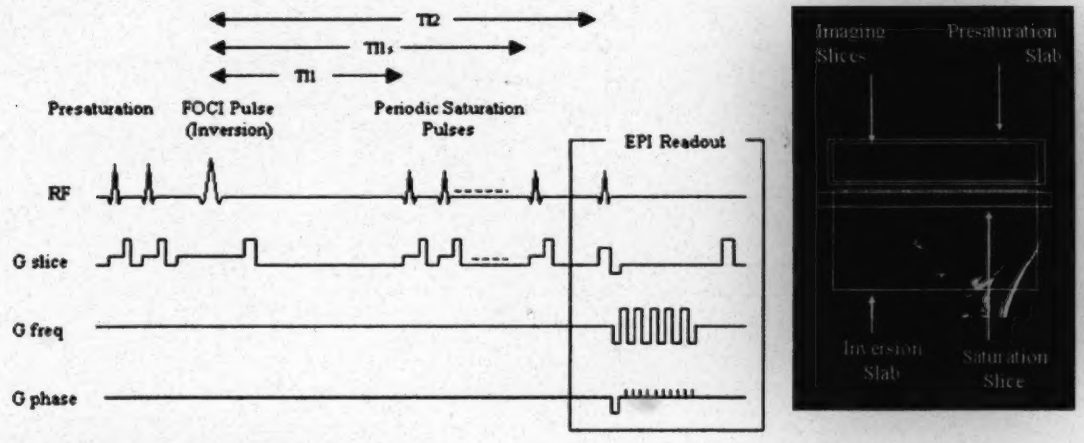

Figure 1-10: Q2TIPS pulse sequence

Periodic saturation pulses are applied to the tagging region from TI_1 to TI_{1s} (TI_1 stop time). Each 90° pulse is followed by a crusher gradient. A delay, Δt, is inserted between the first saturation pulse and the EPI readout; $\Delta t = TI_2 - TI_1$. The saturation pulse defines the time width of the tagged bolus, τ. A presaturation pulse is applied to the imaging slices prior to inversion to reduce signal from static tissue. Adapted from (Luh *et al.*, 1999).

The difference signal, ΔM, in Q2TIPS imaging is independent of both Δt and τ. Therefore, the general kinetic model can be simplified for Q2TIPS by replacing Δt and τ with the time duration of the tagged bolus, TI_1 (Wong *et al.*, 1998b). Because of its transit time insensitivity, Q2TIPS is more amenable to multi-slice imaging than traditional PASL techniques such as FAIR. A more detailed explanation of Q2TIPS CBF quantification, including equations and timing parameters, can be found in the Materials and Methods section of Chapters 2 and 3.

1.4 Implementation of PASL Imaging

Prior to construction of the NMR Research Facility, we developed a FAIR sequence with a QUIPSS-like extension on the 3T MRI scanner. Even though we were successful in producing multi-slice ASL images from normal volunteers, the technique was hindered by: shimming difficulties, which lead to distortions and image shifting in the y-direction between slices, a slower gradient hardware system, and inaccessibility of the scanner to clinical patients. We ultimately wanted to apply ASL to stroke patients, therefore we pursued research on the 1.5T scanner. We were able to continue working with a QUIPSS sequence, specifically Q2TIPS with PICORE tagging, through collaboration with Siemens. In this section I discuss some of our relevant PASL research not mentioned in Chapters 2 and 3, which are essentially journal articles; Chapter 2 has been submitted for review and Chapter 3 has been accepted by JMRI.

To begin with, we implemented a PICORE-Q2TIPS pulse sequence (Siemens, Works in Progress) on the 1.5T scanner, and with preliminary adjustments we were able to generate difference signal (ΔM) images from normal volunteers (Fig. 1-11). We wrote several programs in Matlab (The MathWorks, Inc., Natick, MA) to enable the manual selection of individual difference images to the final perfusion-weighted image in order to avoid motion artifacts and any remaining static tissue signal. Subsequent programs were written for calculation of CBF and transit time.

In optimizing the Q2TIPS pulse sequence, we attempted to (a) select parameters within the limits of the QUIPSS quantification model, and (b) maximize ΔM SNR of individual tag-control pairs so we could decrease the number of averages. In our research, typical ΔM SNR values in whole slice, GM, and WM were 4.4 ± 0.4, 5.6 ± 0.7, and 1.8 ± 0.5, respectively, which are comparable to literature results using Q2TIPS with 2D-EPI readout (Gunther *et al.*, 2005). It is important to note that the difference signal (ΔM) is proportional to cerebral blood flow (see Eq. 1.6), therefore areas with higher signal intensity in ASL difference images, such as the cerebral cortex, have higher perfusion.

Figure 1-11: Q2TIPS difference signal images

PASL-Q2TIPS difference images (a) and corresponding anatomical inversion recovery EPI (IR-EPI) images (b) from a healthy volunteer (22-years-old). The IR-EPI images were used to differentiate gray matter from white matter in the perfusion images. As expected, gray matter displays the highest signal intensity, therefore the highest perfusion. The six slice Q2TIPS data set was acquired with TI_1 = 600 ms, TI_2 = 1200 ms, 5 mm slice thickness, 1.5 mm gap, 1396 Hz/Px, 4:25 min acquisition time, and 63 averages.

1.4.1 TR Optimization

Minimizing PASL sequence repetition time (TR) is important for improving SNR per unit time. However, it is essential to allow enough time between saturation and the next inversion (TR – TI_2) for the entire tag region to be refilled with fully relaxed blood. Using PICORE-QUIPSS II with a 10 cm tag and a 1 cm gap between the inversion slab and imaging slices, Wong *et al.* determined that there is no significant difference in the ASL signal when TR is between 2000 and 3000 ms (Wong *et al.*, 1997). Our research showed that lowering TR from 2800 to 2300 ms did not significantly change ΔM SNR (TI_2 = 1500 ms), yet scan time was reduced by almost 2.5 min. In our first study, where PASL parameters were optimized for an elderly population, we used longer inversion times (TI_2 = 1800 and 2100 ms), therefore it was necessary to increase TR to 2500 ms in

order to refresh the tagging region with fully relaxed spins. In the end, we kept TR = 2500 ms for the remainder of our studies so that comparisons between studies could be made.

1.4.2 TI_1 Optimization

According to the QUIPSS quantification model (Eq. 1.6), the perfusion-weighted signal intensity exhibits a linear dependence on the time of saturation (TI_1): ΔM is 0 when $TI_1 = 0$, increases in proportion to TI_1 at low values, and is constant when $TI_1 > \tau$. Given that the saturation pulse clips the tail end of the tagged bolus, the time of saturation defines the size of the tag as long as the natural time width of the tag produced by the inversion pulse (τ) has not been exceeded. The natural time width can be estimated from a graph of ΔM versus TI_1 as the point at which the linear dependence of ΔM levels off as TI_1 increases. This is the maximum allowable value for TI_1 that satisfies the QUIPSS quantification model.

We measured the GM signal at four values of TI_1 (500, 600, 700, and 800 ms) in three volunteers (age range 24-32 years) using PICORE-Q2TIPS (6 slices, 10 cm tagging plane, TI_2 = 1500 ms) (Fig. 1-12). As expected, gray matter ΔM SNR increases linearly with TI_1 at lower values. Figure 1-12 suggests that most of the tag passes through the distal edge of the tagging region by approximately 800 ms, therefore an optimal value for TI_1 is around 800 ms. This is a relatively common value used for research with PICORE-Q2TIPS (Wong *et al.*, 1998b, Wang *et al.*, 2002, Wang *et al.*, 2003).

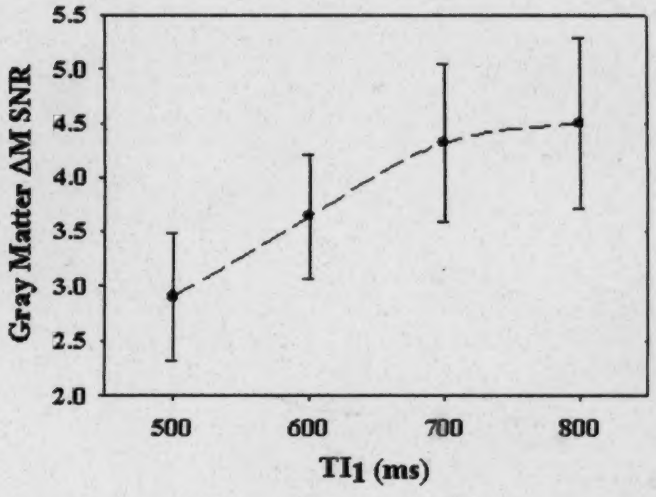

Figure 1-12: TI_1 optimization

Gray matter SNR is calculated from the average signal across six slices in three volunteers. The time width of the tag (τ) appears to be approximately 700-800 ms, the time when GM ΔM SNR levels off. Luh *et al.* show similar results for multi-slice Q2TIPS (Luh *et al.*, 1999).

1.4.3 Reproducibility of ASL Perfusion Values

The noninvasive nature of arterial spin labeling makes it particularly appealing for repeat studies of perfusion, although it will be important to determine the precision of ASL perfusion values (in terms of intra- and intersubject variability) before meaningful conclusions can be drawn from serial measurements. Few studies have assessed the reliability and reproducibility of CBF values in humans measured by ASL. In a FAIR study, the reproducibility of quantitative CBF measurements was found to be satisfactory from day to day, although the authors express concern in drawing conclusions from long term studies (Yen *et al.*, 2002). CASL was used to assess the stability and reproducibility

of perfusion in 34 subjects; CBF was remarkably stable and reproducible in the short term, however intersubject variability was high, up to 100% (Parkes *et al.*, 2004). The authors concluded that intersubject biological variability had a much larger affect on CBF than instrumental error. Finally, the main result of a recent Q2TIPS study was that random noise made the greatest contribution to fluctuation in ASL signal, rather than intrasubject variability; therefore low SNR is the primary limiting factor in the reliability of perfusion measurements (Jahng *et al.*, 2005). At our site, we were concerned with the reliability of ΔM SNR and CBF values measured using PICORE-Q2TIPS, in particular the stability of ΔM SNR over a range of inversion times. This was important to supplement our work concerning PASL imaging in the elderly (Chapter 3), therefore we conducted a small study with repeat measurements of ΔM SNR and CBF values at increasing inversion times.

1.4.3.1 Q2TIPS stability

Three healthy volunteers (24-32 years) were scanned using PICORE-Q2TIPS; sequence parameters and data processing are described in Chapter 3. Four Q2TIPS scans (TI_2 = 900, 1200, 1500, and 1800 ms) were performed on each volunteer per imaging session. Volunteers underwent four imaging sessions on four consecutive days at the same time each day. Stability was determined by monitoring changes in difference image SNR and CBF with time.

The variation in ΔM SNR with increasing TI_2 is consistent over four days in volunteers 1 and 2 (Fig. 1-13a and 1-13b), and over three days in volunteer 3 (Fig. 1-12c), which suggests a relatively low intrasubject variability in the general pattern. Not only is the SNR trend consistent over four days, there is also a small range in SNR values at each TI_2.

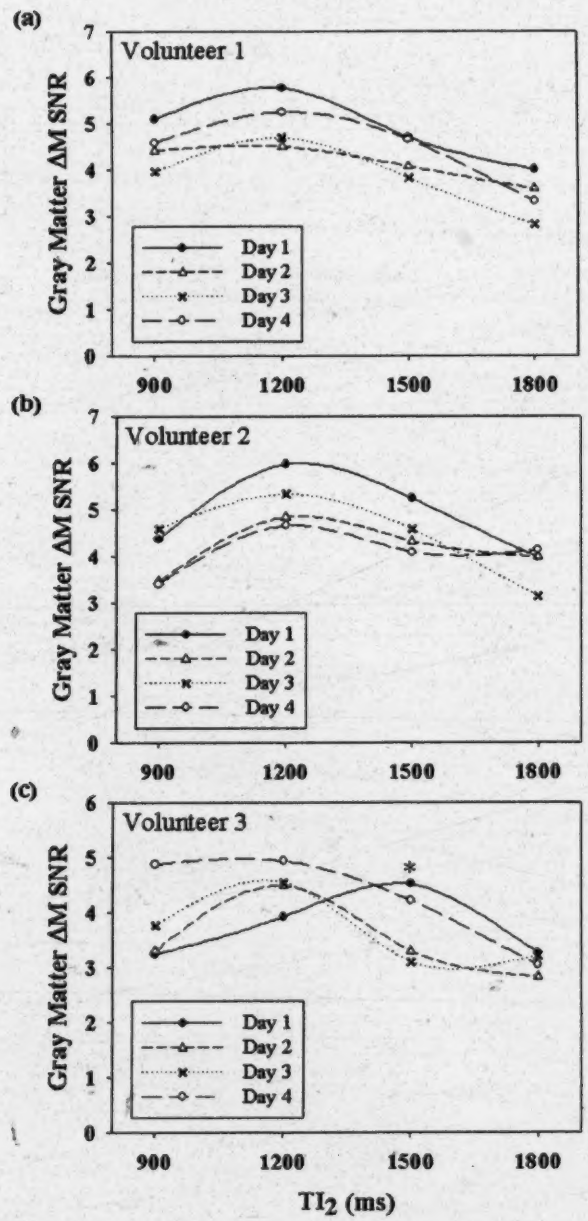

Figure 1-13: Stability of gray matter ΔM SNR with TI_2

The variation in ΔM SNR with TI_2 shows a consistent trend in volunteer 1 (a) and volunteer 2 (b), and a deviation from the general pattern on one day for volunteer 3 (c) (denoted with *). The intrasubject variability in absolute GM SNR with TI_2 also appears to be low, as indicated by the small range in ΔM SNR at each TI_2.

Average cerebral blood flow (6 slices) for each subject over the course of four days is displayed in Fig. 1-14. CBF range and average (mL/100mL/min) for volunteers 1, 2, and 3 are 58-64 (60 ± 3), 48-58 (52 ± 5), and 40-50 (45 ± 5), respectively. The gray matter standard deviation of CBF over the three volunteers is approximately 9%. It is difficult to compare CBF values from different techniques because of partial volume and segmentation effects. However, an interesting comparison can be made between the standard deviation of perfusion measurements, which is a good indicator of intrasubject variability (Parkes *et al.*, 2004). The average gray matter standard deviation in our study is similar to that found in other non-MRI and MRI perfusion studies (Pantano *et al.*, 1984, Herscovitch *et al.*, 1987, Leenders *et al.*, 1990, Schreiber *et al.*, 1998, Parkes *et al.*, 2004). The spread of gray matter perfusion values is higher than that found in white matter and whole brain, and is likely due to changes in metabolism and awareness (Parkes *et al.*, 2004).

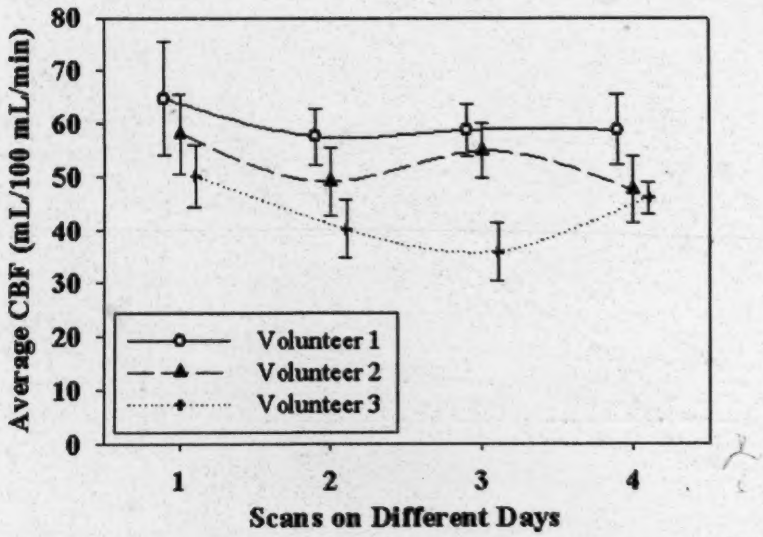

Figure 1-14: Stability of gray matter CBF with PICORE-Q2TIPS

Gray matter CBF (TI_2 = 1500 ms) was measured over four days in three volunteers. CBF values measured with PICORE-Q2TIPS appear to have low intrasubject variability considering the potential for large perfusion fluctuations within the brain. Q2TIPS shows promise as a technique for intersubject comparisons of CBF; across four days, CBF in volunteer 1 > CBF in volunteer 2 > CBF in volunteer 3.

A greater understanding of the causes of perfusion variation, such as caffeine intake, hydration, and physiological factors, would be helpful in reducing the number of variables in perfusion experiments, possible leading to more stable results. Given that an individual's cerebral perfusion can fluctuate considerably (up to 40%), our results demonstrate relatively stable ΔM SNR and CBF with time (Yen *et al.*, 2002).

1.4.4 CBF Quantification

1.4.4.1 Theory: Single-Compartment Model

There are two main approaches to single-compartment modeling that are used to describe the ASL signal. The first approach is based on the Bloch equations which are modified to include flow (Detre *et al.*, 1992). This model describes a well mixed compartment at equilibrium, analogous to the $H_2{}^{15}O$ PET tracer kinetic model, and assumes that (a) labeled blood water exchanges instantaneously and completely into tissue and (b) signal loss occurs with T_{1t}, the tissue longitudinal relaxation time.

Unlike PET imaging, the time scale of an ASL experiment is short (approximately 1 s), and labeled water spends a large percentage of this time in blood, not tissue. Therefore, assuming that the ASL signal is dependent only on local properties, such as M_{0t} (the T_2*-weighted equilibrium magnetization of tissue), λ (blood-brain partition coefficient), and T_{1t}, is incorrect. This model has been shown to give significant errors; approximately 20% and 60% overestimation in gray matter and white matter respectively (Parkes & Tofts, 2002); however, in recent years it has been extended to a two-compartment model that more accurately describes the loss of the tag throughout the experiment (Zhou *et al.*, 2001, Parkes & Tofts, 2002).

The second approach to single-compartment modeling assumes that tagged water remains intravascular throughout the measurement period (i.e. $q(t) = 1$ in the general kinetic model) (Buxton *et al.*, 1998). Solutions to this model are simple; only the global properties of blood, M_{0b} and T_{1b}, are required for quantification. Initially we thought it might be more accurate to (a) relax the assumption in this model, and calculate a value for $q(t)$ based on T_{1b}, T_{1t}, T_{ex}, f, λ, and TI_2, or (b) apply a two-compartment model. However, a recent report suggests that assuming tagged water remains intravascular throughout the measurement period may be reasonable for PASL studies with short measurement times (<2 s). Using this model, errors in CBF were found to be <10% and 20% in gray and white matter, respectively (Parkes, 2005).

1.4.4.2 Q2TIPS Quantification

We used the QUIPSS quantification model to calculate CBF in all studies (Wong *et al.*, 1998b). Prior to quantification, ASL data was imported to Matlab (The MathWorks, Inc., Natick, MA) and processed to yield ASL difference images. Absolute CBF values for GM, WM, and whole slice were determined after regional signal intensity in the difference images was measured in MRVision (MRVision Co., Winchester, MA) and converted to CBF values in Microsoft Excel (Microsoft Co., Seattle, DC). Alternately, quantitative CBF maps could be created in Matlab (The MathWorks, Inc., Natick, MA) (Fig. 1-15). Further details concerning pulse sequence parameters and quantification methods used in our studies can be found in the Materials and Methods sections of Chapters 2 and 3.

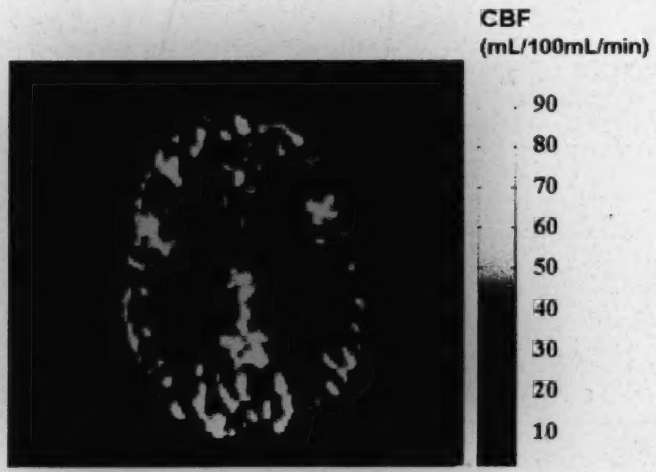

Figure 1-15: Quantitative CBF map

A signal intensity scale corresponding to specific CBF values (mL/100mL/min) is shown to the right of the image. Data was acquired from a normal volunteer using a PICORE-Q2TIPS sequence with TI_1 = 600 ms, TI_2 = 1200 ms, 5 mm slice thickness, 1.5 mm gap, 1396 Hz/Px, 4:25 min acquisition time, and 63 averages.

1.5 Scope of Thesis

The search for a technique to accurately quantify cerebral blood flow has been ongoing ever since the discovery of the cerebral circulation, especially from the time that regional perfusion was coupled to nerve activation and energy metabolism. Although PET imaging was established as the 'gold-standard' for CBF measurement in the 1980's, MRI has been able to advance CBF research by providing a safe, noninvasive, and widely available technique to measure perfusion, with higher SNR and spatial resolution, and shorter scan times than PET.

The two MRI techniques used to assess cerebral blood flow are dynamic susceptibility contrast MRI and arterial spin labeling. Both techniques have been successfully applied in a variety of volunteer and patient studies, although DSC is the technique more frequently used in cerebrovascular disease. DSC has some advantages over ASL in data acquisition; shorter scan times, higher SNR, and superior brain coverage. However, bolus tracking is hindered by computationally intensive postprocessing, and patient exposure to exogenous contrast agent. Alternatively, arterial spin labeling is completely noninvasive, using blood water as an endogenous tracer to track flow. Unlike DSC which measures blood volume, ASL directly measures blood flow, enabling the quantification of CBF without calibration to an independent technique. Postprocessing of ASL images to generate a relative perfusion map entails only image subtraction (control – tag) and averaging, although production of a quantitative CBF map is considerably more difficult. Accurate perfusion quantification requires the use of a model with appropriate assumptions, and acquisition of additional images for calculation of the global properties of blood. Nonetheless, the relative ease of postprocessing extends the practical use of ASL imaging in the acute clinical setting.

Even though ASL has been shown to provide accurate CBF measurements in normal brain tissue, there are many areas for improvement of this technique; pulse sequence optimization, methodological advancements, and technical developments to name a few.

For example, in our preliminary research we noticed signal loss in slices farthest from the tagging plane that could not be accounted for by blood T_1 decay alone, and this prompted research comparing single slice to multi-slice acquisition techniques. This methodological study is presented in Chapter 2. ASL has also been successful in assessing perfusion in various pathologies, such as acute and chronic cerebrovascular disease, epilepsy, Alzheimer's disease, and brain tumors. Specifically, our goal has been to use ASL in acute stroke, and since stroke occurs primarily in the elderly we decided to optimize the Q2TIPS sequence in an elderly population. The results of this study are presented in Chapter 3. It is well known that ASL suffers from low SNR, which limits image resolution and brain coverage. In the final chapter we discuss high field ASL imaging which provides increased perfusion signal and improved image quality. Preliminary results from our work at 3T are also mentioned. Finally, we suggest potential future directions for PASL work at our site, and discuss current state-of-the-art ASL technology.

CHAPTER 2: Comparison of Multi-slice and Single Slice Acquisitions for Pulsed Arterial Spin Labeling Measurements of Cerebral Perfusion

---

A version of this chapter has been submitted for publication

Alison Campbell, Christian Beaulieu (2005) (Submitted)

2.1 Introduction

Arterial spin labeling (ASL) is a noninvasive imaging technique proven to yield accurate measurement of cerebral blood flow in cortical gray matter (Ye *et al.*, 2000). Arterial spins are labeled by changing their state of magnetization in an artery upstream from the site of interest. As these spins flow through the tissue vasculature, water exchange occurs between the labeled blood and tissue. This causes a measurable change in both the apparent tissue T_1 and the tissue magnetization; either change can be measured and used to quantify blood flow. Essentially, perfusion is determined by acquiring one image with spin tagging and one without. The subtraction of these two images results in a difference signal image (ΔM) that is directly proportional to blood flow.

In the early nineties it was shown that either pseudo-continuous saturation or flow driven adiabatic inversion could be used to tag blood water spins in the neck and measure perfusion in a single slice within the brain (Detre *et al.*, 1992, Williams *et al.*, 1992, Kwong *et al.*, 1992). Since the first attempts using continuous arterial spin labeling (CASL), many different arterial labeling schemes have been proposed, such as the pulsed arterial spin labeling (PASL) technique called EPISTAR, whereby a single radio-frequency (RF) pulse is used to label a thick slab close to the imaging slice of interest (Edelman *et al.*, 1994). A 180° inversion pulse is used to apply the upstream tag, and after a delay time to allow the tagged blood to perfuse into the tissue, an image is acquired within the brain. As with CASL, the resultant ΔM image reflects the difference in magnetization of the blood between images acquired with and without the application of a tag pulse. Other PASL variants, such as FAIR (Kwong *et al.*, 1995, Kim, 1995, Schwarzbauer *et al.*, 1996), PICORE (Wong *et al.*, 1997), and Q2TIPS (Wong *et al.*, 1998b) have also been successfully applied. Although the inherent signal-to-noise ratio (SNR) is higher in CASL, PASL has a higher inversion efficiency (close to 1) and lower natural transit delay, making the SNR efficiency between the two techniques similar (Wong *et al.*, 1998a).

With both CASL and PASL the goal is to produce a tag and control image where the signal from static tissue in both images is identical. This is easy to accomplish with single slice techniques, however it is an increasingly complicated task when a multi-slice data set is required for greater brain coverage. A multi-slice acquisition involves applying a single magnetization preparation pulse of the arterial blood tag followed by the sequential acquisition of multiple slices downstream. The major complication in CASL multi-slice imaging is magnetization transfer (MT) effects. It is necessary that the tag image receive the same MT effects as the control image, and this case can only occur if a single slice is acquired. The most effective solution to this problem is to employ a two-coil CASL system (Zhang *et al.*, 1995), however this requires specialized hardware. For PASL, multi-slice acquisitions are difficult because of variable transit delays both within and between slices, and static tissue subtraction errors consistent with slice profile effects of the tag and control pulses (Buxton *et al.*, 1998). Because of these problems with multi-slice acquisitions, single slice CASL and PASL techniques are ideal. However, cerebral perfusion results are often desired at multiple slice locations. To avoid this problem, one could acquire multiple single slice images, however this is time consuming given that lengthy signal averaging is necessary to create perfusion maps with adequate SNR. Therefore, when time constraints are present, which is usually the case, multi-slice ASL acquisitions are necessary for greater brain coverage.

It is well known that SNR in multi-slice scans decreases in more distal slices due to longer inversion times and greater T_1 decay of blood (Luh *et al.*, 1999). However, we have observed signal loss in distal slices which is greater than the loss expected with blood T_1 decay. Several reasons have been proposed for this effect including: the destruction of tagged blood destined for more distal slices by the acquisition of proximal slices (Wong *et al.*, 1997, Wong *et al.*, 1998b), inversion profile imperfection (Wong *et al.*, 1997), and the uncertainty of transit time (Gunther *et al.*, 2005). The purpose of the present study is to determine the cause of the additional signal loss in distal slices, beyond that resulting from blood T_1 decay, by comparing perfusion maps from various single slice acquisitions to those derived from multi-slice acquisitions in healthy

volunteers. This study looks specifically at a Q2TIPS pulse sequence with PICORE tagging and highlights several potential ASL protocol improvements for the study of disease.

2.2 Materials and Methods

2.2.1 MR Imaging

Images were obtained from a group of 17 healthy volunteers (12 males, 5 females, age range 23-34 years), all of whom gave written and informed consent. Three separate studies were conducted for this report, and each volunteer participated in one or more of the studies. Four volunteers participated in all three studies. There were 8 volunteers in study 1, 12 volunteers in study 2, and 9 volunteers in study 3. MR scanning was performed on a 1.5 Tesla Sonata scanner (Siemens Medical Systems, Erlangen, Germany) equipped with gradient coils capable of 40 mT/m amplitude and 200 T/m/s slew rate. Q2TIPS with PICORE tagging (Siemens, Works in Progress) was utilized for all arterial spin labeling perfusion imaging (Luh *et al.*, 1999). PICORE tagging involved slab selective inversion interleaved with no inversion in order to create tag and control images. Gradient-echo (GE) echo-planar imaging (EPI) was used to acquire all slices after application of the labeling pulse.

One multi-slice ASL scan and six single slice ASL scans were acquired in each study. The multi-slice scan consisted of six contiguous 8 mm slices acquired inferior to superior with an interslice delay time of 54 ms. The gap between the inversion band and first imaging slice was set at 20 mm to ensure minimal interaction of slice profiles (Fig. 2-1A). The time of the first saturation pulse (TI_1) was fixed at 800 ms, and the total inversion time (TI_2) for the first slice was 1500 ms. This value of TI_2 was chosen as a result of previous experiments which indicated that $TI_2 = 1500$ ms is optimal for this age range of volunteers (23-34 years) in order to maximize tissue signal and minimize intravascular signal. Other multi-slice Q2TIPS acquisition parameters included: FOV 22

x 22 cm, 64 x 64 matrix, echo time (TE) 15 ms, repetition time (TR) 2500 ms, slice repetition time (TR_{slice}) 54 ms, 3:52 min scan time, 50 tag-control pairs, and bandwidth 3004 Hz/pixel. The six slice locations in both the multi-slice and single slice acquisitions were exactly aligned. In the single slice data sets, slice thickness, TI_1, FOV, matrix, TE, TR, scan time, number of tag-control pairs, and BW were the same as the multi-slice data set. The major differences between single slice and multi-slice acquisition parameters include the width of the gap between the inversion band and imaging slice, and TI_2 of each slice. Basically, the location of each slice was static; however the position of the 10 cm inversion band and the timing of image acquisition (TI_2) were varied between studies.

In study 1, the placement of the inversion band was fixed with respect to the volunteer. Therefore, the gap between the inversion band and the first imaging slice was 20 mm, and this gap increased with increasing slice number (Fig. 2-1B). The distance between the inversion band and the imaging slices were: 20 mm, 28 mm, 36 mm, 44 mm, 52 mm and 60 mm for slices 1 through 6 respectively. The time of image acquisition (TI_2) was fixed at 1500 ms for every slice, regardless of the distance between the inversion band and the slice. In study 2, the inversion band location was fixed and the distances between the inversion band and the imaging slices were the same as study 1 (Fig. 2-1B). As superior slices were imaged, TI_2 increased in accordance with the slice repetition time of the multi-slice acquisitions (54 ms). Therefore, inversion times (TI_2) in study 2 for slices 1 through 6 were: 1500 ms, 1554 ms, 1608 ms, 1662 ms, 1716 ms, and 1770 ms respectively (i.e. exactly the same as they would be in a multi-slice acquisition). In study 3, the inversion band placement varied so that its distance from the imaging slice was constant at 20 mm. As a result, TI_2 was also kept constant at 1500 ms (Fig. 2-1C and D).

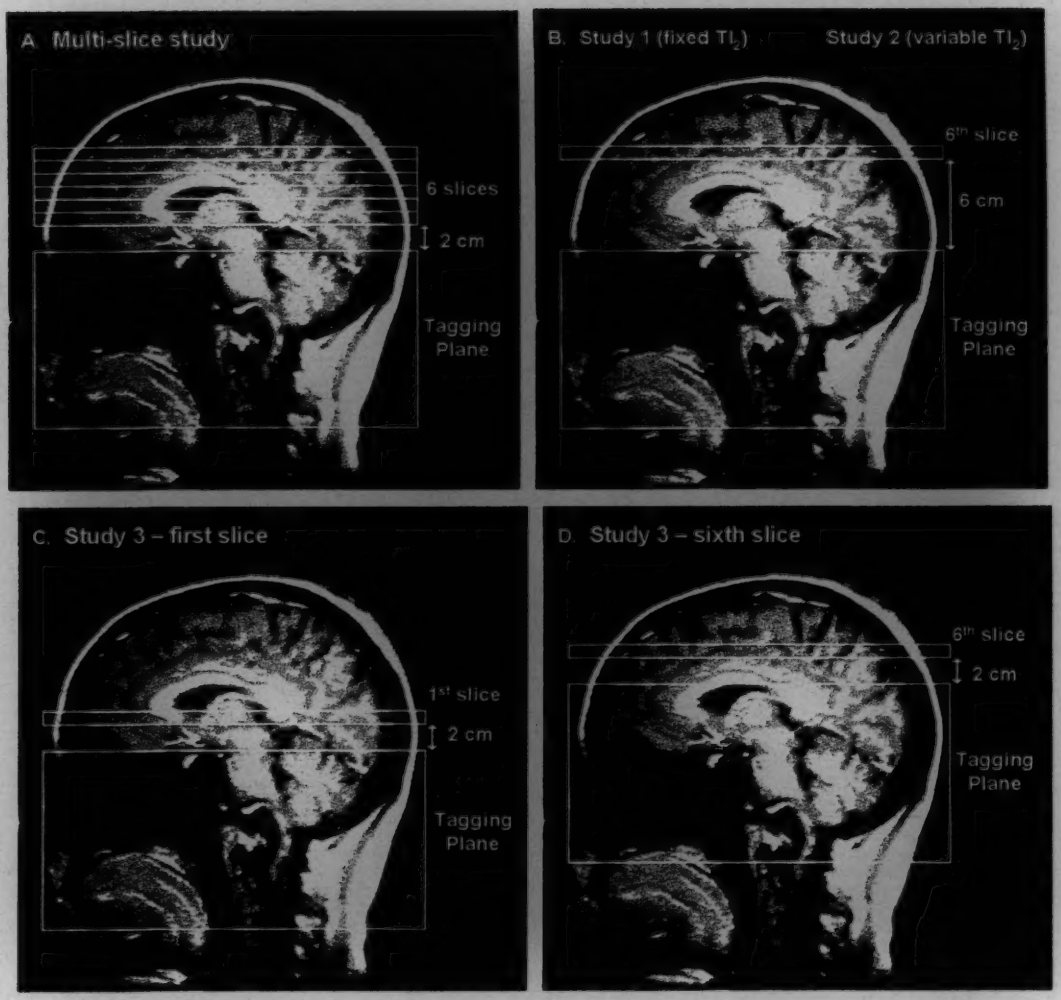

Figure 2-1: Location of the tagging plane and imaging slices in studies 1, 2, and 3

Location of the tagging plane with respect to the imaging slices for: (A) multi-slice study, (B) single slice studies 1 and 2, (C) and (D) single slice study 3. The multi-slice study consists of six 8 mm contiguous slices placed 2 cm from the tagging plane. TI_2 increases incrementally per slice, with a slice repetition time of 54 ms. For studies 1 and 2 the placement of the tagging plane is fixed with respect to the volunteer. The difference between the two studies is that in study 1, $TI_2 = 1500$ ms for every slice, whereas in study 2, TI_2 increases by 54 ms with every increase in slice number (identical to the multi-slice study). In study 3, the tagging plane is adjusted so that it is always located 2 cm from the imaging slice. $TI_2 = 1500$ ms for every slice in study 3.

Several anatomical images were also acquired for each volunteer. An inversion recovery gradient-echo EPI image (TI = 200 ms, TE = 57 ms, TR = 5500 ms) was acquired at each ASL slice location in order to provide an image with adequate gray-white matter contrast for tissue segmentation. Two additional anatomical images were obtained in order to calculate R and M_{owm}, necessary variables for the determination of M_{ob}. A proton density weighted image was acquired (gradient-echo, flip angle = 10°, TE = 5 ms, TR = 1000 ms), so that R, the ratio of proton density of blood in the sagittal sinus to that in white matter, could be determined. M_{owm}, the T_2*-weighted equilibrium signal of white matter, was calculated from a single shot gradient-echo EPI sequence with TE = 15 ms, TR = 20000 ms. These sequences were acquired with the same receiver gain settings as the perfusion images. Together, R and M_{owm} were used to determine M_{ob}, the T_2*-weighted equilibrium signal of blood,

$$M_{ob} = RM_{owm} \exp[(1/T_{2wm}^* - 1/T_{2b}^*)TE] \qquad [2.1]$$

where T_{2wm}* is the T_2* of white matter and T_{2b}* is the T_2* of blood (Wong *et al.*, 1998b). M_{ob} is unique to each volunteer and is necessary for the calculation of cerebral blood flow. The total scan time per volunteer for one study, including the anatomical images, six single slice ASL scans, and one multi-slice ASL scan, was approximately 30 min.

2.2.2 Data Processing

Using the Q2TIPS pulse sequence we acquired a series of tag and control images that were motion corrected and pairwise subtracted to obtain individual ASL difference images. Using MRVision software (MRVision Co., Winchester, MA) each individual difference image was qualitatively assessed and removed if pairwise subtraction had not adequately deleted static tissue. The remaining individual difference images were added together and further processed in Matlab (The MathWorks, Inc., Natick, MA) to create an overall signal difference image (ΔM image). Once ΔM is produced, cerebral blood flow (f) in mL blood / 100 mL tissue / min was calculated using (Wong *et al.*, 1998b),

$$\Delta M(TI_2) = 2M_{ob} f TI_1 \alpha \exp(-TI_2 / T_{1b}) q(T_{1b}, T_{1t}, T_{ex}, f, \lambda, TI_2) \quad [2.2]$$

$$\text{if} \quad TI_1 < \tau \quad \text{and} \quad TI_2 > TI_1 + \Delta t$$

where q(t) is a correction factor accounting for the difference in T_1 decay as tagged water spins move from blood to tissue. In our study q(t) is assumed to be unity (Luh *et al.*, 1999). Δt is the transit time of blood from the labeling plane to the imaging slice, and τ is the time width of the tagged bolus. T_{1b} is the longitudinal relaxation time of blood, assumed to be 1200 ms (Yang *et al.*, 1998).

The inversion recovery anatomical images with good gray-white matter contrast were used for the segmentation of perfusion difference images into gray matter and white matter regions. Signal from whole slice, gray matter, and white matter was calculated for each slice in both the multi-slice and single slice scans. In studies 1 and 3, TI_2 for each slice was constant at 1500 ms. Therefore, the amount of blood T_1 decay is identical for all slices in these two single slice studies. However, in the single slice scans in study 2, as well as all multi-slice acquisitions, TI_2 changes per slice. If not corrected for, SNR would decrease per slice in part because the T_1 decay of blood increases per slice. In order to accurately compare all studies, we corrected for blood T_1 decay prior to making the final SNR calculations.

SNR was calculated for whole slice, gray matter (GM), and white matter (WM) in all slices. In our report, SNR is calculated from the ΔM images and is defined as the signal in brain divided by the standard deviation of the background noise. For the multi-slice experiments, SNR values for all volunteers were averaged per slice, and compared to the average SNR values for all volunteers in the corresponding single slice experiment. In each study, the SNR in the first slice in both the single slice and multi-slice experiments was normalized to 1, as there are no methodological reasons for a difference in SNR in the first slice. For whole slice measurements, the actual difference in slice 1 between single slice and multi-slice experiments before normalization was 4.3% for study 1, 0.7%

for study 2, and 16.6% for study 3. For gray matter, the difference was 3.3% for study 1, 1.9% for study 2, and 12.2% for study 3.

Paired t-tests were performed for all experiments (multi-slice and single slice acquisitions) to determine if significant signal loss occurred in superior slices compared to the first slice. As well, paired t-tests were used to show if any differences in SNR existed between corresponding slices acquired by single slice and multi-slice methods within a study. $P < 0.05$ was considered a statistically significant difference.

2.3 Results

Qualitative assessment of ΔM images in all volunteers demonstrates signal loss in superior slices in multi-slice studies albeit to differing degrees in the 3 single slice studies (Figs. 2-2, 2-3, 2-4). It is not apparent in the initial evaluation of study 1, where the tagging plane was fixed in one position and TI_2 for each slice was held constant at 1500 ms, that any signal in superior slices is recovered (Fig. 2-2). In study 2, the tagging plane is fixed in position, identical to study 1, however TI_2 is increased for slices further from the tagging plane. Imaging superior slices at a later time allows more blood to reach these slices and the perfusion signal increases, as seen in Fig. 2-3. ΔM images in study 3 clearly indicate that signal in superior slices is higher when the tagging plane is moved adjacent to the single acquired slice than the corresponding slice in the multi-slice experiment (Fig. 2-4). Although perfusion signal increases in superior slices for both studies 2 and 3 with single slice acquisition, the increase in signal intensity appears to be greater in study 3.

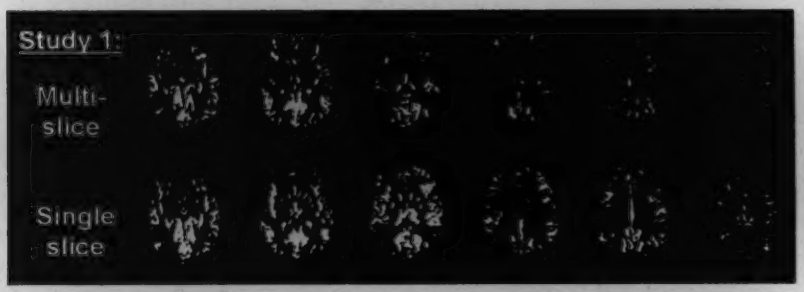

Figure 2-2: ASL single slice and multi-slice perfusion images in study 1

Perfusion difference images normalized to M_{ob} (ΔM / M_{ob}) for the multi-slice and single slice (constant TI_2 = 1500 ms) experiments in study 1 (one volunteer). There is an obvious drop in signal with increasing slice number with the multi-slice and single slice experiments.

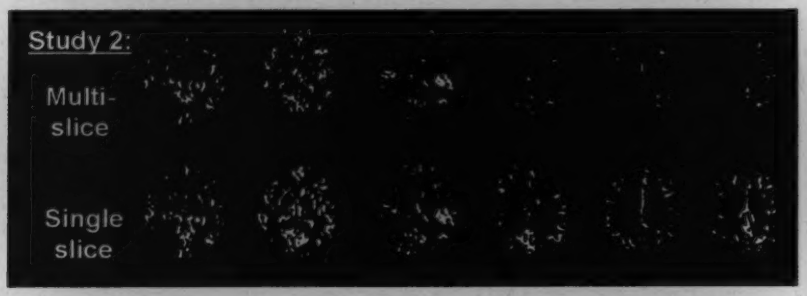

Figure 2-3: ASL single slice and multi-slice perfusion images in study 2

Multi-slice and single slice (incremental TI_2) perfusion images in study 2. There is an obvious drop in signal with increasing slice number in the multi-slice experiment. The images from single slice acquisitions appear to have greater perfusion signal.

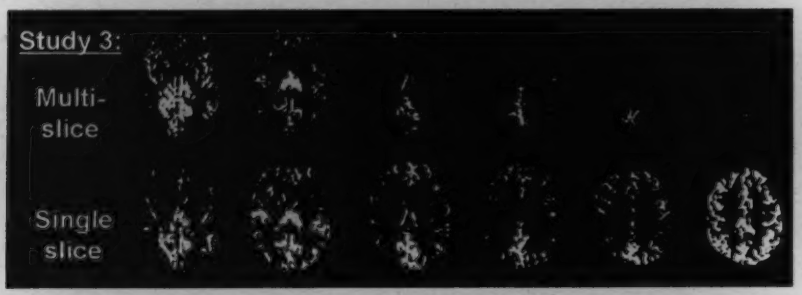

Figure 2-4: ASL single slice and multi-slice perfusion images in study 3

Multi-slice and single slice (adjacent tagging plane and constant TI= 1500 ms) perfusion images in study 3. There is an obvious drop in signal with increasing slice number in the multi-slice experiment. There is a large increase in perfusion signal in the single slice images compared to the multi-slice images.

All perfusion experiments yielded ΔM images with adequate signal to perform SNR and CBF measurements. Difference image SNR values at slice 1 for all single slice and multi-slice acquisitions were: 4.4 ± 0.4 (whole slice), 5.6 ± 0.7 (GM), and 1.8 ± 0.5 (WM). The general pattern of gray matter SNR versus slice number for single slice and multi-slice experiments in each study is demonstrated in Fig. 2-5. SNR measurements from whole slice and white matter demonstrate nearly identical patterns (data not shown). Although the multi-slice acquisition results in all 3 studies would be expected to be identical, deviation occurred due to different volunteers per study and inexact placement of tagging regions and slice locations.

In study 1, with fixed TI_2 of 1500 ms per slice, GM SNR decreases in more distal slices by an amount similar to the multi-slice study (Fig. 2-5A). For each slice, there is no significant difference in GM SNR between the single slice and multi-slice experiments in study 1. As well, there was no significant difference in whole slice and white matter SNR measurements.

In study 2, the tagging plane location was fixed, however TI_2 was increased incrementally with more superior slices. In Fig. 2-5B, gray matter SNR remains relatively constant for all slices in the single slice experiments. Therefore, the additional delay (over study 1) in acquiring more distal slices increases the perfusion signal. GM results for study 2 show that there is a significant difference between SNR measurements of single slice and multi-slice acquisitions in slices 4, 5, and 6 ($P = 0.04$, 0.05, and 0.006 respectively). T-tests on whole slice measurements demonstrate a significant difference in slices 4, 5, and 6 in study 2; WM results indicate that slices 5 and 6 have significantly higher SNR in the single slice experiments compared to multi-slice experiments.

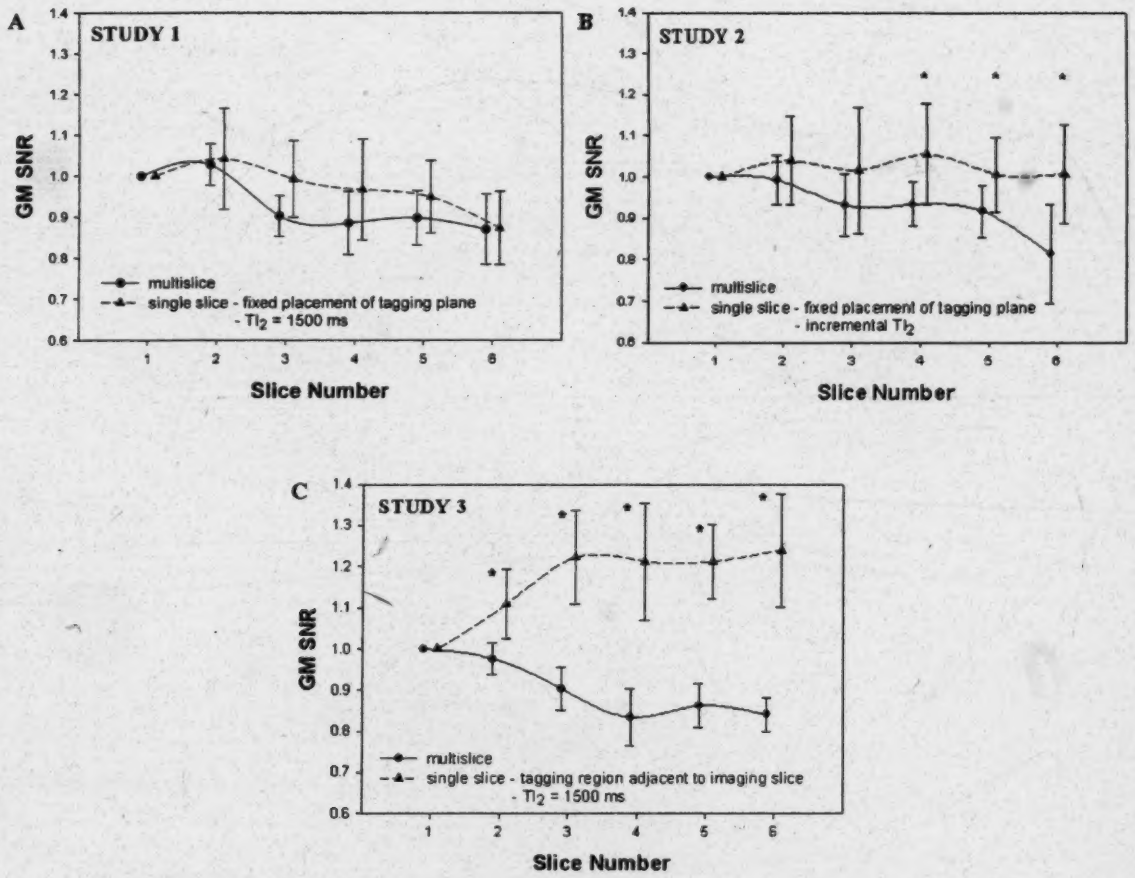

Figure 2-5: Mean gray matter SNR ± SD in both single slice and multi-slice acquisitions

(A) study 1 (N = 8), (B) study 2 (N = 12), and (C) study 3 (N = 9). When the tagging plane location is fixed and TI_2 is held constant at 1500 ms (study 1), single slice GM SNR decreases with slice number by an amount similar to multi-slice studies. SNR in the single slice experiments is not significantly different from the corresponding slice in multi-slice studies. In study 2, most of the signal lost in multi-slice acquisitions is recovered by acquiring multiple single slices. GM SNR in slices 3, 4, and 5 in single slice experiments are significantly higher than slices 3, 4, and 5 in multi-slice experiments, noted with * (paired t-test, $P < 0.05$). In study 3 the tagging plane is kept adjacent (2 cm) to the single slices and hence moves up the brain for superior slices. This results in marked increased GM SNR for single slice acquisitions (slices 2–5) than corresponding slices in the multi-slice studies.

The greatest increase of SNR in whole slice, GM, and WM measurements was found in study 3, when the tagging plane was kept immediately adjacent (2 cm separation) to the single slice. It is apparent in Fig. 2-5C that signal in the superior slices in the single slice experiments is much greater than in the multi-slice experiment (for the same slice), as well as exceeding the signal acquired in studies 1 and 2. Whole slice, GM and WM measurements for all slices are significantly different between multi-slice and single slice acquisitions. Paired t-tests were also performed to indicate whether SNR in slices 2 through 6 differed from SNR in slice 1 for the single slice experiments. Figure 2-5C demonstrates an increase in gray matter SNR in slices 2 through 6 compared to slice 1 for study 3. This is most likely due to the fact that the tagging plane is moved up towards the brain. After comparison to MR angiographic images, it seems that this superior movement of the tagging plane leads to the arteries in the Circle of Willis being tagged. Therefore, it is possible that this greater degree of tagging leads to higher SNR in slices 2–6.

CBF results for single slice and multi-slice experiments were plotted against slice number, similar to the SNR results. The graphs for whole slice, GM and WM for all 3 studies were nearly identical to the SNR graphs (data not shown). White matter displayed the most dramatic drop in CBF in multi-slice experiments when moving from inferior to superior slices. Whereas the average drop in WM CBF between the first 3 slices and the last 3 slices in the multi-slice experiments was 38%, it was 23% and 10% for whole slice CBF and GM CBF respectively. CBF was averaged across all 6 slices to obtain whole brain CBF results, shown in Table 2-1. For study 1, the single slice whole brain, GM, and WM CBF are not significantly different from the corresponding multi-slice CBF values ($P = 0.53$, 0.13, and 0.89 respectively). However, single slice CBF in study 2 is 18% (whole brain, $P = 0.001$), 16% (GM, $P = 0.003$) and 32% (WM, $P = 0.003$) larger than multi-slice CBF. In study 3, single slice CBF is 22% (whole brain, $P = 0.0003$), 13% (GM, $P = 0.0004$) and 32% (WM, $P = 0.02$) larger than multi-slice CBF.

Table 2-1: Average CBF in single slice and multi-slice studies

Average CBF (mL/100 mL/min) over six slices calculated for whole brain, GM, and WM for multi-slice versus single slice PASL imaging in studies 1, 2, and 3 (paired t-tests with * denoting $P < 0.05$).

		CBF (mL / 100 mL / min)		
		Whole Brain	Gray Matter	White Matter
Multi-slice (N = 29)	multi-slice	49 ± 5	70 ± 7	19 ± 4
STUDY 1 (N = 8)	single slice	48 ± 17	63 ± 20	21 ± 12
STUDY 2 (N = 12)	single slice	58 ± 14 *	81 ± 17 *	25 ± 13 *
STUDY 3 (N =9)	single slice	60 ± 15 *	79 ± 17 *	25 ± 15 *

2.4 Discussion

Many PASL schemes have been extended to multi-slice acquisitions and implemented in patient studies. However, accurate cerebral blood flow quantification is difficult since there are differing blood transit times from the tagging plane to each imaging slice. Acquiring slices proximal to distal from the tagging plane means that additional T_1 decay of blood will have occurred in distal slices and blood signal will be lower. This is qualitatively apparent in multi-slice image sets; however it can be corrected for prior to CBF quantification. The introduction of quantitative imaging of perfusion using a single subtraction (Q2TIPS) (Wong *et al.*, 1998b) reduces the problem of various transit time delays. In Q2TIPS, a saturation pulse is applied to the tagging region at a time TI_1 in order to clip the tail end of the tagged bolus. Therefore, the time width of the bolus is known, and the sequence becomes transit time insensitive. Consequently, Q2TIPS appears to be an obvious choice for multi-slice imaging, and is the sequence used in the present report.

As mentioned in the introduction, a major difficulty in PASL multi-slice imaging is the destruction of blood magnetization destined for more distal slices by acquiring more

proximal slices; this causes an underestimation of blood flow. It has been proposed that in order to overcome this problem, one can begin imaging with the superior slice (Yang *et al.*, 1998). However, this is not amenable to Q2TIPS imaging because of the necessary timing parameters involved with this technique. These timing parameters also limit the number of slices that can be acquired. In order to quantify CBF in a single subtraction, the following equation must hold: $TI_2 > TI_1 + \Delta t$, where TI_2 is the time of image acquisition and Δt in the transit time from the tagging plane to the imaging slice. In other words, an image can only be acquired if the entire tagged bolus has been allowed to perfuse the slice and exit by outflow. This equation is unlikely to hold if imaging is carried out with superior to inferior slice acquisition, or if too many slices are acquired. For these two reasons we implemented an inferior to superior slice acquisition scheme while acquiring six slices. Another problem with imaging superior slices prior to inferior slices is the loss and decay of tagged blood signal. The inversion time in such an experiment would have to be long in order to let the tag reach superior slices before imaging occurs. Hence, the inversion time for inferior slices would have to be even longer, and the tag will likely have already passed through these slices prior to imaging. Even if some tag remains, the T_1 decay is likely to be extensive.

The three studies carried out in this report help to demonstrate the extent to which the acquisition of inferior slices dampens the signal in superior slices. In particular, study 2 is identical to a multi-slice acquisition in all ways except for the lack of acquisition of inferior slices. The tagging plane was applied at the same location regardless of slice position, and TI_2 for each slice in the single slice acquisitions were identical to TI_2 in the multi-slice acquisition. Results indicate that a large portion of the signal lost in multi-slice acquisitions is due to this effect. When comparing the first three slices to the last three slices in the multi-slice acquisitions there is a 21% drop in whole slice SNR, however 14% of whole slice SNR is recovered using multiple single slice acquisitions with identical parameters to the multi-slice acquisition.

The difference signal images acquired as single slices in study 3, when the tagging plane is adjacent to the imaging slice and TI_2 is fixed at 1500 ms, show the average GM SNR of the last three slices is 10% higher than the first three slices. This indicates that placing the tagging plane close to the imaging slice prevents blood from taking circuitous routes, increasing the amount of tagged blood reaching the slice by TI_2. As well, superior movement of the tagging plane may cause tagging of additional blood vessels, also increasing the size of the tag reaching the slice by TI_2. By comparison of study 1 to study 3 we are certain the recovery of signal in study 3 is not due to the shortening of TI_2 for more superior slices. Study 1 indicates that the effect of shortening TI_2 in all slices plays little role in the recovery of signal in more distal slices. TI_2 was shortened to 1500 ms in study 3 so as not to miss the tagged bolus, since the distance between the tagging plane and the imaging slice was small (20 mm) and no extra time was required for the tag to enter the slice.

Mean CBF per slice, measured using multi-slice Q2TIPS with sequential slice acquisition, is lower in slices most distal to the tagging region. This is a drawback to 2D multi-slice ASL techniques, since GM and WM CBF should be similar in each slice throughout the brain. The results of this study show that mean CBF of multiple slices, acquired using a single slice technique with optimized parameters, may be more accurate than mean CBF of multi-slice acquisitions, since CBF values are consistent over many slices. However, it is difficult to validate specific CBF values since CBF in different studies is quantified using variable acquisition parameters such as resolution, scan time, and tagging methodology. A recent study compares ASL CBF measurements to the current gold standard $H_2{}^{15}O$ PET, and concludes that ASL GM CBF values (64 ± 12 mL/100mL/min) are not statistically different than PET GM CBF values (67 ± 13 mL/100mL/min) (Ye *et al.*, 2000). Within the ASL literature, GM CBF ranges from 50.9 ± 7.2 (Fernandez-Seara *et al.*, 2005) to 64 ± 12 mL/100mL/min (Ye *et al.*, 2000), with GM/WM CBF ratios from 1.6 (Ye *et al.*, 2000) to 3.2 (Gunther *et al.*, 2005). The multi-slice and single slice (study 2 and 3) GM CBF values (70 ± 7 and 80 ± 17

mL/100mL/min respectively) and GM/WM CBF ratios (3.7 and 3.2 respectively) in the present study are high considering ranges in current literature.

Recently, ASL has been implemented using single-shot 3D readout techniques to remove detrimental signal loss in 2D multi-slice schemes (Talagala *et al.*, 2004, Gunther *et al.*, 2005, Fernandez-Seara *et al.*, 2005). PASL with 3D-GRASE readout schemes result in perfusion images with 2.8-fold higher mean GM SNR than 2D-EPI readouts (13.0 ± 3.5 and 4.7 ± 1.3 respectively) along with equal nominal resolution and acquisition time (Gunther *et al.*, 2005). As well, CASL 3D-GRASE imaging at 3T has been implemented with greater brain coverage in areas of high susceptibility and comparable SNR to CASL 2D-EPI (Fernandez-Seara *et al.*, 2005). Q2TIPS with 2D-EPI readout is a widely accepted sequence for perfusion quantification, however resultant multi-slice data sets have lower SNR and CBF in superior slices due to T_1 decay and slice interference, a problem likely to occur with other PASL sequences using inferior to superior slice acquisition. This problem is amplified with increasing number of slices. Therefore, minimizing slice number to cover only the region of interest (e. g. just the coverage of stroke highlighted on diffusion weighted MRI), and placing the tagging region immediately adjacent to the slices of interest ought to be beneficial for maximizing the signal-to-noise of ASL perfusion images of the brain.

CHAPTER 3: Pulsed Arterial Spin Labeling Parameter Optimization for an Elderly Population

---

A version of this chapter has been accepted for publication

Alison Campbell, Christian Beaulieu (2005) *JMRI* (In Press)

3.1 Introduction

Several imaging techniques such as PET, SPECT, and dynamic susceptibility contrast enhanced MRI are capable of measuring cerebral perfusion. Arterial spin labeling (ASL) uses blood water as an endogenous tracer and has an advantage over other perfusion techniques because it is completely noninvasive. The added advantage over MRI bolus tracking is that ASL permits the absolute quantification of cerebral blood flow (CBF) without knowledge of the arterial input function. Without the need for radioisotopes or injection of contrast agents, ASL cannot cause any dangerous allergic reactions, is much cheaper to implement, and repetitive measurements are possible.

Since the introduction of ASL in the early 1990's (Detre *et al.*, 1992, Williams *et al.*, 1992), there has been a large diversity of schemes proposed for the two broad categories of continuous ASL (CASL) and pulsed ASL (PASL) (Calamante *et al.*, 1999). Typically, arterial spins are inverted (labeled) in an artery upstream from the imaging region of interest, and as labeled blood flows into the imaging area there is an exchange of water between the microvasculature and static tissue through the blood brain barrier. The magnetization state of the tissue changes by an amount determined by blood flow and T_1 relaxation. Two images are acquired, one with spin inversion and one without, and the subtraction of these two images results in a perfusion-weighted image. ASL methods have proven to be accurate for the measurement of CBF in healthy adults (Ye *et al.*, 2000), and have demonstrated perfusion alterations in a variety of disease states, such as stroke (Siewert *et al.*, 1997, Detre *et al.*, 1998, Chalela *et al.*, 2000, Hunsche *et al.*, 2002), epilepsy (Detre & Alsop, 1999, Wolf *et al.*, 2001, Liu *et al.*, 2001), and Alzheimer's disease (Alsop *et al.*, 2000). Stroke and Alzheimer's disease are more prevalent in the elderly and it is unclear whether ASL parameters optimized for a younger adult population, as in most studies, are optimal for measuring perfusion in the elderly.

Numerous studies have been carried out using SPECT and PET to evaluate the change of CBF with age in the elderly. Generally, it is accepted that gray matter flow values in the frontal, temporal, and parietal areas (limbic association regions) decrease with age although there is discrepancy as to the rate of change (Shaw *et al.*, 1984, Martin *et al.*, 1991, Waldemar *et al.*, 1991, Van Laere *et al.*, 2001). Even more controversial is whether or not global CBF has an age-related decline, with most studies rejecting the idea of a global decline with age (Waldemar *et al.*, 1991, Krausz *et al.*, 1998, Nobler *et al.*, 1999). Also of interest are the changes in white matter CBF with age, which has been found to stay relatively constant (Pantano *et al.*, 1984, Marchal *et al.*, 1992). Using the same set of acquisition parameters for all age groups, a continuous ASL study in healthy volunteers as a function of age (20-67 years) has demonstrated a 0.45% per year reduction in gray matter perfusion (Parkes *et al.*, 2004). However, changes in blood flow and transit time could mean that an alternate set of ASL parameters is required to yield optimal perfusion-weighted images in the elderly. The purpose of the present study is to compare the quality (i.e. maximize difference signal in brain, minimizing intravascular signal) of perfusion images obtained with variable delay times for pulsed ASL in both healthy young and older adults.

3.2 Materials and Methods

3.2.1 MR Scanning

Twenty-six healthy volunteers (14 male, 12 female, age range 21-67 years) gave written and informed consent and were scanned using pulsed ASL. Subjects were divided into two categories based on age: young (N = 14, 21-27 years, 7 male, 7 female, mean age = 23 ± 2 years), and elderly (N = 12, 61-67 years, 7 male, 5 female, mean age = 63 ± 2 years). Each person was considered healthy and free of psychiatric and neurologic disorders, diabetes, cardiovascular disease, and psychotropic medications. A questionnaire based on the Framingham Study was used on elderly volunteers to assess for risk of stroke within ten years (Elias *et al.*, 2004). Probability of stroke within ten

years was low in all volunteers. The only risk factor was moderately high systolic blood pressure in two elderly subjects. Perfusion scans were performed on a 1.5 Tesla Sonata scanner (Siemens Medical Systems, Erlangen, Germany) equipped with gradient coils producing a maximum amplitude of 40 mT/m and a maximum slew rate of 200 T/m/s. The Q2TIPS pulse sequence (Siemens, Works in Progress) with PICORE tagging was applied for perfusion imaging in all volunteers (Wong *et al.*, 1998b, Luh *et al.*, 1999). Consequently, slab selective inversion was interleaved with no inversion to obtain tag and control images. A gradient-echo echo-planar imaging (EPI) sequence was used to acquire 6 oblique slices, inferior to superior, with an interslice delay time of 54 ms. Other imaging parameters were: FOV 22 x 22 cm, 64 x 64 matrix, 8 mm thick contiguous slices, echo time (TE) 15 ms, repetition time (TR) 2500 ms, 3:52 min scan time, and bandwidth 3004 Hz/pixel. The time of the saturation pulse (TI_1) was kept constant at 800 ms. Using a TI_1 of 800 ms and a 10 cm tagging region, the tail end of the tagged bolus was clipped while maximal signal was achieved (Wong *et al.*, 1998a, Wang *et al.*, 2002, Wang *et al.*, 2003). The delay time (ω) between saturation and excitation was varied (ω = 100, 400, 700, 1000, 1300 ms) in all volunteers to yield perfusion maps acquired with total inversion times (TI_2) of 900, 1200, 1500, 1800, and 2100 ms. Pairwise subtraction of tag and control images yielded 45 difference images.

For anatomical comparison an inversion recovery gradient-echo EPI image with TI = 200 ms, TE = 57 ms, TR = 5500 ms was acquired to provide good gray-white matter contrast in the slices identical to the perfusion imaging slices. Also, a proton-density weighted image (gradient-echo, flip angle = 10°, TE = 5 ms, TR = 1000 ms) was obtained to measure the value R, the ratio of the signal intensity of white matter to the signal intensity of blood in the sagittal sinus. A single shot gradient-echo EPI image was acquired with TE = 15 ms and TR = 20000 ms so that measurements could be made to determine the T_2*-weighted equilibrium signal of white matter (M_{owm}). These sequences were acquired with the same receiver gain settings as the perfusion images. In the end, the ratio R and M_{owm} were used to calculate M_{ob}, such that (Wong *et al.*, 1998b),

$$M_{ob} = RM_{owm} \exp[(1/T_{2wm}^* - 1/T_{2b}^*)TE] \quad [3.1]$$

where T_{2wm}^* is the T_2^* of white matter and T_{2b}^* is the T_2^* of blood. M_{ob}, the T_2^*-weighted equilibrium signal of blood, is important in the calculation of cerebral blood flow and is unique to each volunteer. T_1 maps were used for the segmentation of gray matter and white matter for blood flow calculations. These were produced using another inversion recovery EPI sequence with varying inversion times, TI = 400, 600, 800, 1000, and 1200 ms.

3.2.2 Data Processing

From the perfusion image series, individual difference images (control - tag) were examined and removed prior to averaging if motion was suspected. Difference images were added together to make a sum image off-line using MRVision (Winchester, MA). Additional processing and calculation of ΔM and CBF images was performed off-line using Matlab (The MathWorks, Inc., Natick, MA). The pulsed ASL difference signal is given by the following equations (Wong *et al.*, 1998b),

$$\Delta M(TI_2) = 2M_{ob} f TI_1 \alpha \exp(-TI_2/T_{1b}) q(T_{1b}, T_{1t}, T_{ex}, f, \lambda, TI_2) \quad [3.2]$$
$$\text{if} \quad TI_1 < \tau \quad \text{and} \quad TI_2 > TI_1 + \Delta t$$

where f is the cerebral blood flow in s^{-1}, ΔM is the difference signal between tag and control images, and T_{1b} is the longitudinal relaxation time of blood. Δt is the transit time of blood from the labeling plane to the imaging slice, and τ is the time width of the tagged bolus. q(t) is a correction factor taking into account the time of exchange of water from blood into tissue, the different relaxation rates of blood and tissue, and the clearance of tag by outflow. For our study q(t) was assumed to be unity (Luh *et al.*, 1999), and T_{1b} was assumed to be 1200 ms (Yang *et al.*, 1998, Wang *et al.*, 2003). In practice, q(t) is close to 1 (typically 0.85-1.0) and plays little role in the overall quantitative value of CBF. $T1_b$ is typically between 1200-1400 ms and is a spatially invariant constant.

CBF was calculated using Eq. 3.2 when $TI_2 = 1500$ and 1800 ms. As long as one time point (TI_2) was obtained when $\omega < \Delta t$, Eq. 3.3 could be used to calculate transit time to each of the slices (Wang *et al.*, 2003).

$$\Delta M(TI_2) = -2M_{ob} f \exp(-TI_2 / T_{1b}) \times [\min(\Delta t - \omega, 0) - (\Delta t - TI_2)] \quad [3.3]$$

Since the T_1 maps were acquired with the same resolution, FOV, and bandwidth (i.e. distortions) as the perfusion images, these T_1 maps were used to segment whole slices into gray matter and white matter, such that white matter consisted of pixels where T_1= 600-800 ms, and gray matter where T_1 was 800-1200 ms. T_1 thresholds were the same in both the elderly and younger groups. Similar T_1 values between young and elderly were confirmed prior to segmentation with production of a T_1 histogram.

As stated above, tissue was first segmented into gray and white matter prior to any measurements. The signal difference (ΔM) was calculated per tissue type per slice and averaged across all 6 slices in each individual, taking into account the T_1 decay of blood for each slice. Before averaging, ΔM measurements were normalized to M_{ob} for accurate intersubject comparisons. Intravascular signal was avoided while taking ΔM measurements of the brain tissue. Next, CBF was calculated using Eq. 3.2 for each tissue type in each individual (e.g. gray matter for the entire brain). Transit time was determined in each individual in the second slice only, keeping to the limitations for transit time calculations ($\omega < \Delta t$). ΔM, CBF, Δt, and R were compared between the younger group and older group using two-tailed unpaired t-tests, and averages and standard deviations are reported for each group. $P < 0.05$ was considered to be significant. Images at each value of TI_2 were examined per individual and across age groups. The time and occurrence of intravascular and tissue signal at each TI_2 was noted, and general qualitative observations were made for each age group.

3.3 Results

3.3.1 ASL Difference Signal

All tissue difference signal (ΔM) in the perfusion-weighted images of each individual was seen to decrease with increasing slice position (inferior to superior), and was most often higher in each young individual than in each older individual. Overall, the average gray matter difference signal normalized to M_{ob} (ΔM / M_{ob}) is higher for the younger group at all time points, and shows a significant difference at TI_2 = 1200 ms and 1500 ms (P = 0.02 and 0.05 respectively). The results of the normalized gray matter difference signal versus inversion time (TI_2) are shown in Fig. 3-1. The white matter ΔM / M_{ob} is similar between the young and old at all values of TI_2, showing no statistically significant difference between the two groups (P = 0.29 and 0.36 at TI_2 = 1200 ms and 1500 ms, respectively). The value of white matter ΔM / M_{ob} increases when TI_2 = 900 ms and 1200 ms followed by a decrease at longer TI_2, similar to the trend in gray matter (Fig. 3-1).

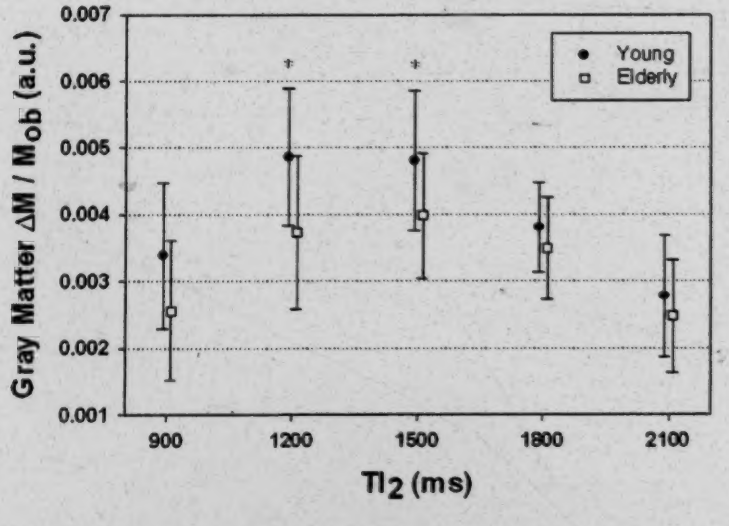

Figure 3-1: Average GM difference signal normalized to M_{ob} (ΔM / M_{ob})

The ΔM / M_{ob} from the younger group is generally larger and tends to peak at shorter TI_2 times (* P < 0.05). The error bars represent the standard deviations.

At shorter inversion times such as $TI_2 = 900$ ms, images from the older population show mostly vascular signal with little tissue signal whereas the younger group has significant signal from tissue but still has regions of high intensity due to intravascular protons. The maximum GM signal occurs at $TI_2 \sim 1500$ ms in the elderly, and at $TI_2 \sim 1300$ ms in the young. Less intravascular signal is observed as TI_2 is increased in both groups; however, the younger group has lost most intravascular signal at $TI_2 = 1500$ ms, whereas the elderly group has persistent intravascular signal. It is not until $TI_2 = 1800$ ms that we see a complete loss of intravascular signal in the elderly (Fig. 3-2). The signal difference between the two age groups can be seen qualitatively in Fig. 3-3 for TI_2 values of 1500 ms and 1800 ms.

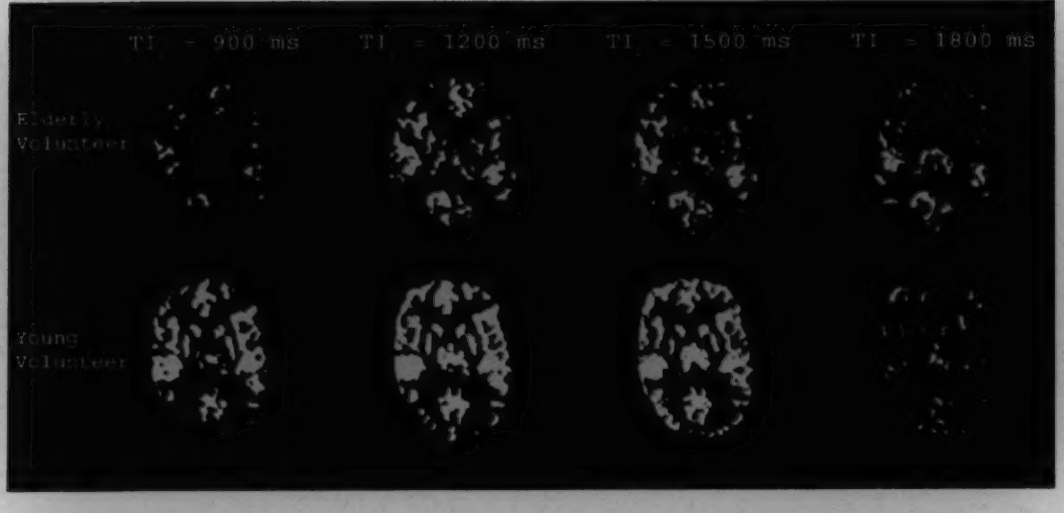

Figure 3-2: Perfusion-weighted difference images at different values of TI_2

The elderly volunteer has mostly intravascular signal at a TI_2 of 900 ms, and still retains some intravascular signal at $TI_2 = 1500$ ms. The young volunteer shows some tissue signal at a TI_2 of 900 ms and most intravascular signal has disappeared by $TI_2 = 1500$ ms. These images clearly display that the tagged blood takes longer to enter the tissue in the elderly. As a result, intravascular signal remains at longer values of TI_2 in the elderly compared to the younger group.

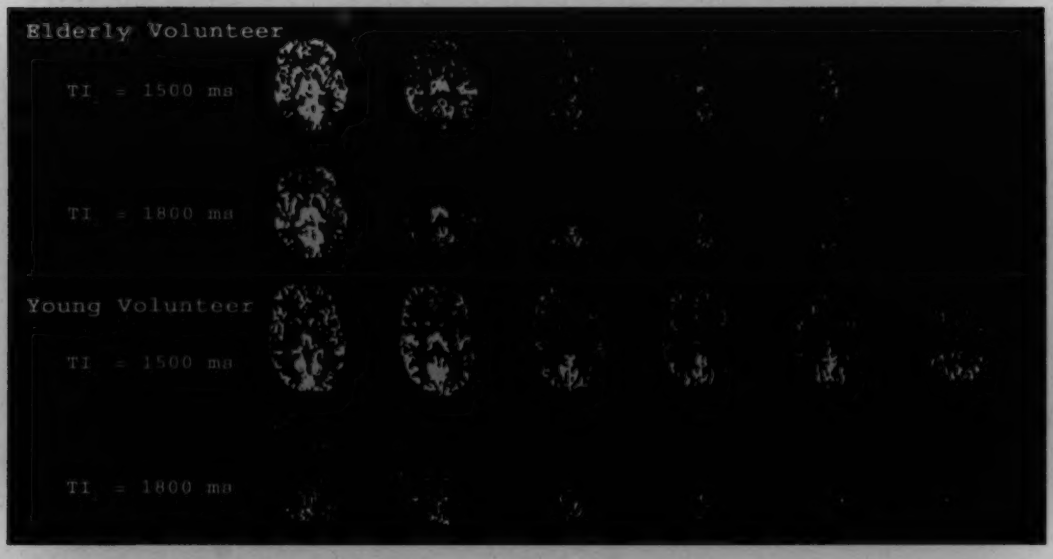

Figure 3-3: Multi-slice perfusion-weighted difference images

For the elderly volunteer, most slices at $TI_2 = 1500$ ms show bright spots representing intravascular signal, whereas at $TI_2 = 1800$ ms the intravascular signal gives way to more dispersed tissue signal. The young volunteer has high signal at $TI_2 = 1500$ ms, with less intravascular signal. Therefore using a TI_2 of 1800 ms causes a loss of tissue signal without reduction of intravascular artifacts, and is not beneficial in the younger adult population. This observation is in contrast to the elderly group in which the absolute tissue difference signal is similar for the two TI_2 times of 1500 ms and 1800 ms. Note that each image is normalized to M_{ob} and all images are globally scaled.

3.3.2 Transit Time

It was possible to calculate the transit time in each individual since perfusion-weighted images were acquired at different values of TI_2. The transit time of blood to gray matter tissue was calculated for the second slice in each individual (Table 3-1). The approximate transit times for the young and elderly were significantly different ($P = 0.03$) and were 522 ± 136 ms and 629 ± 95 ms, respectively, in the cortical gray matter. There is also a statistically significant difference in whole brain transit times between the two age groups ($P = 0.03$), however white matter transit times were similar between the

young and old (P = 0.50). These gray matter results are consistent with previous studies measuring transit time: 416 ± 51 ms (Wang *et al.*, 2003), 730 ± 40 ms (Yang *et al.*, 1998), 514 and 906 ms (visual and motor cortices) (Gonzalez-At *et al.*, 2000), 680 ± 40 ms (Yang *et al.*, 2000), and 680 ± 50 ms (Yongbi *et al.*, 2002).

Table 3-1: Gray matter CBF in the young and elderly

Quantitative perfusion values (mL/100mL/min) in cortical gray matter for both the young and elderly age groups.

Subjects	Age (years)	CBF (mL / 100 mL / min)		Transit Time (ms)	R-value
		TI_2 = 1500ms	TI_2 = 1800ms		
Young (N = 14)	23 ± 2	67 ± 15	68 ± 12	522 ± 136	1.11 ± 0.05
Elderly (N = 12)	63 ± 2	57 ± 12	63 ± 15	629 ± 95	1.08 ± 0.06
Unpaired t-test, P		0.08	0.38	0.03	0.16

3.3.3 Cerebral Blood Flow

The average gray matter cerebral blood flow calculated at a TI_2 of 1500 and 1800 ms for both the young and elderly can be found in Table 3-1. There was no significant difference in cerebral blood flow between the young and the elderly (P = 0.08 and 0.38 for TI_2 = 1500 and 1800 ms, respectively). For the younger group, gray matter CBF is nearly identical regardless of the value of TI_2. However for the older group, there is a significant increase in gray matter CBF when TI_2 increases from 1500 to 1800 ms (P = 0.05). The same pattern holds true for whole brain CBF in the elderly with a significant increase in CBF (P = 0.02) while increasing TI_2 to 1800 ms. Also shown in Table 3-1 are the calculated values of R, which agree well with literature (Wong *et al.*, 1998b).

3.4 Discussion

An ideal pulsed ASL inversion time is one in which tissue signal remains high yet the inversion time is long enough so that intravascular signal is minimal. By varying the inversion time in our experiments it was noticeable that the difference signal was very dependent on the chosen TI_2, with increasing difference signal at lower values of TI_2 until delivery of the entire tag was complete (trailing time) and signal began to drop off. The younger group signal peaks at about $TI_2 = 1300$ ms, however vascular signal still exists at this point. An improved TI_2 is one at 1500 ms where most intravascular signal has disappeared, and there is a loss in tissue signal of only 3%. In the older group the maximum signal occurs when $TI_2 = 1500$ ms, but the loss of intravascular signal occurs at $TI_2 = 1800$ ms, which also results in a 12% loss in tissue signal. Attempting to use the same inversion time in both the young and elderly groups is not ideal since the use of a TI_2 of 1800 ms in the younger group would result in a 22% loss in tissue signal compared to the maximum signal achieved at shorter TI_2 values. In gray matter, the higher tissue signal in the young shows that more tagged blood enters each slice no matter what inversion time is selected. Our findings of similar white matter signal between young and old adults follows the common belief that white matter CBF does not change with age (Davis *et al.*, 1983, Pantano *et al.*, 1984).

The transit time (Δt) results indicate that a 100 ms difference exists between the young and the elderly in the tagging of the blood to the first arrival of tagged blood in the second imaging slice (i.e. first arrival of vascular signal). This suggests that the difference in trailing time between young and old (difference in peak $\Delta M / M_{ob}$ signal) is possibly due to a longer transit time from the tagging region into the imaging slice. Parkes *et al.* noted that a change in capillary permeability as well as slower flow in the larger arterial vessels may be factors in causing the elderly to appear to have lower perfusion (Parkes *et al.*, 2004). These factors may increase the transport time of the entire bolus to the slices of interest in the elderly (i.e. increase in trailing time).

Recent ASL MRI studies measuring cerebral perfusion note a decrease in perfusion with age (Wang *et al.*, 2003, Parkes *et al.*, 2004). Wang *et al.* have shown that a decrease in CBF occurs in the entire brain as we age from children to young adults (Wang *et al.*, 2003). This study was also conducted with varying inversion times. They observed increases in CBF of 30% in children, however these results did not coincide with any changes in transit time. Parkes *et al.* showed a decrease in gray matter perfusion with age at a rate of 0.45% per year (Parkes *et al.*, 2004), which is slightly lower than other reported rates (Pantano *et al.*, 1984, Leenders *et al.*, 1990, Martin *et al.*, 1991). Our study concentrated only on a global change in CBF and does not report any focal measurements. There is no significant difference in CBF values when comparing the young group to the older group at each TI_2. However, the goal of our study was neither to quantify CBF nor to identify how CBF changes with age. Without a gold standard for quantifying CBF it is not possible to tell which one of our CBF values is correct, but it is important to note that all our reported CBF values fall within a reasonably tight range of 57-68 mL/100mL/min.

The purpose of our study was to determine parameters for yielding optimal perfusion-weighted images for scanning an elderly population using the Q2TIPS ASL sequence. We have determined that if we set $TI_1 = 800$ ms that the optimal TI_2 is 1500 ms for the young, and 1800 ms for the elderly. However, these results pertain only to our sequence and TI_1 value and may not be exactly the same for other ASL sequences. Overall, the results of our experiments show that when comparing different age groups it is not necessarily best to use identical acquisition parameters. Differences in the transit time from the tagging region to the imaging slice may play an important role in the amount of difference signal between tagged and untagged images.

In conclusion, inversion timings in arterial spin labeling must be optimized to receive maximum perfusion-weighted tissue signal without deleterious intravascular signal, and these timings may differ between younger and older subjects. Therefore, ASL protocol optimization of the inversion timings should be considered for perfusion studies on diseases that primarily affect the elderly, such as Stroke and Alzheimer's disease.

CHAPTER 4: Discussion

In the following chapter I will briefly summarize the results of Chapter 2 and 3, introduce theory on high field ASL imaging and show preliminary results at 3T, assess the feasibility of applying ASL to stroke, and end with suggestions for future ASL research at our site and current state-of-the-art techniques.

4.1 Multi-slice and Single Slice PASL for CBF Measurement

From the time when pulsed ASL was introduced as a single slice technique for the assessment of CBF, technical advances have permitted multi-slice imaging with reduced sensitivity to transit time effects. Specifically, Q2TIPS implementation has allowed the accurate and efficient quantification of perfusion in multiple slices. Our preliminary work with perfusion quantification showed that CBF values were lower in slices distal to the tagging region, outlining a methodological problem with the acquisition of multiple slices, as there is no physiological basis for decreased perfusion in superior regions of the brain.

The purpose of our study was to determine the reason for the ASL signal loss in superior slices acquired with Q2TIPS that could not be accounted for by blood T_1 decay. Results of the study showed that the signal loss was most likely due to slice interactions, the destruction of blood magnetization destined for more distal slices through the acquisition of proximal slices. The results also highlighted the importance of tagging plane location for maximizing the ASL signal.

Overall, we demonstrate a limitation of 2D-EPI acquisition in ASL when a high number of slices are desired. Emerging techniques using 3D readouts, specifically 3D-GRASE, 3D-FSE-spiral and parallel imaging, are promising especially for ASL imaging at high field and for extended brain coverage (Talagala *et al.*, 2004, Gunther *et al.*, 2005, Fernandez-Seara *et al.*, 2005).

4.2 PASL Parameter Optimization for the Elderly

CBF studies conducted using PET, SPECT, and MRI indicate that regional (cortical) blood flow decreases with age (Martin *et al.*, 1991, Waldemar *et al.*, 1991, Van Laere *et al.*, 2001, Parkes *et al.*, 2004). It has also been stated that blood velocity in large arterial vessels decreases, possibly due to atherosclerosis, implying that the transit time of blood to brain tissue is higher in the elderly (Scheel *et al.*, 2000, Bakker *et al.*, 2004). Optimal ASL sequence parameters, such as the inversion time, are highly dependent on transit time, and it is unclear whether ASL parameters optimized for a younger population, as in most studies, also apply to an elderly population. We hypothesized that sequence parameters would need to be altered for the elderly in order to obtain accurate quantitative results.

Our results show that inversion timings used in PASL imaging should be optimized for the elderly. Due to the increase in transit time with age, a longer inversion time may be necessary to maximize brain tissue signal and minimize intravascular signal. Because stroke is more prevalent in the elderly, optimization of TI should be considered for ASL perfusion studies of stroke.

An example of exceptionally long arterial transit times was observed in a 91-year-old patient recruited into one of our stroke studies. The patient's blood pressure was controlled and the carotid arteries were not significantly diseased. Diffusion images and bolus tracking time-to-peak maps were used to show the area of stroke. ASL perfusion images obtained with TI_2 = 1500 ms show a significant amount of intravascular signal with very little tissue signal, even in areas not affected by the stroke (Fig. 4-1). This is a case example of a patient who appears to have even longer transit times than the healthy elderly volunteers (~ 63-years-old) imaged in our study, and may be an indication of how ASL images may appear in very old subjects. An increase in TI_2 is definitely required, but it is unknown whether an optimized ASL sequence would be able to show more perfusion-weighted signal in this individual, given the limits set by T_1 relaxation.

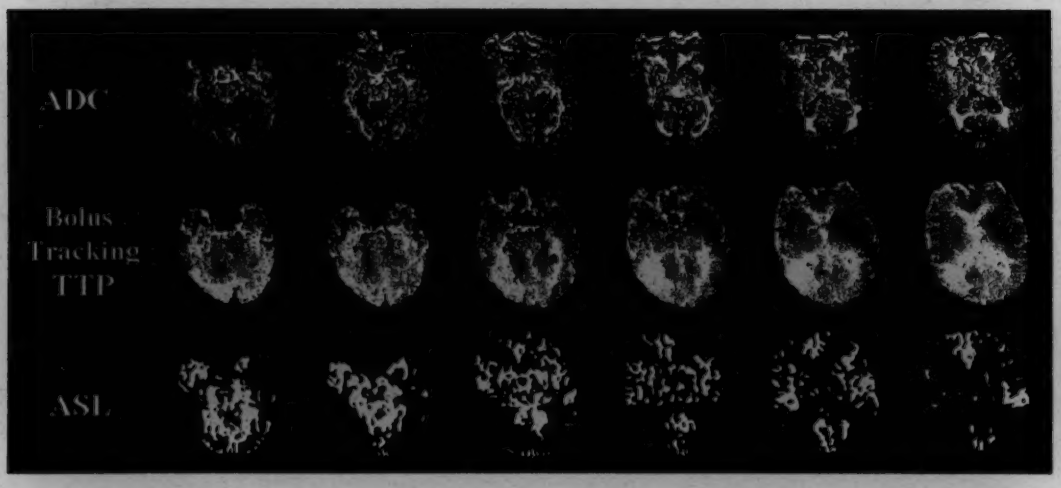

Figure 4-1: ASL images of a 91-year-old stroke patient (time from onset = 20 hours)

The apparent diffusion coefficient (ADC) maps show the region of the stroke (dark area in right posterior brain region). The bright regions on the bolus tracking time-to-peak (TTP) maps represent areas where perfusion is delayed. Arterial spin labeling (ASL) images clearly display reduced perfusion in the area of the stroke. However, tissue perfusion is also reduced in the entire brain, shown by the lack of tissue signal and the presence of focal intravascular signal in the ASL images.

4.2.1 Future Directions

We are currently studying a group of teenagers and young adults (N = 51, age range 12-21 years), using PICORE-Q2TIPS with TI_2 = 900, 1200, 1500, and 1800 ms. We plan to compare ΔM SNR, CBF, and transit time found in teenagers with the results of our young adult population from the previous aging study (N = 14, age range 21-27 years). We propose to (a) determine the variation in ΔM SNR, CBF, and transit time with brain development between 12 and 27 years of age, and (b) offer protocol improvements for ASL perfusion studies in teenagers.

CBF measurement is gaining importance in the diagnosis of several pathologies in childhood and adolescence, such as epilepsy, moyamoya disease, stroke, and metabolic

abnormalities (Liu *et al.*, 2001, Arroyo & Tamer, 2002, Heiniger *et al.*, 2002, Khanna *et al.*, 2004). ASL is a promising technique for perfusion assessment in these cases because of its noninvasive nature and unlimited repeatability. Concerning normal brain development, Wang *et al.* compared healthy children (N = 7) to young adults (N = 5) and demonstrated a linear decline in global CBF with age, although they did not find a significant difference in transit time between the two groups (Wang *et al.*, 2003). It is well known that CBF in children is significantly higher than in young adults. It will be interesting to determine how much of this decline occurs during the teenage years.

4.3 High Field ASL Imaging

4.3.1 SNR Increase with Main Magnetic Field Strength

At the present time, ASL measurement of cerebral blood flow for clinical purposes is somewhat limited by poor spatial resolution, inadequate brain coverage, and long scan times. The raw ASL perfusion signal is less than 1% of the static tissue signal, therefore it is necessary to average many tag-control pairs to increase SNR (SNR is proportional to the square root of the number of averages). High field ASL is appealing, since SNR and contrast-to-noise ratio (CNR) in MR images increase directly with main magnetic field strength (B_0). In addition to the intrinsic SNR increase, ASL has an added labeling advantage due to the approximate cubed root increase in T_1 relaxation time with field strength (Wang *et al.*, 2002). As the longitudinal relaxation time of blood (T_{1b}) increases with field strength, the lifetime of the ASL tag is extended, and ASL sequences with longer inversion times can be implemented. At 1.5T, where T_{1b} ~ 1200-1500 ms (Ye *et al.*, 1997, Luh *et al.*, 1999, Parkes *et al.*, 2004), most ASL sequences use an inversion time of approximately 1200-1600 ms (Wong *et al.*, 1997, Gunther *et al.*, 2005). At high field it may be possible to increase TI substantially; T_{1b} has been measured at 1490 ms (Wansapura *et al.*, 1995) and 1664 ms (Lu *et al.*, 2004) at 3T, and 1620 ms at 4T (Kim *et al.*, 1994). This is particularly important for ASL assessment of cerebrovascular disease,

which often requires long inversion times in order to detect perfusion in regions with long transit delays.

A disadvantage of high field ASL imaging is the linear increase in strength of susceptibility gradients with B_0, resulting in T_2* reduction and signal loss and distortion in areas with high static field inhomogeneities. The spatial resolution of single-shot EPI images is limited by T_2*, therefore an alternate pulse sequence may be better suited for ASL imaging at high field to capitalize on sensitivity gains. The gradient- and spin-echo (GRASE) imaging sequence (Oshio & Feinberg, 1991) is able to maintain signal amplitude in long echo trains. Images from GRASE readout schemes tend to have fewer distortions and higher SNR compared to EPI techniques (Gunther *et al.*, 2005). If EPI is used, minimizing TE to reduce echo train length is beneficial (Fernandez-Seara *et al.*, 2005).

In a study by Wang *et al.* ΔM SNR and CBF values measured using FAIR-QUIPSS at 1.5T were compared to measurements at 4T (Wang *et al.*, 2002). Results demonstrated that high field ASL is feasible and beneficial, with ΔM SNR increasing by a factor of 2.3 and 1.9 in GM and WM, respectively, as well as a 2.8-fold increase in contrast-to-noise ratio (CNR) between gray and white matter at 4T. 4T images show improved delineation of cortical and subcortical gray matter structures, including the caudate, putamen, and thalamus. Another study performing PASL imaging at high field compared FAIR ΔM SNR and CBF values at 1.5T and 3T (Yongbi *et al.*, 2002). GM and WM perfusion SNR values at 3T were 23.7 ± 9.3 and 6.8 ± 2.3, respectively, compared to 8.3 ± 2.2 and 2.7 ± 1.5 at 1.5T. Overall, the authors were able to demonstrate significant SNR gains and consistent CBF measurements at 3T, producing high quality images with excellent suppression of background signal. State-of-the-art 7T ASL imaging is demonstrated in a recent paper discussing methodological improvements for ASL (Duyn *et al.*, 2005). FAIR images acquired in only 5 min with 1.5 x 1.5 x 2.0 mm^3 resolution show excellent delineation of cortical gray matter structures and SNR between 20 and 40.

4.3.2 ASL Pulse Sequence Development at 3T

Using the SMIS programming language we were able to write a flow sensitive sequence at 3T. A global inversion pulse is applied prior to the 90° slice-selective pulse in a single-shot GE-EPI sequence, creating a tagged bolus similar to the FAIR tagging scheme (Kim, 1995). The control image is generated with a slice-selective inversion pulse, and interleaved with the tagging pulse throughout the ASL sequence. An alternate sequence was also written that uses FAIR labeling and a QUIPSS-like extension, with an optional 90° saturation pulse between the labeling and imaging pulses (Wang *et al.*, 2002).

Postprocessing of the MRI signal was performed off-line using programs written in Matlab (The MathWorks, Inc., Natick, MA). These programs were also used to subtract tag-control pairs, add individual difference images, and output ASL signal maps and CBF images. Preliminary results show a good quality multi-slice data set from a normal volunteer (Fig. 4-2). The benefits of 3T ASL are readily apparent; good quality images with adequate SNR are produced by averaging only 10 tag-control pairs acquired in 1:33 min (Fig. 4-3), compared to 50 averages in 3:52 min at 1.5T (see Fig. 1-11 for comparison).

Figure 4-2: FAIR difference images at 3T

FAIR difference images from a normal volunteer scanned at 3T. The multi-slice data set is the sum of 10 averages acquired in 1:33 min, with TI =1200 ms, and an inversion slab thickness 30 mm wider than the imaging slab.

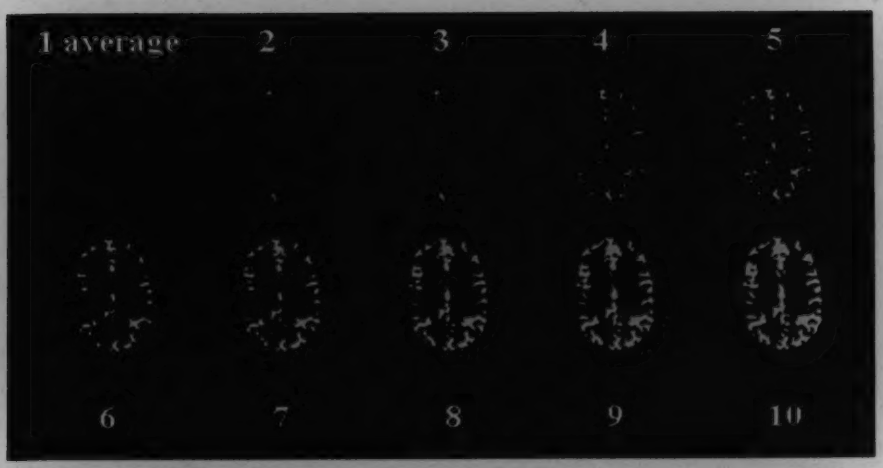

Figure 4-3: Summation of 10 ASL difference images at 3T

The sum of individual FAIR difference images at 3T demonstrates the significant increase in perfusion-weighted signal attained at high field. An ASL perfusion image with adequate SNR can be generated from only 10 averages in 1:33 min.

Overall, high field ASL is appealing because it provides not only an increase in the inherent SNR which is proportional to main magnetic field strength, but also an advantage in terms of labeling due to the increased longitudinal relaxation time of blood (T_{1b}). Consequently, ASL perfusion imaging at high field can produce better quality images with increased SNR and resolution and/or decreased scans times as compared to 1.5T ASL. As well, an increase in the lifetime of the tag implies that longer inversion times may be possible at high field, which is particularly important in the study of cerebrovascular disease where long transit delays often exist in areas supplied by collateral flow. Our preliminary results at 3T clearly demonstrate the significant increase in perfusion signal attained at higher field, reflected in the relatively short scan times required to generate perfusion images with sufficient SNR. Although these results are

promising, echo-planar imaging on the 3T scanner was limited by hardware factors such as lower gradient strength and slew rates, as well as inadequate shimming techniques. Most importantly, however, was that we ultimately wanted to apply ASL to stroke, and the 3T scanner was not accessible to patients. Therefore, upon completion of the new NMR Research Facility in the emergency wing, we decided to concentrate our efforts on ASL development at 1.5T.

4.4 Imaging Evaluation of Stroke

4.4.1 Evaluation and Treatment of Acute Stroke

Stroke is the third leading cause of death and primary cause of adult disability in North America. Stroke occurs when blood flow to part of the brain is suddenly interrupted, and is classified by its cause into two groups: an ischemic stroke (thrombotic or embolic) occurs when a blood vessel becomes occluded, and a hemorrhagic stroke occurs when a blood vessel bursts (~20% of stroke cases) (Mohr *et al.*, 1978). Ischemia reduces the delivery rate of metabolic substrates, causing neuronal ATP deficiency, cytotoxic edema, and eventual cell death (necrotic and apoptotic) (Macdonald & Stoodley, 1998).

The only approved drug for the treatment of acute ischemic stroke, recombinant tissue plasminogen activator (rt-PA), must be given within three hours of stroke onset. Therefore, patients who present with stroke symptoms, for example confusion, aphasia, numbness or weakness, require rapid evaluation. This treatment is potentially dangerous and often contraindicated, as it cannot be given in cases of brain hemorrhage and should not be given to patients without potentially salvageable tissue. At most institutions, including ours, the primary imaging modality used to assess stroke location, type, and severity is x-ray computed tomography (CT). Although CT is highly sensitive to hemorrhagic stroke, it is not an optimal technique for stroke imaging as it cannot differentiate ischemic from infarcted tissue at early time points after stroke onset.

4.4.2 Diffusion- and Perfusion-Weighted MRI

The two emerging imaging techniques for assessment of acute stroke are diffusion- and perfusion-weighted magnetic resonance imaging. In combination with MR angiography, these methods may allow identification of the location, extent, mechanism, and tissue viability of the stroke lesion within the critical first 6 to 12 hours after onset when the greatest therapeutic opportunity exists. Diffusion-weighted MR imaging (DWI) is a technique that permits the measurement of the mobility of water in tissue, therefore providing the earliest known imaging marker of cellular injury in developing ischemic lesions (Baird & Warach, 1998). The degree of water mobility (i.e. diffusion) is quantified as the apparent diffusion coefficient (ADC), such that restricted diffusion is reflected in a low ADC value. In ischemic tissue, decreased blood flow causes energy deficits that result in intracellular ion accumulation, cytotoxic edema and a reduction in extracellular space, which restricts diffusion and leads to signal reduction on ADC maps (Baird & Warach, 1998).

In acute stroke, the presence of mismatch between DWI and PWI lesion volumes may be used to identify abnormally perfused tissue that is at risk for infarction but is salvageable with reperfusion, that is, the ischemic penumbra (Fig. 4-4) (Astrup *et al.*, 1981, Schlaug *et al.*, 1999). It has been postulated that MRI might be able to classify tissue according to reversibility of ischemic damage, predict the extent of infarction, and guide the direction of treatment (Neumann-Haefelin *et al.*, 1999, Rohl *et al.*, 2001). However, recent studies have indicated that stroke evolution is not necessarily predictable using the presence of DWI/PWI mismatch (Rivers *et al.*, 2006), possibly because the area of mismatch does not reliably correlate with the ischemic penumbra (Guadagno *et al.*, 2004). Work is currently under way in a number of centers to define diffusion and perfusion thresholds in order to more accurately define the ischemic penumbra, rather than relying on DWI/PWI mismatch volumes alone (Rohl *et al.*, 2001, Butcher *et al.*, 2003, Moon *et al.*, 2005).

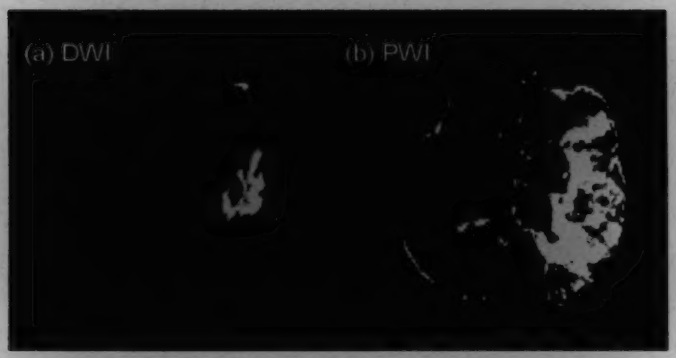

Figure 4-4: DWI and PWI images (DSC-MRI) of an acute stroke patient

The diffusion-weighted image (a) shows a hyperintense region in the left MCA territory that is thought to represent infarcted tissue. The area of perfusion abnormality (b) is significantly larger than the diffusion lesion, revealing an area of mismatch. This mismatch may represent the ischemic penumbra, and is thought to be salvageable if blood flow is restored.

DSC-MRI perfusion imaging with Gd-DTPA is an effective method to determine the physiological status of both healthy and diseased tissue. DSC is the technique most frequently used for the evaluation of cerebral perfusion in stroke, although extensive postprocessing somewhat limits its practical use for immediate perfusion assessment. The clinical application of ASL has been limited by long scan times, poor SNR, and inadequate brain coverage, although recent technical developments to improve ASL temporal and spatial resolution are promising (Duyn *et al.*, 2005). The goal of our research is to develop ASL perfusion imaging techniques that can be applied to acute stroke patients.

4.4.3 ASL Assessment of Perfusion in Stroke

ASL is a robust technique for perfusion quantification in healthy individuals with short (<1s) and consistent transit times (Wong *et al.*, 1999). Perfusion quantification in stroke

patients is considerably more difficult, because the arterial transit times to some brain regions can be extremely long (2-3s) when supplied by collateral flow. Even though the tissue may be adequately perfused, CBF may be underestimated (or not detected) if the transit time exceeds the lifetime of the ASL tag.

Several studies have investigated the potential for the application of ASL to stroke (Table 4-1). In a CASL study of cerebrovascular disease, perfusion images disclosed regional (hemispheric and focal) abnormalities in all patients presenting with cerebral events (Detre *et al.*, 1998). The authors asserted that CASL was a reliable technique for evaluating perfusion in cerebrovascular disease. In another study, CASL identified hypoperfused regions in 10/11 patients presenting with DWI abnormalities (Chalela *et al.*, 2000). Hyperintensities, representing delayed flow and increased transit times, were evident in 7/15 patients, suggesting that an increased post labeling delay may be necessary, even at the expense of SNR. Finally, CASL perfusion images were compared to DSC perfusion maps (relative cerebral blood flow (rCBF), relative cerebral blood volume (rCBV), mean transit time (MTT), and time-to-peak (TTP)) for the assessment of patients with acute and/or chronic cerebrovascular disease (Wolf *et al.*, 2003). CASL images correlated best with DSC TTP maps when all patients were considered, however if patients with a major transit delay were excluded, the correlation was highest between CASL and rCBF. The authors suggest there may be a complementary role for CASL and DSC perfusion MR for the evaluation of patients with cerebrovascular disease.

The remaining studies, using EPISTAR and FAIR, showed a high correlation between PASL hypointensities and DSC-MRI perfusion abnormalities (Siewert *et al.*, 1997, Hunsche *et al.*, 2002). FAIR images correlated best with lesions on rCBF maps compared to rCBV and MTT. EPISTAR hypointensities were consistent with DSC perfusion lesions, except in patients with a major transit delay; DSC maps showed that perfusion was normal (i.e. the area was adequately supplied by collateral flow), whereas EPISTAR images displayed an absence of blood flow. The authors suggest that an increase in EPISTAR inversion time may be necessary to detect regions supplied by

collateral flow. However, TI is limited by T_{1blood} so the tag does not decay before imaging, therefore it may be necessary to image at higher field strength in order to increase the lifetime of the EPISTAR tag and the maximum allowable inversion time.

Overall, stroke patients often experience reduced and/or delayed flow, and it is likely that ASL techniques will need to be modified in order to assess flow in these cases. However, the results are promising for the implementation of PASL imaging in acute stroke, even though this must be confirmed by the extension of this technique to a larger cohort of patients.

Table 4-1: Assessment of cerebrovascular disease using ASL

Technique	Patients	Assessment	Conclusions	References
EPISTAR (single-slice)	21 (acute stroke)	Compared to DSC (qualitative)	1. 17/21 cases, agreement 2. 4/21 cases, disagreement (EPISTAR = no perfusion, DSC = delayed flow)	(Siewert *et al.*, 1997)
CASL (multi-slice)	14 (cerebral events, >24 hrs)	(qualitative and quantitative)	1. able to show hemispheric and focal reduced flow 2. stenosis may lead to increased transit time	(Detre *et al.*, 1998)
CASL (multi-slice)	15 (acute stroke, <24hrs)	Compared to DWI (qualitative, quantitative)	1. 10/11 cases, hypoperfusion matched diffusion lesion 2. 7/15 cases showed hyperintensities	(Chalela *et al.*, 2000)
FAIR (single slice)	12 (acute stroke, <12hrs)	Compared to DSC (qualitative)	1. high correlation – FAIR and DSC rCBF 2. modest correlation - FAIR and rCBV, MTT	(Hunsche *et al.*, 2002)
CASL (multi-slice)	11 (acute and/or chronic cerebrovascular disease)	Compared to DSC (qualitative)	1. CASL and DSC TTP correlated best 2. high correlation – CASL and DSC rCBF (when cases with delayed flow removed) 3. possible complementary role for CASL and DSC	(Wolf *et al.*, 2003)

4.4.4 MRI Stroke Research Program

The MRI stroke research program is designed to follow the evolution of perfusion lesions by scanning stroke patients at four time points: <12 hours after symptom onset, and then 24-36 hours, 5-7 days, and 30 days after the first scan. We predict that a patient with a persistent perfusion deficit may benefit from thrombolytic therapy past the stated 3 hour time limit for treatment. Overall, we anticipate that completion of this study will increase our understanding of stroke pathophysiology as well as our understanding of the role MRI will play in stroke management. The application of ASL with perfusion quantification may help in determining appropriate perfusion thresholds for identifying stroke patients likely to benefit from thrombolysis. Our goal is to improve the treatment of acute stroke patients through the introduction of MRI perfusion imaging as a routine diagnostic tool.

By comparing ASL perfusion lesions to DSC-MRI and DWI abnormalities we plan to: (a) assess the ability of ASL to identify areas of hypoperfusion, normal perfusion, and delayed perfusion, and (b) determine the feasibility of using current ASL techniques to quantify perfusion in acute stroke. To date, we have imaged 22 patients with DSC (6 hyperacute, 9 acute, 7 subacute), 15 patients with ASL (6 acute, 9 subacute), and 10 of these patients have had both ASL and DSC. After qualitative assessment, ASL abnormalities correlate with ADC abnormalities in 5 patients (ASL lesion $\geq$ ADC lesion), and in 3 patients ASL images showed combined hypo- and hyperintense regions, likely indicating delayed flow. Overall, preliminary results have illustrated various degrees of perfusion-diffusion mismatch and agreement between ASL and contrast-enhanced scans (Fig. 4-5).

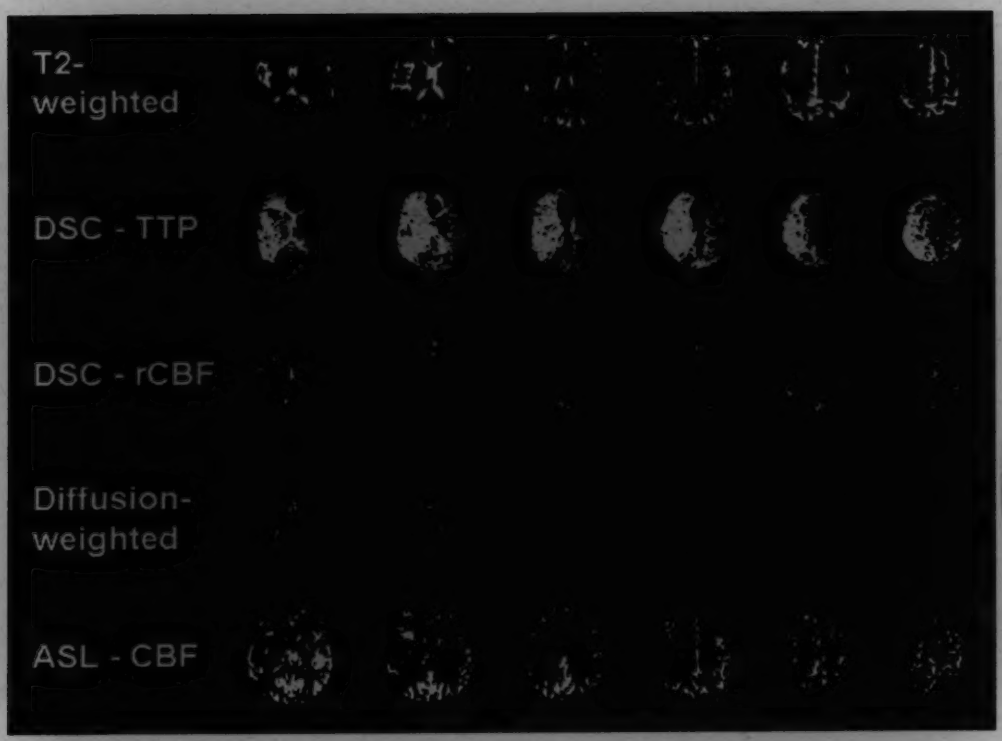

Figure 4-5: DWI, DSC-MRI, and ASL images of an acute stroke patient

This is a representative set of MR images obtained from an acute stroke patient (time from onset = 34 hours), and includes (a) anatomical T_2-weighted images, (b) DSC time-to-peak (TTP) maps, (c) DSC relative CBF (rCBF) maps, (d) CSF-suppressed apparent diffusion coefficient (ADC) maps, and (e) ASL difference images. The area of the perfusion lesion, shown in the TTP maps and ASL images, is larger than the diffusion lesion, indicating potentially salvageable tissue.

4.5 Future Directions

4.5.1 Q2TIPS Sequence Development

The PASL sequence used in our research benefits from several modifications made to the PICORE prototype tagging scheme. Most significantly, the addition of saturation pulses changing the PICORE sequence to Q2TIPS increases the efficiency and accuracy of CBF quantification. Further modifications, in-plane presaturation for reducing static tissue signal, and bipolar crusher gradients for decreasing intravascular signal, were also used in some areas of our research. Presaturation is a widely accepted technique (Wong *et al.*, 1999), however the addition of diffusion gradients may reduce the ASL signal and complicate the quantification process (Ye *et al.*, 1997, Wong, 2005). We did not alter our CBF quantification model to include the effects of diffusion-weighting, although this may be necessary to produce accurate perfusion values.

The location of the tagging region in an ASL experiment has a large effect on the signal that is generated. The ideal location would tag a large amount of blood to increase the signal, avoid venous blood, and tag blood close to the imaging slices to reduce transit times. The importance of tagging plane location was recognized in our research comparing single slice and multi-slice ASL experiments (Chapter 2). As we moved the tagging region further into the brain, possibly tagging the Circle of Willis, we observed a significant increase in ASL signal. There is a possibility that we may be able to improve SNR in our experiments by determining the optimal location of the tagging region in each subject.

4.5.2 Tagging Schemes

A newer form of pulsed ASL has been presented called velocity-selective ASL (VS-ASL), which is advantageous because it is inherently insensitive to transit delays (Duhamel *et al.*, 2003). The tag pulse inverts or saturates blood spins based purely on velocity; blood water flowing faster than the cutoff velocity (V_c) is selected to the tag,

regardless of spatial location. The image acquisition pulse is also velocity selective, consequently only blood that has decelerated through the cutoff velocity during the inversion time will be present in the final image. Good quality VS-ASL images can be produced with cerebral spinal fluid (CSF) suppression, although initial quantification attempts have yielded GM flow values approximately half of that expected (27 mL/100mL/min) (Duhamel *et al.*, 2003). Overall, VS-ASL is a promising technique, especially for the clinical evaluation of acute stroke where transit times can be long due to collateral or slow flow.

Another recently implemented tagging scheme uses selective inversion pulses to create perfusion images of specific territories within the brain (Eastwood *et al.*, 2002, Davies & Jezzard, 2003, Hendrikse *et al.*, 2004, Werner *et al.*, 2004, Golay *et al.*, 2005, Werner *et al.*, 2005). Using either pulsed or continuous tagging schemes, arteries can be selectively tagged to produce multi-slice flow territory maps, i.e. maps of brain regions selectively perfused by the internal carotid artery (ICA), basilar artery (BA), middle cerebral artery (MCA), or anterior cerebral arteries (ACA). Visualization of the flow territories of major feeding arteries is potentially useful for a number of clinical applications, including the assessment of cerebrovascular disease and collateral flow. Additional applications may include the delineation of perfusion territories of smaller cerebral arteries, and selective angiography techniques.

4.5.3 3D Image Acquisition Techniques

Recently, several techniques have been proposed to replace the conventional 2D-EPI readout schemes frequently used in ASL, including PASL with 3D-GRASE at 1.5T (Gunther *et al.*, 2005), CASL with 3D-GRASE at 3T (Fernandez-Seara *et al.*, 2005), and CASL with 3D-FSE and separate labeling coil at 3T (Talagala *et al.*, 2004). All three techniques have been successfully implemented, showing improved SNR, resolution, brain coverage, and scan times. Both GRASE (Feinberg & Oshio, 1991) and FSE (Melki *et al.*, 1991) show better coverage in areas with high susceptibility gradients (e.g.

orbitofrontal cortex) compared to GE-EPI, and marked increase in SNR; PASL with 3D-GRASE yields a 2.8-fold increase in SNR compared to 2D-EPI at the same nominal resolution (Gunther *et al.*, 2005). The resolution of 3D-GRASE images can be improved by increasing the number of phase encoded steps in the slice-encoding direction, although this leads to an increase in echo train length. This is overcome with the addition of parallel imaging techniques to reduce the echo train length, thus decreasing signal loss due to T_2 decay as well as reducing overall scan time (Fernandez-Seara *et al.*, 2005). Parallel techniques combined with 3D-GRASE also provide better separation of the gray-white matter in cerebral blood flow maps. In the end, it may be necessary to use 3D readout techniques to overcome the problem of slice interactions and signal loss that occurs with 2D multi-slice techniques (see Chapter 2).

The latest methodological improvements in ASL are discussed in a recent report by Duyn *et al.*, specifically high field imaging, parallel imaging, and increased pulse sequence efficiency, resulting in increased image acquisition speed and improved SNR (Duyn *et al.*, 2005). The authors present an example of CASL imaging at 7T using FAIR with single-shot SENSE-EPI readout (acceleration factor of 2), which produced high quality images differentiating sulci and giri in the cortex. The images were acquired in approximately 5 min, and had a voxel size of 1.5 mm x 1.5 mm x 2.0 mm (4.5 mm^3), and SNR upwards of 20-40 in gray matter (compared to our resolution of 3.4 mm x 3.4 mm x 8 mm (92 mm^3) and SNR of 5.6 ± 0.7 acquired in 3:52 min at 1.5T).

4.6 Conclusions

Arterial spin labeling is an entirely noninvasive technique that uses endogenous blood water as a tracer to measure cerebral blood flow. Arterial water is magnetically labeled proximal to the tissue of interest, and the effects of this labeling are determined by comparison with images acquired using control labeling. ASL is appealing because it is a

direct measure of blood flow and absolute quantitative values of CBF can be determined with relatively little postprocessing, although the small fractional perfusion signal in ASL (<1%) necessitates lengthy signal averaging of tag-control pairs, which can lead to long scans times. Nonetheless, this technique has been implemented in normal brain studies as well as various disease states, and has been able to provide reproducible and reliable quantitative CBF measurements.

Cerebral blood flow represents an important physiologic parameter for the assessment of normal brain development as well as the diagnosis and management of brain disorders. Using a PICORE-Q2TIPS sequence, we were able to assess CBF in the elderly and demonstrate that changes in the cerebrovasculature with age increase the arterial transit time of blood, requiring a change in PASL parameters, specifically an increase in inversion time, in order to accurately assess blood flow. These results are applicable to the measurement of CBF in stroke, which primarily occurs in the elderly. Current research on CBF in teenagers may provide important insight on brain development and perfusion changes in children, and results could potentially be applied to childhood diseases affecting CBF including stroke, epilepsy, and moyamoya disease.

Further development of quantification methods and technological advances in arterial spin labeling will be important for increasing the clinical utility of this technique. Although quantification of CBF using ASL is feasible at the present time, current models use a variety of assumptions that may not be accurate, such as immediate and complete exchange of labeled water with tissue and single-compartment relaxation of the tag. In addition, methodological problems with tagging schemes and image acquisition can also affect the accuracy of perfusion quantification. Our study comparing single slice to multi-slice image acquisition demonstrates that the perfusion signal in distal slices is reduced because of the acquisition of more proximal slices, resulting in CBF underestimation in multi-slice techniques. Current advancements in the field, specifically ASL with 3D image acquisition techniques, may overcome this problem and allow more accurate CBF quantification over a larger brain coverage.

Overall, arterial spin labeling is appealing for the noninvasive measurement of cerebral blood flow, particularly in research areas where there is a lack of suitable techniques, such as longitudinal studies and the assessment of perfusion in children. Although DSC-MRI is routinely used to measure CBF in stroke patients, caution must be taken in the interpretation of perfusion maps (i.e. relative CBF and CBV, MTT, and TTP maps), due to the fact that several, possibly inaccurate, assumptions are required for their construction (Calamante *et al.*, 2002). This is especially true when absolute quantification is attempted; scaling factors acquired by cross calibration with separate perfusion techniques are likely to vary with pathology. ASL provides an attractive alternative to DSC especially for perfusion quantification, and although ASL is presently limited by fundamental difficulties with long transit delays due to the short lifetime of the tag, it may become the imaging method of choice in the future when high field scanners are more widely distributed. Our contributions to the ASL field include PASL parameter optimization in the elderly and demonstration of signal loss in traditional multi-slice acquisition techniques which may cause perfusion underestimation. In the end, we hope our work will play a role in the development of arterial spin labeling as a routine diagnostic tool for the measurement of cerebral blood flow.

REFERENCES

Alsop, D. C. & Detre, J. A. (1996). Reduced transit-time sensitivity in noninvasive magnetic resonance imaging of human cerebral blood flow. *J Cereb Blood Flow Metab*, **16**, 1236-49.

Alsop, D. C. & Detre, J. A. (1998). Multisection cerebral blood flow MR imaging with continuous arterial spin labeling. *Radiology*, **208**, 410-6.

Alsop, D. C., Detre, J. A. & Grossman, M. (2000). Assessment of cerebral blood flow in Alzheimer's disease by spin-labeled magnetic resonance imaging. *Ann Neurol*, **47**, 93-100.

Arroyo, H. A. & Tamer, I. (2002). [Cerebrovascular disease in childhood and adolescence. Ischaemic cerebral accidents]. *Rev Neurol*, **34**, 133-44.

Astrup, J., Siesjo, B. K. & Symon, L. (1981). Thresholds in cerebral ischemia - the ischemic penumbra. *Stroke*, **12**, 723-5.

Back, T. (1998). Pathophysiology of the ischemic penumbra--revision of a concept. *Cell Mol Neurobiol*, **18**, 621-38.

Baird, A. E. & Warach, S. (1998). Magnetic resonance imaging of acute stroke. *J Cereb Blood Flow Metab*, **18**, 583-609.

Bakker, S. L., de Leeuw, F. E., den Heijer, T., Koudstaal, P. J., Hofman, A. & Breteler, M. M. (2004). Cerebral haemodynamics in the elderly: the rotterdam study. *Neuroepidemiology*, **23**, 178-84.

Bell, B. A. (1984). A history of the study of the cerebral circulation and the measurement of cerebral blood flow. *Neurosurgery*, **14**, 238-46.

Belliveau, J. W., Rosen, B. R., Kantor, H. L., Rzedzian, R. R., Kennedy, D. N., McKinstry, R. C., Vevea, J. M., Cohen, M. S., Pykett, I. L. & Brady, T. J. (1990). Functional cerebral imaging by susceptibility-contrast NMR. *Magn Reson Med*, **14**, 538-46.

Belliveau, J. W., Kennedy, D. N., Jr., McKinstry, R. C., Buchbinder, B. R., Weisskoff, R. M., Cohen, M. S., Vevea, J. M., Brady, T. J. & Rosen, B. R. (1991). Functional mapping of the human visual cortex by magnetic resonance imaging. *Science*, **254**, 716-9.

Bogousslavsky, J., Delaloye-Bischof, A., Regli, F. & Delaloye, B. (1990). Prolonged hypoperfusion and early stroke after transient ischemic attack. *Stroke*, **21**, 40-6.

Boxerman, J. L., Hamberg, L. M., Rosen, B. R. & Weisskoff, R. M. (1995). MR contrast due to intravascular magnetic susceptibility perturbations. *Magn Reson Med*, **34**, 555-66.

Brooks, R. A. & Di Chiro, G. (1976). Principles of computer assisted tomography (CAT) in radiographic and radioisotopic imaging. *Phys Med Biol*, **21**, 689-732.

Butcher, K., Parsons, M., Baird, T., Barber, A., Donnan, G., Desmond, P., Tress, B. & Davis, S. (2003). Perfusion thresholds in acute stroke thrombolysis. *Stroke*, **34**, 2159-64.

Buxton, R. B., Frank, L. R., Wong, E. C., Siewert, B., Warach, S. & Edelman, R. R. (1998). A general kinetic model for quantitative perfusion imaging with arterial spin labeling. *Magn Reson Med*, **40**, 383-96.

Calamante, F., Thomas, D. L., Pell, G. S., Wiersma, J. & Turner, R. (1999). Measuring cerebral blood flow using magnetic resonance imaging techniques. *J Cereb Blood Flow Metab*, **19**, 701-35.

Calamante, F., Gadian, D. G. & Connelly, A. (2002). Quantification of perfusion using bolus tracking magnetic resonance imaging in stroke: assumptions, limitations, and potential implications for clinical use. *Stroke*, **33**, 1146-51.

Carpenter, D. A., Grubb, R. L., Jr. & Powers, W. J. (1990). Borderzone hemodynamics in cerebrovascular disease. *Neurology*, **40**, 1587-92.

Carter, C. C., Eichling, J. O., Davis, D. O. & Ter-Pogossian, M. M. (1972). Correlation of regional cerebral blood flow with regional oxygen uptake using 15 O method. *Neurology*, **22**, 755-62.

Chalela, J. A., Alsop, D. C., Gonzalez-Atavales, J. B., Maldjian, J. A., Kasner, S. E. & Detre, J. A. (2000). Magnetic resonance perfusion imaging in acute ischemic stroke using continuous arterial spin labeling. *Stroke*, **31**, 680-7.

Davies, N. P. & Jezzard, P. (2003). Selective arterial spin labeling (SASL): perfusion territory mapping of selected feeding arteries tagged using two-dimensional radiofrequency pulses. *Magn Reson Med*, **49**, 1133-42.

Davis, S. M., Ackerman, R. H., Correia, J. A., Alpert, N. M., Chang, J., Buonanno, F., Kelley, R. E., Rosner, B. & Taveras, J. M. (1983). Cerebral blood flow and cerebrovascular CO2 reactivity in stroke-age normal controls. *Neurology*, **33**, 391-9.

Detre, J. A., Leigh, J. S., Williams, D. S. & Koretsky, A. P. (1992). Perfusion imaging. *Magn Reson Med*, **23**, 37-45.

Detre, J. A., Alsop, D. C., Vives, L. R., Maccotta, L., Teener, J. W. & Raps, E. C. (1998). Noninvasive MRI evaluation of cerebral blood flow in cerebrovascular disease. *Neurology*, **50**, 633-41.

Detre, J. A. & Alsop, D. C. (1999). Perfusion magnetic resonance imaging with continuous arterial spin labeling: methods and clinical applications in the central nervous system. *Eur J Radiol*, **30**, 115-24.

Detre, J. A., Samuels, O. B., Alsop, D. C., Gonzalez-At, J. B., Kasner, S. E. & Raps, E. C. (1999). Noninvasive magnetic resonance imaging evaluation of cerebral blood flow with acetazolamide challenge in patients with cerebrovascular stenosis. *J Magn Reson Imaging*, **10**, 870-5.

Drayer, B. P., Wolfson, S. K., Reinmuth, O. M., Dujovny, M., Boehnke, M. & Cook, E. E. (1978). Xenon enhanced CT for analysis of cerebral integrity, perfusion, and blood flow. *Stroke*, **9**, 123-30.

Duhamel, G., de Bazelaire, C. & Alsop, D. C. (2003). Evaluation of systematic quantification errors in velocity-selective arterial spin labeling of the brain. *Magn Reson Med*, **50**, 145-53.

Duyn, J. H., van Gelderen, P., Talagala, L., Koretsky, A. & de Zwart, J. A. (2005). Technological advances in MRI measurement of brain perfusion. *J Magn Reson Imaging*, **22**, 751-3.

Eastwood, J. D., Holder, C. A., Hudgins, P. A. & Song, A. W. (2002). Magnetic resonance imaging with lateralized arterial spin labeling. *Magn Reson Imaging*, **20**, 583-6.

Eastwood, J. D., Lev, M. H. & Provenzale, J. M. (2003). Perfusion CT with iodinated contrast material. *AJR Am J Roentgenol*, **180**, 3-12.

Edelman, R. R., Siewert, B., Darby, D. G., Thangaraj, V., Nobre, A. C., Mesulam, M. M. & Warach, S. (1994). Qualitative mapping of cerebral blood flow and functional localization with echo-planar MR imaging and signal targeting with alternating radio frequency. *Radiology*, **192**, 513-20.

Elias, M. F., Sullivan, L. M., D'Agostino, R. B., Elias, P. K., Beiser, A., Au, R., Seshadri, S., DeCarli, C. & Wolf, P. A. (2004). Framingham stroke risk profile and lowered cognitive performance. *Stroke*, **35**, 404-9.

Feinberg, D. A. & Oshio, K. (1991). GRASE (gradient- and spin-echo) MR imaging: a new fast clinical imaging technique. *Radiology*, **181**, 597-602.

Fernandez-Seara, M. A., Wang, Z., Wang, J., Rao, H. Y., Guenther, M., Feinberg, D. A. & Detre, J. A. (2005). Continuous arterial spin labeling perfusion measurements using single shot 3D GRASE at 3 T. *Magn Reson Med*, **54**, 1241-7.

Fick, A. (1870). Ueber die Messung des Blutquantums in den Herzventrikeln. *Sitz ber Physik-Med Ges Wurzburg*, **2**, 16-28.

Gobbel, G. T., Cann, C. E. & Fike, J. R. (1991). Measurement of regional cerebral blood flow using ultrafast computed tomography. Theoretical aspects. *Stroke*, **22**, 768-71.

Golay, X., Petersen, E. T. & Hui, F. (2005). Pulsed star labeling of arterial regions (PULSAR): a robust regional perfusion technique for high field imaging. *Magn Reson Med*, **53**, 15-21.

Gonzalez-At, J. B., Alsop, D. C. & Detre, J. A. (2000). Cerebral perfusion and arterial transit time changes during task activation determined with continuous arterial spin labeling. *Magn Reson Med*, **43**, 739-46.

Guadagno, J. V., Donnan, G. A., Markus, R., Gillard, J. H. & Baron, J. C. (2004). Imaging the ischaemic penumbra. *Curr Opin Neurol*, **17**, 61-7.

Gunther, M., Oshio, K. & Feinberg, D. A. (2005). Single-shot 3D imaging techniques improve arterial spin labeling perfusion measurements. *Magn Reson Med*, **54**, 491-8.

Gur, A. Y., Bova, I. & Bornstein, N. M. (1996). Is impaired cerebral vasomotor reactivity a predictive factor of stroke in asymptomatic patients? *Stroke*, **27**, 2188-90.

Heiniger, P., el-Koussy, M., Schindler, K., Lovblad, K. O., Kiefer, C., Oswald, H., Wissmeyer, M., Mariani, L., Donati, F., Schroth, G. & Weder, B. (2002). Diffusion and perfusion MRI for the localisation of epileptogenic foci in drug-resistant epilepsy. *Neuroradiology*, **44**, 475-80.

Hendrikse, J., van der Grond, J., Lu, H., van Zijl, P. C. & Golay, X. (2004). Flow territory mapping of the cerebral arteries with regional perfusion MRI. *Stroke*, **35**, 882-7.

Herscovitch, P., Raichle, M. E., Kilbourn, M. R. & Welch, M. J. (1987). Positron emission tomographic measurement of cerebral blood flow and permeability-surface area product of water using [15O]water and [11C]butanol. *J Cereb Blood Flow Metab*, **7**, 527-42.

Hossmann, K. A. (1994). Viability thresholds and the penumbra of focal ischemia. *Ann Neurol*, **36**, 557-65.

Hunsche, S., Sauner, D., Schreiber, W. G., Oelkers, P. & Stoeter, P. (2002). FAIR and dynamic susceptibility contrast-enhanced perfusion imaging in healthy subjects and stroke patients. *J Magn Reson Imaging*, **16**, 137-46.

Ingvar, D. H. & Lassen, N. A. (1961). Quantitative determination of regional cerebral blood flow in man. *Lancet*, 806-07.

Jahng, G. H., Song, E., Zhu, X. P., Matson, G. B., Weiner, M. W. & Schuff, N. (2005). Human brain: reliability and reproducibility of pulsed arterial spin-labeling perfusion MR imaging. *Radiology*, **234**, 909-16.

Jaszczak, R. J. & Coleman, R. E. (1988). Instrumentation for single-photon-emission computed tomographic studies of the brain. *Am J Physiol Imaging*, **3**, 67-70.

Kety, S. S. & Schmidt, C. F. (1945). The determination of cerebral blood flow in man by the use of nitrous oxide in low concentrations. *Am J Physiol*, **143**, 53-66.

Kety, S. S. & Schmidt, C. F. (1948a). The nitrous oxide method for the quantitative determination of cerebral blood flow in man: Theory, procedure, and normal values. *J. Clin. Invest.*, **27**, 475-83.

Kety, S. S. & Schmidt, C. F. (1948b). The effects of altered arterial tensions of carbon dioxide and oxygen on cerebral blood flow and cerebral oxygen consumption of normal young men. *J.Clin.Invest.*, **27**, 484-92.

Kety, S. S. (1951). The theory and applications of the exchange of inert gas at the lungs and tissues. *Pharmacol Rev*, **3**, 1-41.

Kety, S. S. (1991). The circulation, metabolism, and functional activity of the human brain. *Neurochem Res*, **16**, 1073-8.

Khanna, P. C., Lath, C., Gadewar, S. B. & Patkar, D. P. (2004). Role of magnetic resonance perfusion studies in moyamoya disease. *Neurol India*, **52**, 238-40.

Kidwell, C. S., Alger, J. R. & Saver, J. L. (2004). Evolving paradigms in neuroimaging of the ischemic penumbra. *Stroke*, **35**, 2662-5.

Kim, S. G., Hu, X. & Ugurbil, K. (1994). Accurate T1 determination from inversion recovery images: application to human brain at 4 Tesla. *Magn Reson Med*, **31**, 445-9.

Kim, S. G. (1995). Quantification of relative cerebral blood flow change by flow-sensitive alternating inversion recovery (FAIR) technique: application to functional mapping. *Magn Reson Med*, **34**, 293-301.

Krausz, Y., Bonne, O., Gorfine, M., Karger, H., Lerer, B. & Chisin, R. (1998). Age-related changes in brain perfusion of normal subjects detected by 99mTc-HMPAO SPECT. *Neuroradiology*, **40**, 428-34.

Kwong, K. K., Belliveau, J. W., Chesler, D. A., Goldberg, I. E., Weisskoff, R. M., Poncelet, B. P., Kennedy, D. N., Hoppel, B. E., Cohen, M. S., Turner, R. & et al. (1992). Dynamic magnetic resonance imaging of human brain activity during primary sensory stimulation. *Proc Natl Acad Sci U S A*, **89**, 5675-9.

Kwong, K. K., Chesler, D. A., Weisskoff, R. M., Donahue, K. M., Davis, T. L., Ostergaard, L., Campbell, T. A. & Rosen, B. R. (1995). MR perfusion studies with T1-weighted echo planar imaging. *Magn Reson Med*, **34**, 878-87.

Latchaw, R. E., Yonas, H., Hunter, G. J., Yuh, W. T., Ueda, T., Sorensen, A. G., Sunshine, J. L., Biller, J., Wechsler, L., Higashida, R. & Hademenos, G. (2003). Guidelines and recommendations for perfusion imaging in cerebral ischemia: A scientific statement for healthcare professionals by the writing group on perfusion imaging, from the Council on Cardiovascular Radiology of the American Heart Association. *Stroke*, **34**, 1084-104.

Leblanc, R., Yamamoto, Y. L., Tyler, J. L., Diksic, M. & Hakim, A. (1987). Borderzone ischemia. *Ann Neurol*, **22**, 707-13.

Leenders, K. L., Perani, D., Lammertsma, A. A., Heather, J. D., Buckingham, P., Healy, M. J., Gibbs, J. M., Wise, R. J., Hatazawa, J., Herold, S. & et al. (1990). Cerebral blood flow, blood volume and oxygen utilization. Normal values and effect of age. *Brain*, **113 (Pt 1)**, 27-47.

Liu, H. L., Kochunov, P., Hou, J., Pu, Y., Mahankali, S., Feng, C. M., Yee, S. H., Wan, Y. L., Fox, P. T. & Gao, J. H. (2001). Perfusion-weighted imaging of interictal hypoperfusion in temporal lobe epilepsy using FAIR-HASTE: comparison with H(2)(15)O PET measurements. *Magn Reson Med*, **45**, 431-5.

Lou, H. C., Edvinsson, L. & MacKenzie, E. T. (1987). The concept of coupling blood flow to brain function: revision required? *Ann Neurol*, **22**, 289-97.

Lu, H., Clingman, C., Golay, X. & van Zijl, P. C. (2004). Determining the longitudinal relaxation time (T1) of blood at 3.0 Tesla. *Magn Reson Med*, **52**, 679-82.

Luh, W. M., Wong, E. C., Bandettini, P. A. & Hyde, J. S. (1999). QUIPSS II with thin-slice TI1 periodic saturation: a method for improving accuracy of quantitative perfusion imaging using pulsed arterial spin labeling. *Magn Reson Med*, **41**, 1246-54.

Macdonald, R. L. & Stoodley, M. (1998). Pathophysiology of cerebral ischemia. *Neurol Med Chir (Tokyo)*, **38**, 1-11.

Marchal, G., Rioux, P., Petit-Taboue, M. C., Sette, G., Travere, J. M., Le Poec, C., Courtheoux, P., Derlon, J. M. & Baron, J. C. (1992). Regional cerebral oxygen consumption, blood flow, and blood volume in healthy human aging. *Arch Neurol*, **49**, 1013-20.

Martin, A. J., Friston, K. J., Colebatch, J. G. & Frackowiak, R. S. (1991). Decreases in regional cerebral blood flow with normal aging. *J Cereb Blood Flow Metab*, **11**, 684-9.

Melki, P. S., Mulkern, R. V., Panych, L. P. & Jolesz, F. A. (1991). Comparing the FAISE method with conventional dual-echo sequences. *J Magn Reson Imaging*, **1**, 319-26.

Mohr, J. P., Caplan, L. R., Melski, J. W., Goldstein, R. J., Duncan, G. W., Kistler, J. P., Pessin, M. S. & Bleich, H. L. (1978). The Harvard Cooperative Stroke Registry: a prospective registry. *Neurology*, **28**, 754-62.

Moon, W. J., Na, D. G., Ryoo, J. W., Roh, H. G., Byun, H. S., Chon, Y. H. & Chung, E. C. (2005). Assessment of tissue viability using diffusion- and perfusion-weighted MRI in hyperacute stroke. *Korean J Radiol*, **6**, 75-81.

Nabavi, D. G., Cenic, A., Craen, R. A., Gelb, A. W., Bennett, J. D., Kozak, R. & Lee, T. Y. (1999). CT assessment of cerebral perfusion: experimental validation and initial clinical experience. *Radiology*, **213**, 141-9.

Nabavi, D. G., Cenic, A., Henderson, S., Gelb, A. W. & Lee, T. Y. (2001). Perfusion mapping using computed tomography allows accurate prediction of cerebral infarction in experimental brain ischemia. *Stroke*, **32**, 175-83.

Neumann-Haefelin, T., Wittsack, H. J., Wenserski, F., Siebler, M., Seitz, R. J., Modder, U. & Freund, H. J. (1999). Diffusion- and perfusion-weighted MRI. The DWI/PWI mismatch region in acute stroke. *Stroke*, **30**, 1591-7.

Nighoghossian, N., Trouillas, P., Philippon, B., Itti, R. & Adeleine, P. (1994). Cerebral blood flow reserve assessment in symptomatic versus asymptomatic high-grade internal carotid artery stenosis. *Stroke*, **25**, 1010-3.

Nobler, M. S., Mann, J. J. & Sackeim, H. A. (1999). Serotonin, cerebral blood flow, and cerebral metabolic rate in geriatric major depression and normal aging. *Brain Res Brain Res Rev*, **30**, 250-63.

Ordidge, R. J., Wylezinska, M., Hugg, J. W., Butterworth, E. & Franconi, F. (1996). Frequency offset corrected inversion (FOCI) pulses for use in localized spectroscopy. *Magn Reson Med*, **36**, 562-6.

Oshio, K. & Feinberg, D. A. (1991). GRASE (Gradient- and spin-echo) imaging: a novel fast MRI technique. *Magn Reson Med*, **20**, 344-9.

Ostergaard, L., Weisskoff, R. M., Chesler, D. A., Gyldensted, C. & Rosen, B. R. (1996a). High resolution measurement of cerebral blood flow using intravascular tracer bolus passages. Part I: Mathematical approach and statistical analysis. *Magn Reson Med*, **36**, 715-25.

Ostergaard, L., Sorensen, A. G., Kwong, K. K., Weisskoff, R. M., Gyldensted, C. & Rosen, B. R. (1996b). High resolution measurement of cerebral blood flow using intravascular tracer bolus passages. Part II: Experimental comparison and preliminary results. *Magn Reson Med*, **36**, 726-36.

Ostergaard, L., Smith, D. F., Vestergaard-Poulsen, P., Hansen, S. B., Gee, A. D., Gjedde, A. & Gyldensted, C. (1998a). Absolute cerebral blood flow and blood volume measured by magnetic resonance imaging bolus tracking: comparison with positron emission tomography values. *J Cereb Blood Flow Metab*, **18**, 425-32.

Ostergaard, L., Johannsen, P., Host-Poulsen, P., Vestergaard-Poulsen, P., Asboe, H., Gee, A. D., Hansen, S. B., Cold, G. E., Gjedde, A. & Gyldensted, C. (1998b). Cerebral blood flow measurements by magnetic resonance imaging bolus tracking: comparison with [(15)O]H2O positron emission tomography in humans. *J Cereb Blood Flow Metab*, **18**, 935-40.

Pantano, P., Baron, J. C., Lebrun-Grandie, P., Duquesnoy, N., Bousser, M. G. & Comar, D. (1984). Regional cerebral blood flow and oxygen consumption in human aging. *Stroke*, **15**, 635-41.

Parkes, L. M. & Tofts, P. S. (2002). Improved accuracy of human cerebral blood perfusion measurements using arterial spin labeling: accounting for capillary water permeability. *Magn Reson Med*, **48**, 27-41.

Parkes, L. M., Rashid, W., Chard, D. T. & Tofts, P. S. (2004). Normal cerebral perfusion measurements using arterial spin labeling: reproducibility, stability, and age and gender effects. *Magn Reson Med*, **51**, 736-43.

Parkes, L. M. (2005). Quantification of cerebral perfusion using arterial spin labeling: Two-compartment models. *J Magn Reson Imaging*, **22**, 732-6.

Paulson, O. B., Strandgaard, S. & Edvinsson, L. (1990). Cerebral autoregulation. *Cerebrovasc Brain Metab Rev*, **2**, 161-92.

Paulson, O. B. (2002). Blood-brain barrier, brain metabolism and cerebral blood flow. *Eur Neuropsychopharmacol*, **12**, 495-501.

Raichle, M. E., Grubb, R. L., Jr., Gado, M. H., Eichling, J. O. & Ter-Pogossian, M. M. (1976). Correlation between regional cerebral blood flow and oxidative metabolism. In vivo studies in man. *Arch Neurol*, **33**, 523-6.

Reivich, M. (1964). Arterial Pco2 and Cerebral Hemodynamics. *Am J Physiol*, **206**, 25-35.

Rempp, K. A., Brix, G., Wenz, F., Becker, C. R., Guckel, F. & Lorenz, W. J. (1994). Quantification of regional cerebral blood flow and volume with dynamic susceptibility contrast-enhanced MR imaging. *Radiology*, **193**, 637-41.

Rivers, C. S., Wardlaw, J. M., Armitage, P. A., Bastin, M. E., Carpenter, T. K., Cvoro, V., Hand, P. J. & Dennis, M. S. (2006). Do acute diffusion- and perfusion-weighted MRI lesions identify final infarct volume in ischemic stroke? *Stroke*, **37**, 98-104.

Rohl, L., Ostergaard, L., Simonsen, C. Z., Vestergaard-Poulsen, P., Andersen, G., Sakoh, M., Le Bihan, D. & Gyldensted, C. (2001). Viability thresholds of ischemic penumbra of hyperacute stroke defined by perfusion-weighted MRI and apparent diffusion coefficient. *Stroke*, **32**, 1140-6.

Rosen, B. R., Belliveau, J. W., Vevea, J. M. & Brady, T. J. (1990). Perfusion imaging with NMR contrast agents. *Magn Reson Med*, **14**, 249-65.

Roy, C. S. & Sherrington, C. S. (1890). On the regulation of the blood-supply of the brain. *J Physiol*, **11**, 85-108.

Scheel, P., Ruge, C. & Schoning, M. (2000). Flow velocity and flow volume measurements in the extracranial carotid and vertebral arteries in healthy adults: reference data and the effects of age. *Ultrasound Med Biol*, **26**, 1261-6.

Schellinger, P. D., Fiebach, J. B. & Hacke, W. (2003). Imaging-based decision making in thrombolytic therapy for ischemic stroke: present status. *Stroke*, **34**, 575-83.

Schlaug, G., Benfield, A., Baird, A. E., Siewert, B., Lovblad, K. O., Parker, R. A., Edelman, R. R. & Warach, S. (1999). The ischemic penumbra: operationally defined by diffusion and perfusion MRI. *Neurology*, **53**, 1528-37.

Schreiber, W. G., Guckel, F., Stritzke, P., Schmiedek, P., Schwartz, A. & Brix, G. (1998). Cerebral blood flow and cerebrovascular reserve capacity: estimation by dynamic magnetic resonance imaging. *J Cereb Blood Flow Metab*, **18**, 1143-56.

Schwarzbauer, C., Morrissey, S. P. & Haase, A. (1996). Quantitative magnetic resonance imaging of perfusion using magnetic labeling of water proton spins within the detection slice. *Magn Reson Med*, **35**, 540-6.

Shaw, T. G., Mortel, K. F., Meyer, J. S., Rogers, R. L., Hardenberg, J. & Cutaia, M. M. (1984). Cerebral blood flow changes in benign aging and cerebrovascular disease. *Neurology*, **34**, 855-62.

Siewert, B., Schlaug, G., Edelman, R. R. & Warach, S. (1997). Comparison of EPISTAR and T2*-weighted gadolinium-enhanced perfusion imaging in patients with acute cerebral ischemia. *Neurology*, **48**, 673-9.

Simonsen, C. Z., Ostergaard, L., Smith, D. F., Vestergaard-Poulsen, P. & Gyldensted, C. (2000). Comparison of gradient- and spin-echo imaging: CBF, CBV, and MTT measurements by bolus tracking. *J Magn Reson Imaging*, **12**, 411-6.

Smith, A. M., Grandin, C. B., Duprez, T., Mataigne, F. & Cosnard, G. (2000). Whole brain quantitative CBF and CBV measurements using MRI bolus tracking: comparison of methodologies. *Magn Reson Med*, **43**, 559-64.

Speck, O., Chang, L., DeSilva, N. M. & Ernst, T. (2000). Perfusion MRI of the human brain with dynamic susceptibility contrast: gradient-echo versus spin-echo techniques. *J Magn Reson Imaging*, **12**, 381-7.

Talagala, S. L., Ye, F. Q., Ledden, P. J. & Chesnick, S. (2004). Whole-brain 3D perfusion MRI at 3.0 T using CASL with a separate labeling coil. *Magn Reson Med*, **52**, 131-40.

Ter-Pogossian, M. M., Phelps, M. E., Hoffman, E. J. & Mullani, N. A. (1975). A positron-emission transaxial tomograph for nuclear imaging (PETT). *Radiology*, **114**, 89-98.

Thijs, V. N., Somford, D. M., Bammer, R., Robberecht, W., Moseley, M. E. & Albers, G. W. (2004). Influence of arterial input function on hypoperfusion volumes measured with perfusion-weighted imaging. *Stroke*, **35**, 94-8.

Tomita, M., Suzuki, N., Hamel, E., Busija, D. & Lauritzen, M. (2000). Regulation of cerebral microcirculation--update. *Keio J Med*, **49**, 26-34.

Van Laere, K., Versijpt, J., Audenaert, K., Koole, M., Goethals, I., Achten, E. & Dierckx, R. (2001). 99mTc-ECD brain perfusion SPET: variability, asymmetry and effects of age and gender in healthy adults. *Eur J Nucl Med*, **28**, 873-87.

Villringer, A., Rosen, B. R., Belliveau, J. W., Ackerman, J. L., Lauffer, R. B., Buxton, R. B., Chao, Y. S., Wedeen, V. J. & Brady, T. J. (1988). Dynamic imaging with lanthanide chelates in normal brain: contrast due to magnetic susceptibility effects. *Magn Reson Med*, **6**, 164-74.

Waldemar, G., Hasselbalch, S. G., Andersen, A. R., Delecluse, F., Petersen, P., Johnsen, A. & Paulson, O. B. (1991). 99mTc-d,l-HMPAO and SPECT of the brain in normal aging. *J Cereb Blood Flow Metab*, **11**, 508-21.

Wang, J., Alsop, D. C., Li, L., Listerud, J., Gonzalez-At, J. B., Schnall, M. D. & Detre, J. A. (2002). Comparison of quantitative perfusion imaging using arterial spin labeling at 1.5 and 4.0 Tesla. *Magn Reson Med*, **48**, 242-54.

Wang, J., Licht, D. J., Jahng, G. H., Liu, C. S., Rubin, J. T., Haselgrove, J., Zimmerman, R. A. & Detre, J. A. (2003). Pediatric perfusion imaging using pulsed arterial spin labeling. *J Magn Reson Imaging*, **18**, 404-13.

Wansapura, J. P., Holland, S. K., Dunn, R. S. & Ball, W. S. (1995). 3.0 Tesla study of NMR relaxation times in the human brain. In: *Proceedings of the 3rd Annual Meeting of SMR*, Nice, France, p 685.

Webster, M. W., Makaroun, M. S., Steed, D. L., Smith, H. A., Johnson, D. W. & Yonas, H. (1995). Compromised cerebral blood flow reactivity is a predictor of stroke in patients with symptomatic carotid artery occlusive disease. *J Vasc Surg*, **21**, 338-44; discussion 44-5.

Weisskoff, R. M., Zuo, C. S., Boxerman, J. L. & Rosen, B. R. (1994). Microscopic susceptibility variation and transverse relaxation: theory and experiment. *Magn Reson Med*, **31**, 601-10.

Werner, R., Alfke, K., Schaeffter, T., Nabavi, A., Mehdorn, H. M. & Jansen, O. (2004). Brain perfusion territory imaging applying oblique-plane arterial spin labeling with a standard send/receive head coil. *Magn Reson Med*, **52**, 1443-7.

Werner, R., Norris, D. G., Alfke, K., Mehdorn, H. M. & Jansen, O. (2005). Continuous artery-selective spin labeling (CASSL). *Magn Reson Med*, **53**, 1006-12.

Widder, B., Kleiser, B. & Krapf, H. (1994). Course of cerebrovascular reactivity in patients with carotid artery occlusions. *Stroke*, **25**, 1963-7.

Williams, D. S., Detre, J. A., Leigh, J. S. & Koretsky, A. P. (1992). Magnetic resonance imaging of perfusion using spin inversion of arterial water. *Proc Natl Acad Sci U S A*, **89**, 212-6.

Wintermark, M., Sesay, M., Barbier, E., Borbely, K., Dillon, W. P., Eastwood, J. D., Glenn, T. C., Grandin, C. B., Pedraza, S., Soustiel, J. F., Nariai, T., Zaharchuk, G., Caille, J. M., Dousset, V. & Yonas, H. (2005). Comparative overview of brain perfusion imaging techniques. *Stroke*, **36**, e83-99.

Wirestam, R., Andersson, L., Ostergaard, L., Bolling, M., Aunola, J. P., Lindgren, A., Geijer, B., Holtas, S. & Stahlberg, F. (2000). Assessment of regional cerebral blood flow by dynamic susceptibility contrast MRI using different deconvolution techniques. *Magn Reson Med*, **43**, 691-700.

Wolf, R. L., Alsop, D. C., Levy-Reis, I., Meyer, P. T., Maldjian, J. A., Gonzalez-Atavales, J., French, J. A., Alavi, A. & Detre, J. A. (2001). Detection of mesial temporal lobe hypoperfusion in patients with temporal lobe epilepsy by use of arterial spin labeled perfusion MR imaging. *AJNR Am J Neuroradiol*, **22**, 1334-41.

Wolf, R. L., Alsop, D. C., McGarvey, M. L., Maldjian, J. A., Wang, J. & Detre, J. A. (2003). Susceptibility contrast and arterial spin labeled perfusion MRI in cerebrovascular disease. *J Neuroimaging*, **13**, 17-27.

Wong, E. C., Buxton, R. B. & Frank, L. R. (1997). Implementation of quantitative perfusion imaging techniques for functional brain mapping using pulsed arterial spin labeling. *NMR Biomed*, **10**, 237-49.

Wong, E. C., Buxton, R. B. & Frank, L. R. (1998a). A theoretical and experimental comparison of continuous and pulsed arterial spin labeling techniques for quantitative perfusion imaging. *Magn Reson Med*, **40**, 348-55.

Wong, E. C., Buxton, R. B. & Frank, L. R. (1998b). Quantitative imaging of perfusion using a single subtraction (QUIPSS and QUIPSS II). *Magn Reson Med*, **39**, 702-8.

Wong, E. C., Buxton, R. B. & Frank, L. R. (1999). Quantitative perfusion imaging using arterial spin labeling. *Neuroimaging Clin N Am*, **9**, 333-42.

Wong, E. C. (2005). Quantifying CBF with pulsed ASL: Technical and pulse sequence factors. *J Magn Reson Imaging*, **22**, 727-31.

Yang, Y., Frank, J. A., Hou, L., Ye, F. Q., McLaughlin, A. C. & Duyn, J. H. (1998). Multislice imaging of quantitative cerebral perfusion with pulsed arterial spin labeling. *Magn Reson Med*, **39**, 825-32.

Yang, Y., Engelien, W., Xu, S., Gu, H., Silbersweig, D. A. & Stern, E. (2000). Transit time, trailing time, and cerebral blood flow during brain activation: measurement using multislice, pulsed spin-labeling perfusion imaging. *Magn Reson Med*, **44**, 680-5.

Ye, F. Q., Mattay, V. S., Jezzard, P., Frank, J. A., Weinberger, D. R. & McLaughlin, A. C. (1997). Correction for vascular artifacts in cerebral blood flow values measured by using arterial spin tagging techniques. *Magn Reson Med*, **37**, 226-35.

Ye, F. Q., Berman, K. F., Ellmore, T., Esposito, G., van Horn, J. D., Yang, Y., Duyn, J., Smith, A. M., Frank, J. A., Weinberger, D. R. & McLaughlin, A. C. (2000). H(2)(15)O PET validation of steady-state arterial spin tagging cerebral blood flow measurements in humans. *Magn Reson Med*, **44**, 450-6.

Yen, Y. F., Field, A. S., Martin, E. M., Ari, N., Burdette, J. H., Moody, D. M. & Takahashi, A. M. (2002). Test-retest reproducibility of quantitative CBF measurements using FAIR perfusion MRI and acetazolamide challenge. *Magn Reson Med*, **47**, 921-8.

Yongbi, M. N., Yang, Y., Frank, J. A. & Duyn, J. H. (1999). Multislice perfusion imaging in human brain using the C-FOCI inversion pulse: comparison with hyperbolic secant. *Magn Reson Med*, **42**, 1098-105.

Yongbi, M. N., Fera, F., Yang, Y., Frank, J. A. & Duyn, J. H. (2002). Pulsed arterial spin labeling: comparison of multisection baseline and functional MR imaging perfusion signal at 1.5 and 3.0 T: initial results in six subjects. *Radiology*, **222**, 569-75.

Zhang, W., Silva, A. C., Williams, D. S. & Koretsky, A. P. (1995). NMR measurement of perfusion using arterial spin labeling without saturation of macromolecular spins. *Magn Reson Med*, **33**, 370-6.

Zhou, J., Wilson, D. A., Ulatowski, J. A., Traystman, R. J. & van Zijl, P. C. (2001). Two-compartment exchange model for perfusion quantification using arterial spin tagging. *J Cereb Blood Flow Metab*, **21**, 440-55.